Disentangling the control of tectonics, eustasy, trophic conditions and climate on shallow-marine carbonate production during the Aalenian-Oxfordian interval: From the western France platform to the western Tethyan domain

Simon Andrieu, Benjamin Brigaud, Jocelyn Barbarand, Eric Lasseur, Thomas Saucède

Disentangling the control of tectonics, eustasy, trophic conditions and climate on shallow-marine carbonate production during the Aalenian-Oxfordian interval: from the western France platform to the western Tethyan domain

Simon Andrieu[a], Benjamin Brigaud[a], Jocelyn Barbarand[a] , Eric Lasseur[b], and Thomas Saucède[c]

[a] GEOPS, Univ. Paris-Sud, CNRS, Université Paris Saclay, Rue du Belvédère, Bât. 504, 91405 Orsay, France
[b] BRGM, 3 avenue Claude Guillemin, BP 36009, 45060 Orléans, France
[c] UMR 6282 Biogéosciences, Univ. Bourgogne Franche-Comté, CNRS, 6 Bd Gabriel, 21000 Dijon, France

Corresponding author

simon.andrieu@u-psud.fr; Tel.: +33 169156126; fax: +33 169154911

Abstract

The objective of this work is to improve our understanding of the processes controlling changes in the architecture and facies of intracontinental carbonate platforms. We examined the facies and sequence stratigraphy of Aalenian to Oxfordian limestones of western France. Seventy-seven outcrop sections were studied and thirty-one sedimentary facies identified in five depositional environments ranging from lower offshore to backshore. Platform evolution was reconstructed along a 500 km cross-section. Twenty-two depositional sequences were identified on the entire western France platform and correlated with European third-order sequences at the biozone level, demonstrating that eustasy was the major factor controlling the cyclic trend of accommodation. The tectonic subsidence rate was computed from accommodation measurements from the Aalenian to the Oxfordian in key localities.Tectonism controlled the sedimentation rate and platform architecture at a longer time scale. Tectonic subsidence triggered the demise of carbonate production at the Bathonian/Callovian boundary while the uplift made possible the recovery of carbonate platform from Caen to Le Mans during the mid Oxfordian. Topography of the Paleozoic basement mainly controlled lateral variations of paleodepth within the western France platform until the mid Bathonian. A synthesis of carbonate production in the western Tethyan domain at that time was conducted. Stages of high carbonate production during the Bajocian/Bathonian and the middle to late Oxfordian are synchronous with low $\delta^{13}C$, high eccentricity intervals, and rather dry climate promoting (1) evaporation and carbonate sursaturation, and (2) oligotrophic conditions. Periods of low carbonate production during the Aalenian and from the middle Callovian to early Oxfordian correlate with high $\delta^{13}C$ and low eccentricity intervals, characterized by wet climate and less oligotrophic conditions. Such conditions tend to diminish growth potential of carbonate platforms. This work highlights the importance of climate control on carbonate growth and demise at large scale in western Tethyan epicontinental seas.

Keywords: Carbonate platform, Facies, Sequence stratigraphy, Tectonics, Jurassic

1. Introduction

In recent decades, numerous studies have been conducted on Jurassic carbonate platforms of the Western Tethys to characterize their architectures, facies, and discontinuities. They highlighted the importance of interactions among the multiple processes that control the evolution of carbonate depositional systems, that is: (1) eustasy, (2) tectonism in that it modifies accommodation, and (3) environmental conditions including seawater temperature, depth, salinity, chemistry, trophic conditions and productivity, with this last aspect determining the nature of carbonate producers and production rates (Pomar et al., 2001; Brigaud et al., 2009, Carpentier et al., 2010). Deciphering the precise influence of each factor on depositional sequences, on carbonate platform architecture, growth, and demise, and on facies distribution and composition is still a challenge (Mutti and Hallock, 2003; Léonide et al., 2007; Merino-Tomé et al., 2012), especially because accommodation and carbonate production are interdependent factors (Pomar et al., 2001). For instance, intracratonic basins were considered stable until recent studies showed that tectonics influenced sedimentation (Guillocheau et al., 2000; Carcel et al., 2010; Brigaud et al., 2014; Wright et al., 2014). Nevertheless, determining the specific control of tectonics on carbonate platform development is complex, especially because vertical movements are of low amplitude and detected over long wavelengths. Moreover, the control of the inherited basement structure over the architecture of carbonate platform is rarely discussed (Allenbach et al., 2002).

Western Tethyan carbonate platforms underwent several stages of growth and demise during the Jurassic, which are particulary well-marked in the Paris Basin (Brigaud et al., 2014). However, no large-scale synthesis of such changes in sedimentation patterns and facies has been conducted, while it could provide new insights on the main factors controlling the type of carbonate producers and production rate.

From the Aalenian to the Oxfordian (about 17 My, Gradstein et al., 2012), a vast carbonate platform developed in western France. Several stratigraphic studies based on the distribution of ammonite and brachiopod species provide a precise and reliable biostratigraphic framework within which to study the evolution of this platform at the biozone level. However, such studies remain limited to specific geographic areas or stages (Caen to Alençon: Dugué, 1989; Rioult et al., 1991; Préat et al., 2000; Dugué, 2007; Poitiers region: Mourier, 1983; Lorenz, 1992; Gonnin et al., 1992, 1993, 1994; Lenoir, 2012; Saint-Maixent l'École to Montbron: Foucher, 1986; Faugeras, 1988; Branger, 1989). The western France platform has tremendous potential for improving our understanding of Jurassic intracratonic carbonate systems because (1) it offers a continuous record of 17 My that can be studied through numerous outcrops and boreholes with a good time control based on biostratigraphy, (2) it rests upon a highly structured Hercynian basement, and (3) it has never been studied as a whole.

The first objective of this work is to reconstruct changes in facies and architecture of the western France platform and to determine the respective influences of eustasy, tectonics, environmental conditions, and the topography of the Paleozoic basement on platform evolution. The second objective is to compare our results at broad scale with other platforms in western Tethyan epicontinental sea. Facies were described and classified so as to define depositional environments. A 500 km-long north–south cross-section from Deauville to Montbron is examined within a sequence stratigraphy framework to model the evolution of the platform from the Aalenian to the Oxfordian. Four accommodation curves are established to quantify the amplitude of vertical movements and precisely identify tectonic control over the evolution of this intracontinental carbonate platform. A synthesis of sedimentation patterns in western Tethyan domain during the Middle Jurassic and the Oxfordian is

conducted and a large-scale model for western Tethyan carbonate platforms evolution is provided.

2. Geological setting

The Paris and Aquitaine Basins are two intracontinental sedimentary basins filled with Triassic to Quaternary deposits. They developed respectively over a Cadomian and Variscan basement (Paris Basin, Guillocheau et al., 2000) and a Variscan basement (Aquitaine Basin, Biteau et al., 2006). The study area stretches from Deauville, in the northwestern Paris Basin, to Angouleme, in the northern Aquitaine Basin, along an approximately 500-km transect (Fig. 1). From Aalenian to Oxfordian times, western France was positioned at subtropical latitudes (20–30°N) and was covered by a shallow epicontinental sea. Sediments are predominantly composed of shallow marine carbonates deposited over a vast platform open to the Atlantic, Tethys, and Artic oceans (Fig. 2A-B; Enay and Mangold, 1980; Thierry and Barrier, 2000).

Several studies of ammonite and brachiopod fauna have been conducted for Middle and Late Jurassic outcrops in areas around Caen (Rioult et al., 1991), Argentan (Kuntz et al, 1989; Ménillet et al., 1997; Moguedet et al., 1998), Poitiers (Gabilly et al., 1978; Mourier, 1983; Cariou and Joubert, 1989a; Lorenz, 1992), and between Saint-Maixent l'École and Montbron (Cariou et al., 1973; Foucher, 1986; Faugeras, 1988; Branger, 1989; Cariou et al., 2006). They have made it possible to define a precise and reliable biostratigraphical framework at the ammonite biozone level (Fig. 3). The stratigraphic framework is briefly described for the five areas of our study, displaying numerous outcrops and various facies: Caen, Argentan/Alençon, Poitiers Saint-Maixent-l'École, and Montbron. Readers should refer to Mégnien and Mégnien (1980) for a detailed description of lithostratigraphic units of the study area.

The Caen area was more or less isolated from the Paris Basin during the Trias and at the onset of the Jurassic, and remained separated from Argentan by emersive basement reliefs until the

116 end of the Bathonian (Enay and Mangold, 1980; Dugué, 2007). Around Caen, the Bajocian to
117 Oxfordian succession includes two major episodes of carbonate platform growth, (1) from the
118 late Bajocian (*parkinsoni* Zone) to the late Bathonian (*discus* Zone) and (2) from the mid
119 (*densiplicatum* Zone) to late Oxfordian (*glosense* Zone; Fig. 3, Rioult et al., 1991). From the
120 late Bajocian to the late Bathonian, bioclastic facies rich in echinoderms (*Calcaires de Caen*,
121 *Calcaires de Creully*, *Calcaires de Ranville* Formations), bryozoans (*Calcaires de Lagrune*
122 Formation), and sponge bioconstructions (*Caillasses de Basse-Ecarde* Formation) dominated.
123 The middle to upper Oxfordian deposits display ooid- and coral-dominated facies (*Calcaires*
124 *d'Auberville*, *Calcaires oolithiques de Trouville*, *Coral Rag* Formations; Fig. 3; Rioult et al.,
125 1991). The Aalenian to late Bajocian (*garantiana* Zone) was, like the Toarcian, a period of
126 low carbonate production, with highly condensed ferruginous levels (*Oolithe ferrugineuse*
127 *aalénienne*, *Couche verte*, *Conglomérat de Bayeux*, *Oolithe de Bayeux* Formations, Rioult et
128 al., 1991). A carbonate platform demise occurred from the very late Bathonian (*discus* Zone)
129 to late early Oxfordian (*cordatum* Zone), a period characterized by clayey deposits (*Argiles de*
130 *Lion*, *Marnes d'Escoville*, *Marnes d'Argences*, *Marnes à Belemnopsis latesulcata*, *Marnes et*
131 *calcaires sableux de Crevecoeur*, *Marnes de Dives*, *Marnes de Villers*, *Oolithe ferrugineuse*
132 *de Villers* and *Argiles à Lopha gregarea* Formations; Fig. 3).
133 The area from Argentan to Alençon formed a small basin, separated from Caen by emersive
134 basement reliefs (Dugué, 2007). Detrital deposits formed during the Aalenian (*Sables et*
135 *graviers de Tessé* Formation), displaying brachiopods and ammonites (*Graphoceras* sp.,
136 *Graphoceras cornu*) from the *murchisonae* and *concavum* Zones (Fig. 3; Juignet et al., 1984).
137 During the Bajocian to late Bathonian (*discus* Zone), a bioclastic to oolitic carbonate platform
138 grew (*Oolithe à pentacrines*, *Oolithe de Vilaines-la-Carelle*, *Calcaires d'Ecouché*, *Calcaires*
139 *de Sarceaux* and *Calcaires d'Argentan* Formations; Fig. 3; Juignet et al., 1984; Kuntz et al,
140 1989). The very late Bathonian (*discus* Zone), Callovian, and early Oxfordian deposits are

141 characterized by clays to sands (*Marnes de Montcel*, *Marnes du Chevain*, *Oolithe de Suré*,
142 *Marnes et calcaires sableux*, *Oolithe ferrugineuse de Chemilli*, *Marnes de Montarlo*, *Sables*
143 *de Saint-Fulgent*, *Marnes à Pernes*, *Sables de Mortagne* Formations; Fig. 3 ; Ménillet et al.,
144 1997). The mid to late Oxfordian limestone displays ooid and coral rich facies (*Calcaires*
145 *coralliens de Mortagne*, *Calcaires à Astrates*; Fig. 3; Moguedet et al., 1998).
146 Around Poitiers, the marl/limestone alternations (*Calcaires argileux d'Airvault* Formation) of
147 the early Aalenian pass upwards into bioclastic to oolitic limestones (*Calcaires finement*
148 *dolomitiques à silex*, *Calcaires roux bioclastiques à oncolithes*, *Calcaires dolomitiques à*
149 *bioclastiques de Poitiers*, *Calcaires graveleux de Poitiers*, and *Pierre des Lourdines*
150 Formations; Fig. 3 ; Mourier et al., 1986 ; Cariou and Joubert, 1989a). There is a sedimentary
151 gap between the late Callovian and the late early Oxfordian (*athleta*, *lamberta* and *mariae*
152 Zones; Cariou and Joubert, 1989a). Middle and upper Oxfordian deposits are composed of
153 crinoid limestones (*Pierre grise de Bonnillet*, *Calcaires crinoïdiques* Formations) and clayey
154 sedimentary sets (*Banc de Pierre sublithographique*, *Calcaires argileux et glauconieux de*
155 *Mirebeau* Formations; Fig. 3 ; Cariou and Joubert, 1989a).
156 The Saint-Maixent-l'École area was located on a relatively low-energy platform at the margin
157 of the *Golfe Charentais* basin during the Mid Jurassic (Enay and Mangold, 1980). The Saint-
158 Maixent-l'École area is dominated by marl/limestone alternations overlying the Aalenian
159 (*Marnes bleues* Formation) and from the early Callovian to the late Oxfordian
160 (*macrocephalus* to *bimmamatum* zones; *Calcaires argileux de Pamproux*, *Marnes de Velluire*,
161 *Pierre chauffante*, *Marnes gris-bleues à ammonites pyriteuses*, *Marnes grises à spongiares*,
162 *Marnes Schisteuses* and *Calcaires blancs de Fors* Formations; Cariou et al., 2006). The
163 Bajocian and Bathonian limestones are characterized by bioclast-rich facies (*Calcaires*
164 *ponctués de Saint-Maixent*, *Calcaires à silex* Formations; Cariou et al., 2006).

In the Montbron area, in the western part of the high-energy Central Platform (Figs 2A and 3), dolomite (*Dolomies de Montbron* Formation) and shallow carbonate facies (*Calcaires de Combe Brune*, *Calcaires de Saint-Sauveur*, *Calcaires de Vilhonneur*, *Calcaires crayeux à stromatolithes de Montbron*, *Calcaires oolithiques et coralliens de Garat* Formations; Foucher, 1986; Le Pochat et al., 1986) were deposited from the Bajocian to Oxfordian. The biostratigraphy of brachiopod faunas (Foucher, 1986) reveals a sedimentary gap during the early Callovian. The Aalenian deposits are characterized by clay and marl facies (*Argiles et marnes grises* Formation).

3. Material and methods

3.1. Sedimentology

This study is based on the detailed examination of 77 outcrop sections lying between the cities of Deauville and Montbron. Observations were completed with data from previous works carried out on 13 outcrop sections (Foucher, 1986; Dugué, 1989; Louail et al., 1989; Maire, 1983; Rioult et al., 1991) and 37 boreholes (Guyader et al., 1970; Bourgueil et al., 1971; Roger et al., 1979; Rioult and Doré, 1989; Ménillet et al., 1999 and from borehole data of the French Geological Survey avaible online http://infoterre.brgm.fr/, Fig. 1). Outcrop sections were logged in detail: lithology, texture (Dunham, 1962; Embry and Klovan, 1971; Insalaco, 1998), allochem content, and sedimentary structures were reported. A total of 268 thin sections were examined to determine the microfacies using a polarizing microscope. The proportion of facies components (bioclasts and non-bioclastic elements), texture, granulometry, grain sorting, and early cement types were characterized in each thin section. We followed the definition (1997) of James for photozoan and heterozoan grain associations. Photozoan grain association is rich in hermatypic corals, chlorophytes, benthic foraminifera and non-bioclastic components as ooids, peloids and aggregates. Heterozoan facies association displays abundant rhodophytes, molluscs, echinoderms and bryozoans.

Transitional facies designates grain associations in which neither heterozoan or photozoan producers are prevailing.

3.2. Sequence stratigraphy

Following Embry's definition (2009), outcrop sections and boreholes were interpreted in terms of sequence stratigraphy to establish a stratigraphic cross-section. In this sequence stratigraphy model, units are bounded either by a subaerial unconformity (SU) when the surface was exposed, or by a maximum regressive surface (MRS) when the surface was not exposed. Maximum regressive surfaces, also called transgressive surfaces (Van Wagoner et al., 1988) or flooding surfaces (Homewood et al., 1992), coincide with shifts in stacking patterns between shallowing-upward and deepening-upward trends, and correspond to the shallowest depositional environment recorded within a sequence (Embry, 2009). Maximum flooding surfaces (MFSs) mark a shift between deepening-upward and shallowing-upward trends, and correspond to the deepest facies encountered within a sequence. Subaerial unconformities or maximum regressive surfaces form sequence boundaries (SBs). Depositional sequences are composed of transgressive and regressive systems tracts (TSTs and RSTs). The transgressive systems tract is characterized by retrograding architectures, with more distal facies upward and the regressive systems tract is characterized by prograding architectures, with more proximal facies upward.

3.3. Decompacted depth, accommodation, subsidence, and tectonic subsidence calculation

Decompacted depth, also called total subsidence, corresponds to the thickness of sediments after decompaction (Steckler and Watts, 1978; Allen and Allen, 2005). Goldhammer (1997) demonstrates that, in mud-supported carbonates at least, compaction mainly occurs during shallow burial with 100 to 400 m overburden. Considering that all the formations of the Middle and Upper Jurassic were buried beneath more than 500 m of sedimentary deposits, the following compaction factors were used for the entire sedimentary series: 1.2 for grainstones,

1.5 for packstones, 2 for wackestones, 2.5 for mudstones, and 3 for marls (Hillgärtner and Strasser, 2003).

Accommodation space can be defined as the sum of the decompacted thickness of sediments and of paleodepth variations (Robin et al., 2000). For each facies, paleodepths were estimated based on the examination of sedimentary structures and fossil fauna (especially corals, Lathuilière et al., 2005). The classic wave zonation is used, considering depths of 10–15 m for the fair-weather wave base and more than 40 m for the storm wave base (Walker and James, 1992; Sahagian et al., 1996).

Subsidence corresponds to the increase in accommodation that is not due to eustasy, and so created by basement movements. It was calculated by subtracting eustasy variations from accommodation using the eustasy curve of Haq et al. (1987). The curve was placed in the European context of third-order sequences as defined by Hardenbol et al. (1998b). Although there is debate about this curve (Miller et al., 2005), it is the only eustasy curve precise enough to estimate eustatic variations at the time resolution used in this study, and so the only curve that can be used to reconstruct subsidence variations at the third-order sequence scale. Current criticisms of Haq's charts claim that it overestimates the amplitude of eustatic variations. In Cretaceous and Cenozoic times, Rowley et al., (2013), based on worldwide continental flooding, have identified large overestimations of the magnitude of variations and restored elevations of eustatic level. No reassement of the kind has yet been published for the Jurassic, but this could be a major bias in estimates of subsidence amplitudes. However, as the eustasy values substracted from the measured accommodation are all from the same chart (Haq, 1987), this misestimate may affect the amplitude but not the trend. We therefore focus mainly on the trend and variations between sites.

Tectonic subsidence is independent of the isostatic adjustment due to sediment deposition or paleodepth variations. It was calculated using the equation of Steckler and Watts (1978):

$$Y = S\left(\frac{\rho m - \rho b}{\rho m - \rho w}\right) - \Delta SL\left(\frac{\rho m}{\rho m - \rho w}\right) + Wd$$

Y is tectonic subsidence, S is decompacted sediment thickness, ρm is mantle density, ρb is mean sediment density, ρw is water density, ΔSL is eustasy variation, and Wd is paleodepth variation. Mean densities of 3.3 g.cm^{-3}, 2.6 g.cm^{-3}, and 2.4 g.cm^{-3} were used for mantle rocks, carbonates, and marls respectively.

Decompacted sediment thickness, accommodation, subsidence, and tectonic subsidence values were calculated for each third-order sequence top, corresponding to maximum regressive surfaces, and with an average time step of 0.8 My (Gradstein et al., 2012), to reconstruct sequence evolution over the Aalenian to Oxfordian time interval.

Uncertainties in accommodation, subsidence, and tectonic subsidence calculation may be due to uncertainties in the estimates of (1) the decompacted sediment thickness, (2) paleodepth, and (3) eustasy (for subsidence and tectonic subsidence only). Uncertainties in the decompacted sediment thickness depend on the chosen compaction law (Hillgärtner and Strasser, 2003). Uncertainties in paleodepth estimates are 60 m +/-15 m for the lower offshore, 30 m +/-10 m for the upper offshore, 10 m +/-5 m for the shoreface and the lagoon, and 0 m to 10 m above sea level for continental environments. A +/-5 m uncertainty was used to take into account reading precision of the curve by Hardenbol et al. (1998b). However, as explained above, the eustasy variations used (Haq, 1987) are probably overestimated and the subsidence and tectonic subsidence curve should not be regarded as absolute values but as trends.

4. Results

4.1. Sedimentary Facies

Thirty-one different facies were identified in the limestones under study. The facies were grouped into five positions within the downdip profile (Fig. 4): (1) the lower offshore for facies deposited below the storm wave base, (2) upper offshore for facies deposited between

265 the storm wave base and the fair-weather wave base, (3) shoal/barrier environments for wave-
266 and tide-dominated facies deposited above the fair-weather wave base, (4) lagoon to intertidal
267 environments for most mud-supported carbonate rocks deposited in calm and shallow
268 environments, and (5) backshore for facies deposited in sebkha, brackish, or continental
269 environments, above high tides. Observations and descriptions are summarized in Table 1.
270 Five synthetic sedimentological logs synthesize the succesion of Aalenian to Oxfordian
271 deposits in the Caen, Alençon, Poitiers, Saint-Maixent-l'École, and Montbron areas (Fig. 5).
272 *4.1.1. Lower offshore: facies F1a to F1f*
273 Claystones and marls with micritic limestone alternations (F1a-b-c, Fig. 6A-B), ferruginous
274 ooid wackestones to packstones (F1d, Fig. 6C-D), ferruginous oncoid floatstones (F1e, Fig.
275 6C-E-F), and glauconitic to phosphatic bioclastic wackestones to floatstones (F1f, Fig. 6G)
276 are present in the lower offshore. Fauna are composed of ammonites, belemnites, bivalves,
277 brachiopods, benthic and planktonic foraminifers, sponge spicules, ostracods, echinoderms,
278 dinoflagellates, serpulites, and gastropods. Bioturbation is frequent and trace fossils abundant
279 (*Chondrites, Thalassinoïdes, Walthonensis*; Dugué, 1989). Ferruginous oncoids of facies F1e
280 are composed of microstromatolitic iron mats dominated by filamentous bacteriae and fungi
281 living below the photic zone in dysaerobic waters (Préat et al., 2000). The very fine grain size,
282 the absence of sedimentary structures, the absence of scleractinian corals that are typical of
283 the euphotic zone, the abundant bioturbation, and the presence of ammonites and belemnites
284 indicate a very calm depositional environment, probably below the storm wave base (Pomar,
285 2001; Lathuilière et al., 2005).
286 *4.1.2. Upper offshore: facies F2a to F2f*
287 Mostly bioclastic limestones, intercalated with thin marl interbeds are present in the upper
288 offshore environments (Fig. 7A). Six facies were identified: (1) alternations of marl and
289 echinoderm/peloid packstones to grainstones (F2a, Fig. 7A-B), (2) alterning marls and

bivalve/brachiopod wackestones to packstones (F2b, Fig. 7C), (3) marl/ooid grainstone alternations (F2c), (4) sponge wackestones to floastones (F2d, Fig. 7D-E), (5) sheetstone to platestone facies with lamellar corals, and (6) sponge bioconstructions in marls (F2e-f, Fig. 7F). The dominant fauna is composed of echinoderms, bivalves, sponges, lamellar microsolenid corals, brachiopods, bryozoans, and foraminifers. It indicates normal oxygenation and salinity conditions. The dominance of lamellar microsolenid corals argues for an environment located within the photic zone. In the eastern Paris Basin, similar coral associations developed in paleodepths ranging between 20 m and 40 m during the Oxfordian (Lathuilière et al., 2005). The upper surface of the limestone beds is often bioturbated by vertical burrows filled in with the overlying clays. The accumulation of fragmented bivalve shells forming shell-graded layers (F2a-b), gutter casts (F2a-b-c, Fig. 7A), hummocky cross-stratification (HCS, F2b), and upturned sponges (F2c) suggests that sedimentation was under storm influence in the upper offshore between the storm wave base and the fair-weather wave base.

4.1.3. Shoreface: facies F3a to F3l

Twelve facies are distinguished in shoreface environments: (1) very fine peloidal grainstones (F3a, Fig. 8A), (2) superficial ooid grainstones (F3b), (3) bivalve grainstones to rudstones (F3c, Fig. 8B), (4) bioclastic peloidal grainstones (F3d, Figs 8C and 9A), (5) quartz bioclastic sands to sandstones (F3e, Fig. 9B), (6) sponge bioconstructions in bioclastic grainstones (F3f, Fig. 9C), (7) mixstone to domestone coral bioconstructions (*Isastrea*, *Thecosmilia*, Rioult et al., 1989) in oolitic grainstones (F3g), (8) echinoderm grainstones (F3h, Figs 8D and 9D), (9) bryozoan grainstones to rudstones (F3i, Fig. 8E), (10) ooid grainstones to sands (F3j, Figs 8F and 9E-F-G), (11) lithoclast-ooid grainstones to rudstones (F3k, Figs 8G and 9F), (12) lithoclast-oyster calcareous conglomerates (F3l, Figs 8H and 9H). The presence of grainstone to rudstone textures, common low-angle large-scale clinobeds (Fig. 9A), tabular to trough

315 cross bedding in dunes (Figs. 9B and G), erosive channels (Fig. 9A), wedges in clinobedded
316 oolitic grainstones (Fig. 9F), and herringbone cross bedding suggests a high-energy wave- or
317 tide-influenced environment located above the fair-weather wave base. This is congruent with
318 the mixstone to domestone texture of coral bioconstructions and with the occurrence of the
319 coral genera *Isastrea* and *Thecosmilia*, which characterize paleodepths between 20 m and 0 m
320 in the eastern Paris Basin during the Oxfordian (Lathuilière, 2005).
321 *4.1.4. Lagoon and intertidal environments: facies F4a to F4d*
322 Four facies are distinguished in : (1) coral bioconstructions (mixstones to domestones) in
323 micritic limestones (F4a), (2) bioclastic/peloid/quartz mudstones (F4b, Fig. 10A), (3)
324 pellet/peloid grainstone/packstones (F4c, Fig. 10B), and (4) oncoid-ooid rudstones to
325 packstones associated with grapstones and lithoclasts (F4d, Fig. 10C-D-E). In these mud-
326 dominated facies, the fauna is mainly composed of bivalves, corals, gastropods, and miliolids.
327 Brachiopods, bryozoans, and echinoderms occur in low numbers. From Argentan to the
328 Alençon area, these facies may be directly transgressive on the basement highs and alternate
329 with oolitic shoal deposits (Fig. 10F). The dominance of peloid to oncoid facies and the
330 presence of miliolids and well-preserved gastropods (especially nerineids) argue for protected
331 lagoonal environments. However, washover deposits in facies F4b are characteristic of events
332 of high-hydrodynamism (storms probably). Tangential cross bedding in dunes, and grain-
333 supported to mud-supported textures in facies F4c and F4d indicate variable hydrodynamic
334 conditions. Microbialites and microbial peloids are common in facies F4c and F4d (Fig. 10C).
335 Microstalactitic and meniscus cements also occur in both facies (Fig. 10D); they are
336 characteristic of cementation occurring in a vadose diagenetic environment. The local
337 occurrence of birdseyes (Fig. 10E) and of planar-bedding in facies F4c and F4d indicate that
338 they can form in intertidal environments.
339 *4.1.5 Supratidal to continental environments: facies F5a to F5c*

340 Three facies can be present in supratidal to continental environments: (1) dolomitic facies
341 (F5a, Fig. 10G), (2) lignite-rich facies (F5b), and (3) paleosoil layers (F5c). The dolomitic
342 facies (F5a, Fig. 10G), exclusively present at Montbron, includes stromatolites (Le Pochat et
343 al., 1986). It is characteristic of supratidal environments of high salinity or evaporation rates
344 present in sabkha environments. The lignite facies (F5b) consists of organic matter rich
345 deposits, of very fine grain size (silt), and displays characeae gyrogonites and ostracods
346 (Foucher, 1986) suggesting a very calm and protected brackish depositional environment.
347 Paleosoils (F5c) are described by Dugué (1989) and Ménillet et al. (1999) around Caen and
348 Argentan. They are composed of silts, clays, and quartz grains of about 0.1 mm diameter. The
349 occurrence of characeae gyrogonites and roots suggests environments of coastal plain deposits
350 (Dugué, 1989).

351 *4.2. Facies architecture and depositional sequences*

352 The spatial distribution and temporal evolution of the facies defined above is described below.
353 Twenty-two transgressive–regressive cycles were identified between the early Aalenian and
354 the late Oxfordian, whose maximum flooding surfaces are underlined by clays (Figs 5 and
355 11). Considering a time range of about 17 My for the entire interval (Gradstein et al., 2012), a
356 rough estimate of the average duration of each cycle comes to 0.8 My, which is close to the
357 duration range of third-order cycles as reported by several authors (Haq et al., 1987;
358 Hardenbol et al., 1998a; Schlager, 2004). Moreover, it corresponds to a multiple of 0.4 My,
359 which is the duration of Earth's eccentricity cycle, often considered as the controlling factor
360 for third-order sequences (e.g. Strasser et al., 2000).

361 These cycles are arranged into lower-order cycles from an Aalenian regressive hemicycle
362 topped by the maximum regressive surface Bj1 (Caen) or Bj3 (Montbron); a Bajocian–
363 Bathonian cycle topped by the maximum regressive surface Bt2 (Caen) of Bt4 (Montbron;

maximum flooding surface *zigzag*); and a Callovian–mid Oxfordian cycle until the maximum regressive surfaces Ox6 (maximum flooding surface *mariae* or *tenuiserratum*).

A constant characteristic of the western France platform throughout the Aalenian to Oxfordian interval is the presence of clayey lower offshore environments from La Flèche to Mirebeau, where sedimentation only occurred during sequences MJIV, MJVII , LJVI and LJVII (Figs 11 and 12).

4.2.1. Aalenian to early Bathonian: detrital to bioclastic ramp (sequences MJI to MJVIII)

This interval contains eight third-order sequences from Deauville to Montbron (Figs 5 and 11): MJI (Middle Jurassic I, *opalinum* Zone), MJII (*opalinum* to *murchisonae* Zones), MJIII (*bradforensis* to *concavum* zones), MJIV (*discites* and *laeviuscula* Zones), MJV (*propiquans* and early *humphriesianum* Zones), MJVI (late *humphriesianum* and *niortense* Zones), MJVII (*parkinsoni* Zone), and MJVIII (*zigzag/progracilis* Zones). The Aalenian to early Bathonian is characterized by ramp geometries that are either detritic (Aalenian) or bioclastic (echinoderms, bivalves, and sponge bioherms; Bajocian/early Bathonian; Figs 11 and 12A to D). The *zigzag* Zone maximum flooding surface is marked by an increase in paleodepth leading to large-scale retrogradations and maximum expansion of clayey facies in the study area (Figs 5, 11, and 12D).

Offshore environments dominate from Argentan to Deauville, where a ramp deepens northward. Sequence MJI consists in 1 meter of ferruginous oncoid facies (F1d, *Oolithe ferrugineuse aalénienne* Formation, *opalinum* Zone) and is capped with marly to silty limestones of sequences MJII to MJIV (facies F1c, *Malière* Formation, *murchisonae* to *concavum* Zones, Figs 5, 11, and 12A). Sequences MJV and MJVI are located in a condensed succession composed of glauconitic limestones (F1f, *Couche verte* Formation, *propiquans* Zone), oncoid ferruginous facies (F1e, *Conglomérat de Bayeux* Formation, *humphriesianum* zone), and ooid ferruginous facies (F1d, *Oolithe ferrugineuse de Bayeux* Formation,

389 *garantiana* to *niortense* Zones, Figs 5, 11, and 12B). Sequence MJVIII is marked by a mid
390 ramp rich in sponges that progrades northward (F2d, *Calcaires à spongiaires* Formation, Figs
391 5A, 11, and 12C). Around Caen, the maximum regressive surface between sequences MJVII
392 and MJVIII (Bj5) is characterized by upper offshore sponge facies sharply overlain by lower
393 offshore marl/limestone alternations of sequence MJVII (F1a-b, *Marnes de Port-en-Bessin*
394 Formation, Figs 5D, 11, and 12D).
395 Over the Aalenian to early Bathonian, the shallowest environments were located on
396 Ordovician basement highs, between Argentan and Le Mans. For the Aalenian, facies are
397 clastic sands with rare ammonites (*Graphoceras* sp. and *Graphoceras cornu*) characterizing
398 the *concavum* Zone (facies F3e-l, *Sables et graviers de Tessé* Formation, Figs 5B, 11, and
399 12A). Sequence MJIII is bounded at the top by a maximum regressive surface marked by a
400 perforated hardground with encrusting bivalves, also characterizing a sedimentary gap that
401 occurs during sequences IV to VI (Bj1, Figs 5, 11, and 12B). Over sequence MJVII, basement
402 highs are covered with oolitic sands to grainstones (F3j, *Oolithe de Vilaines-la-Carelle*
403 Formation, Figs 5B, 11, and 12C) that prograde toward Saumur. These shallow oolitic facies
404 were dated to the *niortense* and *parkinsoni* Zones based on ammonites *Pseudogarantiana* sp.
405 and *Parkinsonia cf parkinsoni* respectively. At the top of sequence MJVII, the maximum
406 regressive surface Bt5 is underlined by (1) a lignite layer attesting to emersion at Argentan
407 (French Geological Survey, http://infoterre.brgm.fr/) and (2) a perforated hardground
408 encrusted with oysters around Le Mans, which also marks a sedimentary gap of sequence
409 MJVIII (Juignet et al., 1989).
410 From Saumur to Poitiers, a ramp gently shallowed southward from lower offshore to
411 shoreface environments, dominated by echinoderms and bivalve mud-supported facies (F2a-b,
412 *Calcaires dolomitiques à bioclastiques de Poitiers*, *Calcaires graveleux de Poitiers*, and
413 *Calcaires à silex* Formations; Figs 5C, 11, and 12a to D). Maximum regressive surfaces are

414 marked by bioclastic to superficial ooid grainstones at Poitiers changing to micritic limestones
415 toward Saumur (Aa1 to Bt1; F3b-h, F2a-b, *Calcaires roux bioclastiques à oncolithes* and
416 *Calcaires graveleux de Poitiers* Formations; Figs 5 and 11). Sequence MJVI is condensed
417 from Mirebeau to Saint-Maixent-l'École.
418 Depositional environments deepen again towards Saint-Maixent-l'École and Ruffec, where
419 upper offshore bioclastic mud-supported facies to lower offshore marls and glauconitic
420 limestones were deposited (F2b, F1f, and F1b, *Calcaires ponctués de Saint-Maixent, Banc*
421 *pourri* and *Marnes bleues* Formations, Figs 5D, 11, and 12A to D).
422 Towards Ruffec then Montbron, the ramp became shallower during the Aalenian to early
423 Bajocian with the deposition of upper offshore detrital to bioclastic facies (sequences MJII to
424 MJV, Figs 11, 12A, and B). Paleodepth decreased abruptly from offshore to shoreface,
425 marking the platform edge around Montbron over sequences MJV to MJVIII. An oolitic shoal
426 protected lagoonal/supratidal environments where dolomite precipitated over the regressive
427 systems tracts of sequences MJV and MJVI (Fig. 11). During sequences MJVII and MJVIII,
428 the lagoon was filled by mud-supported facies. The maximum regressive surfaces Bj3 to Bj5
429 correspond to periods of maximum expansion of lagoon environments prograding to the
430 northwest during the deposition of regressive systems tracts. The maximum regressive surface
431 at the top of sequence MJVIII (sequence boundary Bt1) is marked by lignite, characterizing
432 subaerial exposure (F5b; Fig. 11; Foucher, 1986).

433 *4.2.2. Mid and late Bathonian: echinoderm/bryozoan ramp from Deauville to Le Mans, oolitic*
434 *platform at Montbron (sequences MJIX-X-XI).*

435 The middle to late Bathonian is composed of three third-order sequences: MJIX
436 (*subcontractus* to early *morrisi* Zones), MJX (late *morrisi* to *orbis* Zones), and MJXI (early
437 *discus* Zone). Maximum regressive surfaces (Bt2-3-4) are marked either by marine perforated
438 surfaces encrusted with bivalves in upper offshore and shoreface environments, or by
439 exposure surfaces with vadose cements, stromatolites, or lignite levels in shoal and lagoonal

environments (Figs 5A-B-E and 11). During sequences MJIX and MJX, an echinoderm-rich shallow ramp, prograding northwards, stretched from Argentan to Deauville (F3h, *Calcaires de Saint-Pierre-du-Mont* and *Calcaires de Ranville* Formations, Figs 5A, 11 and 12E). A protected lagoon composed of peloidal mudstones to packstones (F4b-c-d, *Calcaires de Valframbert* Formation, Figs 11 and 12E) developed between the basement highs from Argentan to Alençon. Basement highs were overlain by shallow shoreface and lagoonal facies during the Bathonian (Figs 11 and 12A; *Calcaires de Villedieu*, *Calcaires de Valframbert*, *Calcaire et oolithe ferrugineuse à Montlivaltia* Formations; Dassidat et al., 1982; Juignet et al., 1989, Ménillet et al., 1994 and 1997). The brachiopod fauna in the *Calcaires de Valframbert* Formation is composed of *Burmirhynchia turgida*, *Rhynchonelloidella elegantula*, and *Epithyris oxonica* that indicate a mid Bathonian age (*Subcontractus* to *Morrisi* Zones; sequence MJIX; Rioult and Fily, 1975; Rioult et al., 1991). The *Calcaire et oolithe ferrugineuse à Montlivaltia* Formation displays cephalopods (*Paroecotraustes waageni*, *Grossouvria bathonica*, *Homoeplanulites* sp., *Cosmoceras contrarium*, *Opis lorierei*, and *O. similis)* and brachiopods (*Rioultina triangularis* and *Avonothyris* sp.) indicating the early late Bathonian, *hodsoni* Zone (sequence MJX; Juignet et al., 1989; Le Gall et al., 1998). The fauna can be used to date the flooding of the basement highs to the mid and late Bathonian, *subcontractus* to *hodsoni* Zones (sequence MJIX and MJX). During sequence XI (*Discus* Zone), a flat and shallow bryozoan to bivalve-rich ramp stretched from Deauville to Le Mans (F3i-c; Figs 11 and 12F). Oolitic limestones prograde from Le Mans to La Flèche (Fig. 11).

For sequences MJIX and MJXI, a ramp shallowing southward developed between Poitiers and Saumur. Facies alternate between echinoderm to sponge wacke/packstones (sequences MJIX and MJXI; F2a-d; *Calcaires à silex* and *Calcaires graveleux de Poitiers* Formation) and prograding superficial ooid grainstones (sequence MJX and regressive systems tract of sequence MJXI; F3b; *Calcaires graveleux de Poitiers* Formation; Figs 5C-D, 11, and 12E).

Another ramp profile deepened southwards from Poitiers (shoreface to upper offshore) to Saint-Maixent-l'École (upper to lower offshore; Figs 11, 12E, and F). Around Montbron, shallow lagoon environments rich in peloids and oncoids (F3b-c-d, *Calcaires de Saint-Sauveur* and *Calcaires de Vilhonneur* Formations, Figs 5E, 11, and 12E-F) were edged by ooid/lithoclast wedges progading to the northwest over the mid to late Bathonian (F3j-k, *Calcaires de Combe Brune* Formation).

4.2.2. Callovian and early Oxfordian: clayey ramp (sequences MJXII-XIII-XIV-V and LJI-II)

The Callovian to early Oxfordian contains six third-order sequences: MJXII (*herveyi* and early *koegini* Zones), MJXIII (late *koegini* and *calloviense* Zones), MJXIV (*jason* and *coronatum* Zones), MJXV (*athleta* and *lamberti* Zones), LJI (*mariae* and early *cordatum* Zones), and LJII (Late *cordatum* Zone). Transgressive systems tracts are characterized by increasingly clayey sedimentation upward, with a gradual disappearance of carbonate beds. The upper reaches of regressive systems tracts are commonly marked by prograding sandy to carbonate deposits until maximum regressive surfaces, corresponding to marine surfaces (Cal1 to Cal4, Ox1), which can display encrusting bivalves and phosphate coatings (Cal4, Foucher 1986), or exposure surfaces, with early meniscus cements (Ox 1; *Sables ferrugineux de Varais* Formation; Figs 5 and 11). From Deauville to Le Mans, the study area is dominated by a flat clayey ramp (F1a-b-c; Figs 5A-B-C-D; 11 and 12G). From Mirebeau to Poitiers, a ramp progressively shallowed to upper offshore environments dominated by echinoderm to bivalve wackestones/packstones during Callovian sequences MJXII to MJXIV (F2a-b, *Pierre des Lourdines* and *Calcaires argileux de Pamproux* Formations, Figs 5C, 11, and 12G). Sequences MJXV and LJI are missing (gap of the *athleta* to *mariae* Zones) and sequence LJII is condensed in a less than 1 m-thick carbonate level in Poitiers. A ramp gradually deepened from Poitiers to Ruffec, and the paleodepth then abruptly shallowed at Montbron, with the development of a shallow platform lagoon protected by an oolitic shoal over sequence MJXIV

(F3j and F4b; *Calcaires Crayeux à Stromatolithes* de Montbron Formation; Figs 5E, 11, 12G). Brachiopod-based biostratigraphy indicates a gap for sequences MJII and MJXIII (Foucher, 1986), and sequences MJXV to LJI might be missing as well (Figs 5C-D-E and 11).

4.2.3. Middle to late Oxfordian: Coral/ooid platforms development (sequences LJIII-IV-V-VI-VII)

The mid to late Oxfordian interval is composed of five third-order sequences: LJIII (Early *plicatilis* Zone), LJIV (Late *plicatilis* Zone), LJV (*tenuiserratum* Zone), LJVI (*glosense* to early *serratum* Zones), and LJVII (late *serratum* to *rosenkranzi* Zones). Ooid/coral shallow platform geometries predominate, with very steep slopes (Figs 11 and 12H-I).

Transgressive systems tracts are characterized by major retrogradations from Deauville to Argentan, from La Flèche to Le Mans, and from Saint-Maixent l'École to Montbron. The maximum flooding surfaces are marked by the deposition of marl to mud-supported upper offshore facies over the entire study area. Regressive systems tracts are marked by major progradations of lagoonal to shoreface environments from Argentan to Deauville, from Le Mans to Saumur, and from Montbron to Saint-Maixent-l'École (e.g. *Calcaire oolithique de Lisieux* Formation, Fig. 11). Maximum regressive surfaces correspond to periods of maximum expansion of lagoonal and shoreface facies, and may be either marine (Ox4, Ox5 and Ox6) or emersive, with the occurrence of meniscus cements (Ox4, Argentan to Alençon) or soils (Ox6, Caen to Le Mans, Fig. 11 and 12I).

Sequence LJIII occurs only in the northern part of the study area, where it is composed of clayey offshore facies. Over sequence LJIV and LJV, a shallow platform stretches from Caen to Le Mans, where a 100 km-long lagoon developed (F4d and F4a; *Calcaires coralliens de Mortagne* and *Calcaires coralliens de la Ferté-Bernard* Formations; Figs 5A-B, 11, and 12H). An oolitic to coral barrier delimited the northern and southern lagoon (F3a-j, Figs 11 and 12H). During the regressive systems tract of sequence LJVI, cross-bedded sands prograded from Caen towards Deauville (F3e, *Sables de Glos* Formation, Fig. 11). They

516 change abruptly to lower offshore clays around Deauville (*Argiles de Villers* Formation, Fig.
517 11). These are overlain by the lagoon, mud-supported facies of sequence LJVII (F5c;
518 *Calcaires à Astrates* Formation; Figs, 5B, 11, 12I; Dugué, 1989; Ménillet, 1999).
519 During sequence LJV, facies changed suddenly from marls (*Marnes à spongiaires* Formation)
520 to fine peloid/echinoderm grainstones between Mirebeau and Poitiers (F3a-h; *Pierre grise de*
521 *Bonnillet* and *Calcaires crinoïdiques* Formations), and a ramp deepened from Poitiers to
522 Ruffec, where lower offshore facies dominated. Over sequences LJVI and LJVII, lower
523 offshore clayey environments predominate from Saumur to Ruffec (F1c; *Banc de pierre*
524 *sublithographique*, *Calcaires argileux et glauconieux de Mirebeau*, *Marnes grises à*
525 *spongiaires* Formations; Figs 5C, 11, and 12H-I). During the mid/late Oxfordian, the
526 Montbron area saw the emplacement of an ooid/peloidal barrier with coral bioconstructions
527 ahead of a calm lagoon where coral/peloidal mudstones accumulated (F3a-d-j, F4b, *Calcaires*
528 *oolithiques et coralliens de Garat* Formation, Figs 5E, 11, and 12H-I).
529 *4.3. Decompacted sedimentation, accommodation, subsidence, and tectonic subsidence*
530 - *Early to early mid Aalenian (sequences MJI and MJII).* This interval is characterized
531 by stable accommodation and near-zero decompacted sediment thickness rates (Figs 13 and
532 14). Notable decompacted accumulation (13 m/My) and subsidence rates (5 m/My) are only
533 present in the Poitiers area.
534 - *Late mid Aalenian to early Bajocian (sequences MJIII to MJV).* Accommodation and
535 decompacted sediment thickness rates for the entire interval range from 0 m/My in Argentan
536 to 15 m/My in Montbron (Fig. 13). A substantial accommodation rate is only recorded in
537 Poitiers for sequence MJIV (70 m/My, Fig. 14). This interval is marked by a tectonic uplift,
538 synchronous over the entire western France platform (Fig. 13).
539 - *Late Bajocian to late Bathonian (sequences MJVI to MJXI).* In this time interval,
540 decompacted sedimentation rates vary from 27 m/My in Poitiers to 46 m/My in Caen, and

accommodation rates vary from 27 m/My in Poitiers to 34 m/My in Argentan (Fig. 13). The highest accommodation rates are recorded for sequence MJXI, with values of 83 m/My in Montbron, 130 m/My in Caen and Poitiers, and 240 m/My in Argentan. Continuous subsidence and tectonic subsidence are recorded in the Argentan, Poitiers, and Montbron areas.

- *Early Callovian (sequence MJXII).* The Caen and Argentan areas show high rates of decompacted sedimentation (respectively 76 m/My and 65 m/My) and accommodation (104 m/My, Figs 13 and 14), whereas Poitiers and Montbron are characterized by decompacted sedimentation and accommodation rates of about zero. High positive subsidence and tectonic subsidence rates are recorded for Caen and Argentan, whereas negative tectonic subsidence rates characterized the Poitiers and Montbron areas (Fig. 13).

- *Late early Callovian to mid Oxfordian (sequences MJXIII to LJIV).* Over this interval, high decompacted sedimentation rates (respectively 51 m/My and 58 m/My) and accommodation rates (41 m/My and 46 m/My) are recorded in Caen and Argentan. A negative accommodation rate (-17 m/My) coupled with a high negative tectonic subsidence rate mark an uplift in Caen during sequence LJIV, following a period of relative stability (Figs 13 and 14). Stage 5 is characterized by near-zero rates of decompacted sedimentation, accommodation, and subsidence (Figs 13 and 14). Subsidence and tectonic subsidence curves display negative rates in Poitiers and Montbron over the entire interval. Only sequence MJXIV displays a different pattern in Montbron, with high decompacted sedimentation (154 m/My) and accommodation rates (163 m/My).

- *Late mid to late Oxfordian (sequences LJV to LJVII).* This last phase is characterized in Caen by high rates of decompacted sedimentation (109 m/My) and accommodation (124 m/My), which correlate with major tectonic subsidence (Figs 13 and 14). In Argentan, stage 6 exhibits low decompacted sedimentation and accommodation rates of 27 m/My and 34 m/My,

and steady tectonic subsidence. The Poitiers area recorded a very high accommodation rate over sequence LJV (192 m/My), contemporaneous with significant tectonic subsidence (Figs 13 and 14). During deposition of sequences LJVI and LJVII, a stable tectonic phase is recorded in Poitiers, where the decompacted sedimentation and accommodation rates are 34 m/My (Figs 13 and 14). Around Montbron, the decompacted sedimentation rate (67 m/My) and accommodation rate (67 m/My) might have been constant over the last stage, and the area was subsiding (Figs 13 and 14).

5. Discussion

5.1. Accomodation changes on the western France carbonate platform – Global and regional trends

Platform architecture and sedimentary dynamics change with time from Deauville to Montbron over the Mid Jurassic and the Oxfordian, raising questions about the factors controlling this evolution. Sedimentary sequences, systems tracts, and platform architectures depend directly on the ratio between accommodation space (A) and sedimentation rate (S); (Jervey, 1988; Schlager, 1993, 2005; Catuneanu et al., 2009). The A/S ratio controls the progradational, aggradational, or retrogradational geometries of sediments. Retrograding structures and facies that are more distal upward mark the transgressive systems tract, when the A/S ratio is higher than 1. Prograding structures and upwardly more proximal facies characterize the regressive system tract, when the A/S is lower than 1. Accommodation space is generated by changes in (1) global eustasy and/or (2) subsidence, the latter being associated with (3) isostatic adjustment due to sediment deposition or paleodepth variation, and with (4) tectonics. At local scale, tectonic subsidence can be explained by syn-sedimentary active faults. Sedimentation rate relates to (1) terrigenous input or to (2) in-situ carbonate production and its redistribution, which is largely influenced by environmental conditions (e.g. trophic conditions and seawater temperature).

591 Overall eustasy variations in European basins have been modeled by Hardenbol et al. (1998b)
592 and are presented in Figures 13 and 15. Changes in depth, decompacted sediment thickness
593 (observed total subsidence, Steckler and Watts, 1978; Alen and Alen, 2005), accommodation
594 (total subsidence +/- depth variation), subsidence, and tectonic subsidence (Steckler and
595 Watts, 1978; Fig. 13) were reconstructed in four key localities to discuss the factors
596 controlling sediment architectures (Caen, Argentan, Poitiers, and Montbron, Fig. 13). By
597 reconstructing long-distance depositional sequences and dating basement flooding it was
598 possible to reconstruct the ante-Aalenian topography and discuss its influence on platform
599 architecture.

600 *5.1.1. Eustasy as the major control on 3rd-order transgressive–regressive systems tracts*

601 The overall correlation between European third-order sequences and the 22 depositional
602 sequences along with their continuity over the entire western France platform suggests that
603 eustasy is the main factor affecting accommodation variations at the scale of third-order
604 sequences (Hardenbol et al., 1998a, Fig. 15). The maximum flooding surfaces identified were
605 also found in other European basins of similar ages at the biozone scale (Hardenbol et al.,
606 1998a). However, five third-order sequences described in other European basins were not
607 identified in the study area: two within the Bathonian deposits (*zigzag/progracilis* Zones
608 transition and *discus* subzone maximum flooding surfaces), two within the Callovian
609 succession (*koegini* and *lamberti* Zones maximum flooding surfaces), and one within the late
610 Oxfordian (*bimmamatum* Zone; Fig. 15; Hardenbol et al., 1998a). The absence of several
611 European basin sequences from western France can be explained by (1) non
612 deposition/preservation in proximal areas (hardgrounds and exposure surfaces), especially at
613 the Bathonian/Callovian boundary (Figs 5 and 11), and by (2) condensation in deep clay-
614 dominated environments, which is the case for Callovian and early Oxfordian sequences
615 (*koegini*, *lamberti* and *bimmamatum* Zones; Fig. 11).

However, there are significant differences in second-order transgressive–regressive cycles between European basins and the western France platform, but also within the western France platform (Figs 11 and 15). Lateral dissimilarities in sedimentation rate and carbonate production, and the sharp local depth variations recorded over the western France platform cannot have been under global or eustatic control and must be related to local tectonics (Fig. 11).

5.1.2.Tectonics contribution on sedimentation rate, carbonate platform architecture, growth, and demise

Several episodes of facies and platform architecture change are interpreted to be connected with tectonic activity over all or part of western France. The major tectonic uplift, associated with an accommodation rate of about zero, that occurred over the entire study area from the mid Aalenian to the early Bajocian (sequences MJIII to MJV, Fig. 13) corresponds to the Mid-Cimmerian Unconformity, a subtle deformation event identified all around the Paris Basin (Guillocheau et al., 2000; De Graciansky and Jacquin, 2003) and in Western Europe related to North Sea doming (Underhill and Partington, 1993). Eustatic rise between sequences MJIII and MJV was not sufficient to offset the loss of accommodation due to the uplift (Haq et al., 1987). The consequences were the very low sedimentation rates (0 to 15 m/My) and overall shallowing (Figs 11 and 13). Around Montbron, lagoon environments expanded northwards during the *humphriesianum* Zone, marking the regressive maxima of a second-order cycle, and oolitic wedges formed in Poitiers over sequences MJIV and MJV, (Figs 11 and 15). In Caen, uplift was active until the end of sequence MJVII (negative accommodation rate of -17 m/My, Fig. 14) and may have induced the shallowing trend marked by upper offshore sponge facies prograding northwards.

During the late Bajocian and the Bathonian, about 150 m of accommodation space was created, despite a global sea-level fall (Figs 13 and 14; Hardenbol et al., 1998b). This

641 indicates that the western France platform underwent a major phase of tectonic subsidence
642 (estimated at about 100 m considering a sea-level fall of 45 m; Fig. 13; Hardenbol et al.,
643 1998b). The accommodation generated by tectonics, coupled with the subsidence related to
644 sediment loading, made it possible for 100 to 150 m of decompacted carbonates to accumulate
645 (Fig. 13). Over sequences MJIX to MJXI, the Caen and Montbron shallow platforms
646 prograded northwards, indicating that carbonate production was sufficient to fill the
647 accommodation space generated by tectonic subsidence (Fig. 11). Significant variations in
648 decompacted sedimentation/accommodation rate were observed within sequence MJXI
649 between Falaise (decompacted sedimentation/accommodation rate about 36 m/My) and
650 Argentan (about 240 m/My; Gradstein et al., 2012; Figs 11 and 14). This implies a local
651 tectonic subsidence of about 40 m/My in the Argentan area, the remaining subsidence being
652 controlled by sediment loading. Argentan is bordered by three faults affecting the Mesozoic
653 series, which may have controlled this tectonic subsidence for the latest Bathonian: the
654 Montabard-Gouffern fault to the north (Ménillet et al., 1997; Gigot et al., 1999), the
655 Pommereux-Sentilly fault to the west, and the Sées fault to the southwest (Kuntz et al., 1989;
656 Fig.1). The Montabard-Gouffern fault displays a high subvertical dip and a vertical offset of
657 between 30 and 40 m. At its northwestern extremity, Bajocian to Bathonian limestones were
658 brought into contact with Triassic to Ordovician deposits, indicating Bathonian to post-
659 Bathonian activity (Gigot et al., 1999).
660 The early Callovian is marked by a sudden carbonate demise that is commonly explained by a
661 eustatic rise and a consequent extensive drowning event within the Paris Basin (Jacquin et al.,
662 1992, 1998; Jacquin and de Graciansky, 1998; Brigaud et al., 2014). The sudden
663 disappearance of carbonates in favor of clay sedimentation occurred from Deauville to Le
664 Mans during deposition of the early transgressive systems tract of sequence MJXII (Figs 11,
665 12G and 13). The progressive rise in the overall eustatic level, estimated at about 15 m, was

not sufficient to explain sudden shallowing of at least 40 m (Hardenbol et al., 1998b; Figs 11 and 13). From Deauville to Le Mans, the steep deepening resulting in carbonate demise for the earliest Callovian was triggered by prominent tectonic subsidence of an amplitude between at least 35 m in Argentan and 55 m in Caen (Fig. 13). The increased accommodation was then maintained through the Callovian and into the early Oxfordian due to a eustatic rise (Hardenbol et al., 1998b). Several reactivated basement faults affecting the Mesozoic series from Falaise to Alençon may have caused this tectonic subsidence: the Cordey-Ronai, Montabard-Gouffern, Merlerault, Courtomer, and Fresnay-sur-Sarthe faults (Fig. 1). The Merlerault and Courtomer faults display a vertical offset varying between 50 m and 130 m in the Mesozoic succession (Ménillet et al., 1997 and 1998). Northwards, the Cordey-Ronai and Montabard-Gouffern faults affect the Middle Jurassic series with a vertical offset of about 40 m (Ménillet et al., 1998).

In Montbron, the accommodation rate was zero for sequences MJXII and MJXIII over a period of eustatic rise (about +20 m, Figs 13 and 14, Hardenbol et al., 1998b). This implies an uplift, the amplitude of which is estimated at about 40 m, preceding emersion, which occurred during a second-order transgression in European basins, and accounting for the absence of sequences MJXII and MJXIII at Montbron (Fig. 11; Hardenbol et al., 1998a). This local tectonics implies that the sequence boundary between the two complete second-order cycles in western France corresponds to Bt4 in Montbron whereas it corresponds to Bt2 in Caen and Argentan (Figs 11 and 15). In Poitiers and Montbron, the uplift phase remained constant until the end of sequence LJIV (Middle Oxfordian, Fig. 13). The postulated lack of deposition of sequences MJXV to LJIV in Montbron was certainly due to emersion due to uplift. Over sequences LJII to LJIV, uplift in the Poitiers area controlled sedimentation despite global eustatic rise, leading to the non-deposition of sequences LJII and LJIII and to the shallowing-upward trend marked by the deposition of cross-bedded bioclastic grainstones during

691 sequence MJXIV (Figs 11 and 13). From Poitiers to Montbron, the maximum flooding
692 surface of the Callovian–Oxfordian cycle cannot be positioned in the *mariae* Zone as for the
693 Caen and Argentan areas or for European second-order cycles, but is located in the
694 *tenuiserratum* Zone (Figs 11 and 15).
695 In Argentan, the accommodation rate was zero for sequences LJII and LJIII over a period of
696 eustatic rise (about +15 m, Figs 13 and 14, Hardenbol et al., 1998b). This implies an uplift of
697 about 30 m, leading to the progradation of shoreface sands topped by an exposure surface
698 (*Roussier de Gacé* and *Sables ferrugineux de Vairais* Formations, Ox1, Figs 11 and 13). In
699 Caen, drastic shallowing from lower offshore to shoreface between sequences LJII and LJIV
700 during a period of eustatic rise (about +10 m, Hardenbol et al., 1998b) implies a major uplift,
701 of about 40 m (Fig. 13). This early/mid Oxfordian uplift made possible the growth of a
702 shallow carbonate platform prograding northwards during sequence LJIV. This carbonate
703 platform persisted until the end of the Oxfordian from Caen to Le Mans. However, the sharp
704 carbonate demise resulting in the deposition of lower offshore clays and in retrograding
705 environments southwards cannot have been the consequence of the eustatic rise alone (about
706 12 m, Hardenbol et al., 1998b) and must also have been due to intense tectonic subsidence
707 occurring in Deauville over sequences LJV and LVI (Figs 11 and 13). Deauville is separated
708 from Caen by the Viller-Reux fault which diplays a vertical offset of about 55 m and brought
709 Jurassic and Cretaceous series into contact (Fig. 1, Pareyn, 1970). This fault may have been
710 reactivated during the Late Jurassic, causing the major tectonic subsidence recorded in
711 Deauville. The deepening from shoreface to lower offshore around Poitiers during sequence
712 LJV, in a context of relative eustatic stability (+3 m Hardenbol et al., 1998b), and leading to
713 carbonate demise, was the consequence of sudden and intense tectonic subsidence. This event
714 may have been due to the late Oxfordian reactivation of the Lusignan fault: a 100 km-long
715 basement structure oriented NW–SE and affecting Jurassic series to the north of Poitiers

716 (Cariou and Joubert, 1989b). In Montbron, the increased accommodation due to gradual and
717 slow tectonic subsidence coupled with a global eustatic rise over sequences LJV to LJVII
718 (Hardenbol et al., 1998b, Fig. 13) accelerated sedimentation and led to the deposition of about
719 180 m of decompacted carbonates (Figs 11 and 13).

720 *5.2. Basement topography as a major control of paleodepth on the western France*
721 *carbonate platform*

722 The Jurassic platform of western France developed over a pre-structured bottom surface. This
723 includes basement rocks that are mostly Cambrian and Ordovician quartz sandstones,
724 displaying major paleotopographic changes that can be directly observed in the field (Juignet
725 et al., 1989; Ménillet et al., 1994; Cariou et al., 2006). Post-Variscan relief of the basement
726 has been partly lowered by the deposition of Liassic series, for example in the Montbron area
727 that is filled by about 250 m of Triassic to Liassic deposits (Roger et al., 1979). The
728 topography of the basement was reconstructed for the time interval under study from borehole
729 data with paleobathymetric interpretations (Fig. 12).

730 Between Argentan and Alençon, sequences MJI to MJVIII are not found overlying the
731 basement, indicating an emerged area from the early Aalenian to the mid Bathonian (Figs 11
732 and 12A to D). These areas were flooded over sequences MJI to MJIX, during which shallow
733 environments were essentially located on basement highs: from Argentan to Alençon and in
734 Poitiers (Fig. 12A to D). From sequence MJI to MJIX, deep platform environments (lower
735 offshore) were located in basement depressions in Caen and from Le Mans to Saumur (Fig.
736 12A to D).

737 Over the Aalenian to early Bathonian, the basement topography was the major factor
738 determining lateral variations of paleodepth, as shallow environments were located on
739 basement highs and deeper environments in basement depressions (Fig. 12A to E). From the
740 late Bathonian to late Oxfordian, the basement depressions were filled by sediments and

741 flattened, and the influence of the basement topography on bathymetries became negligible,
742 except from Le Mans to Saumur, where lower offshore environments persisted (Fig. 12F to I).
743 Local tectonic subsidence and uplifts changed basement topography through time as described
744 in part 4.1.2. However, tectonic movements were rather homogenous across western France
745 through the Aalenian to early Bathonian and the basement topography remained
746 approximately the same (Figs 12A to E and 13). From the late Bathonian to late Oxfordian,
747 local tectonic movements greatly modified the basement topography (Figs 12F to I and 13).

748 *5.3. Growth and demise of carbonate platforms in western Tethyan domain*

749 A bibliographic synthesis of sedimentation in western Tethyan domain was conducted and
750 coupled with our results to propose a model of sedimentary evolution and carbonate
751 production in Western Tethys from Aalenian to Oxfordien (see Table 2 for references and
752 Figure16 for maps).

753 Two periods of global carbonate platform growth were identified in Western Tethys in
754 France, England, Spain and Italy platforms during this period: one during Bajocian/Bathonian
755 and the subsequent during middle/late Oxfordian in France, England, Spain, and Italy
756 platforms. In shoreface environments, marked by facies with grainstone texture and cross-
757 bedding, photozoan facies are dominant and include abundant ooids, peloids, and hermatypic
758 corals (Fig. 17A). Heterozoan facies, characterized by the predominance of mollusk,
759 echinoderms and bryozoans (Fig. 17A), are rather found in micritic limestones and
760 limestone/marl alternations forming in offshore environments. However, shallow facies in
761 northern Germany and Scotich Cleveland basin are dominated by sandstones.

762 Two general period of low carbonate production occurred during the Aalenian and middle
763 Callovian to early Oxfordian intervals. The middle Callovian to early Oxfordian period is
764 marked by thick clayey accumulations in offshore environments. On the contrary, condensed
765 levels, often ferruginous, prevailed during the Aalenian, while thick marly deposits locally

766 formed in Switzerland, Germany and southern Poland. Shallow environments are marked by
767 crossbedded siliciclastic sands (Scotland, northern Germany, and northwestern France) or
768 heterozan to transitional carbonate grain associations (southern France), except in England
769 (London platform) where oolitic grainstones were deposited during the Aalenian. In low
770 latitude areas (Apennines and Apulia platforms in Italy, Morocco) no neat carbonate
771 production demises are recorded during the Aalenian and Callovian to early Oxfordian
772 intervals, which could be the consequence of more favorable environmental conditions for
773 carbonate growth induced by a drier climate, as suggested by Dera et al. (2009) for the early
774 Jurassic.

775 *5.4. A comprehensive model for western Tethyan carbonate platform growth and demise*

776 *5.4.1. High an low eccentricity cycles*

777 Martinez and Dera (2015) synthetized the evolution of $\delta^{13}C$ measured in well-preserved
778 belemnite rostra over the Jurassic in western European basins (Fig. 15). Changes in carbonate
779 production on western Tethyan platforms during the Middle Jurassic and Oxfordian correlates
780 with stable $\delta^{13}C$ values as long-term $\delta^{13}C$ maxima are synchronous with low carbonate
781 production rates (Aalenian and from middle Callovian to early Oxfordian) and long-term $\delta^{13}C$
782 minima correspond to periods of high carbonate production (Bajocian/Bathonian and from
783 middle to late Oxfordian). Martinez and Dera (2015) interpreted these long-term $\delta^{13}C$
784 variations as resulting from a 9.1 My eccentricity orbital cycle.

785 *5.4.2. Carbonate production during high-eccentricity intervals*

786 The late Bajocian-Bathonian and middle-late Oxfordian intervals are characterized by clay
787 fraction with small kaolinite amounts in the eastern Paris Basin (0-10%, Pellenard and
788 Deconinck, 2006; Brigaud et al., 2009). Due to relative low burial depth and temperatures that
789 never exceeded 50 °C in this area (Clauer et al., 2007), mineralogical clay associations can be

790 considered as detrital, which can be used as an environmental proxy (Debrabant et al., 1992;
791 Dera et al., 2009). High kaolinite content may indicate either intense chemical weathering of
792 kaolinite soils or reworking of ancient kaolinite-bearing rocks (Chamlet, 1989, Dera et al.,
793 2009), and low kaolinite amount in the Bajocian-Bathonian and middle-late Oxfordian
794 limestones may then characterize an arid climate. This is consistent with results of Ma et al.
795 (2011) who suggested that high eccentricity intervals induced a dry climate disturbed by short
796 episodes of intensive rainfalls and storms. Although these moosonal episodes intensified the
797 net transfer of nutrient, organic carbon and carbonates ions to the ocean, organic carbon burial
798 was prevented because of the prevailing dry climate and the efficient oxidizing conditions in
799 seawater (Fig. 17B; Martinez and Dera, 2015). This lead to (1) an enrichment of seawater in
800 ^{12}C and a consequent decrease of $\delta^{13}C$ values in the oceanic reservoir, and to (2) carbonate
801 sursaturation in epicontinental seas due to high evaporation (Martinez and Dera, 2015). This
802 model is consistent with the high carbonate production rate recorded in western Tethyan
803 epicontinental seas during the Bajocian/Bathonian and middle/ late Oxfordian intervals. The
804 ratio between photozoan and heterozoan associations is mainly controlled by seawater
805 temperature, trophic conditions, and bathymetry (Fig. 17A; James, 1997, Mutti and Hallock,
806 2003). Photozoan association development is favored by high seawater temperatures
807 (subtropical to tropical, >18°C) and low trophic resources (oligotrophic to mesotrophic), but
808 can also be found in temperate waters under oligotrophic conditions (Fig. 17A; Mutti and
809 Hallock, 2003). Heterozoan grain association dominates in warm waters (>18°C) under
810 eutrophic conditions or in cool waters (<18°C) whatever the trophic conditions. In western
811 Tethyan platforms, during the Bajocian/Bathonian and middle/late Oxfordian, photozoan
812 producers were distributed in shoreface environments, indicating prevailing olitrophic
813 conditions, whereas heterozoan producers are mainly present in offshore environments (Figs.
814 16 and 17B). Nevertheless, heterozoan producers can also be found locally in shallow wave to

tide-dominated environments, as in northwestern France during the Bathonian (Fig. 16). This could be induced by local changes in environmental conditions as an increase of trophic inputs or a decrease of seawater temperatures (e.g. Lécuyer et al., 2003).

5.4.3. Carbonate production during low-eccentricity intervals

During the Jurassic, low eccentricity intervals induced wet conditions, which promoted high weathering rates, nutrient inputs, productivity levels, and organic burial in the ocean, and led to an increase of $\delta^{13}C$ values (Martinez and Dera, 2015). This happened during the Aalenian and from the middle Callovian to early Oxfordian (Fig. 17B; Martinez and Dera, 2015). The high kaolinite ratio in the Paris Basin (> 20% of the clay mineralogical association; Pellenard and Deconinck, 2006; Brigaud et al., 2009), and vascular plant biomarkers used as a proxy for palaeoflora (Hautevelle et al., 2006) support enhanced weathering conditions under a humid climate during the middle Callovian to early Oxfordian. Moreover, organic-rich layers are found in Central Atlantic (Dromart et al., 2003) and in the western Tethyan domain (England, Kenig et al., 1994; Saudi Arabia, Carrigan et al., 1995) during the middle Callovian. The Aalenian clay mineralogical association is also dominated by kaolinite in the southern Paris Basin (Delavenna et al., 1989) and in England (Sellwood and Sladen, 1981). The presence of anoxic conditions at the sea bottom is evidenced in southern Poland by the presence of agglutinated foraminifera, but the association with organic-rich deposists is not obvious (Tyszka, 1994; Tyszka and Kaminski, 1995). It is likely that organic carbon was either (1) locked up but disseminated in shelf mudstones and therefore, is not readily identified, (2) stored in deep marine areas or (3) stored in terrestrial settings (Price, 2010). Clay contents and palaeoflora data, as well as evidences of prevailing anoxic conditions at the sea-floor during the Aalenian and from the middle Callovian to early Oxfordian are consistent with the hypothesis of a wet climate during low-eccentricity intervals leading to high nutrient inputs. Such an eutrophication of sea waters is noxious for photozoan carbonate producers and tends

840 to diminish the growth potential of carbonate platforms (Weissert and Mohr, 1996; Bartolini
841 et al., 1996; Bartolini et al., 1999; Bartolini and Cecca, 1999; Mutti and Hallock, 2003),
842 promoting siliciclastic sedimentation (Figs. 15, 16 and 17B). On the western France platform,
843 decompacted carbonate accumulation rate was over 60 m/My during the Bathonian and
844 middle/late Oxfordian but fell down under 20 m/My at the Aalenian and during the middle
845 Callovian/early Oxfordian interval. The mean biological carbonate content in marls varies
846 from 35% to 20% in the Callovian to early Oxfordian, the lowest values being recorded in the
847 *mariae* Zone (Dugué, 1989), which correlates with the $\delta^{13}C$ maxima (Martinez and Dera,
848 2015). Proximal deposits are sandstone or heterozoan to transitional grain associations, whose
849 development is favored by eutrophic conditions (Figs. 16 and 17B). Photozoan facies can
850 develop locally, probably due to local changes in trophic conditions or seawater temperatures
851 (e.g. London platform during the Aalenian). Low sedimentation rates (mainly between 0 and
852 10 m/My), the abundance of condensed ferruginous deposits and gaps during the Aalenian are
853 the consequence of a decrease of accommodation space related to a global uplift in Western
854 Europe. This event corresponds to the Mid-Cimmerian unconformity (Figs. 16 and 17B;
855 Underhill and Partington, 1993; Guillocheau et al., 2000; De Graciansky and Jacquin, 2003).
856 High clayey sedimentation rates during the middle Callovian to early Oxfordian, generally
857 between 20 and 50 m/My, was allowed by an increase in accommodation space both due to
858 (1) the global eustatic sea-level rise (Hardenbol et al., 1998b) and (2) increase of subsidence
859 rate (Fig. 17B). In western France, the demise of the carbonate platform initiated at the
860 Bathonian/Callovian boundary because of a sharp, local tectonic subsidence, but it persisted
861 in deeper and shallower environments until the middle Oxfordian due to (1) the eutrophic
862 conditions of neritic environments and to (2) the global eustatic sea level rise.

863 **6. Conclusions**

Thirty-one facies were characterized in Aalenian to Oxfordian formations of western France, deposited in lower offshore to backshore settings. Changes in platform geometry and facies were identified over a time interval of ~17 Ma (Aalenian to Oxfordian) and across a long distance (500 km). A high-resolution correlation scheme was realized at the ammonite biozone scale in a sequence stratigraphy framework. Twenty-two third-order depositional sequences have been defined. They are bounded by maximum regressive surfaces that are either marine (e.g. perforated hardgrounds encrusted with bivalves) or emersive (microstalactitic, meniscus, and dogtooth cements, lignite, paleosoils). Depositional sequences of the western France platform correlate at the ammonite biozone scale with the third-order sequences of European basins, indicating that eustasy is the major factor controlling third-order transgressive–regressive systems tracts (Hardenbol et al., 1998a). Topography of the Paleozoic basement controlled lateral depth variations until the mid Bathonian, resulting in the development of (1) shoreface environments from Argentan to Le Mans and in Poitiers and to (2) lower offshore environments in Caen and from La Flèche to Mirebeau. Evolution of tectonic subsidence was reconstructed in four key areas of western France: Caen, Argentan, Poitiers, and Montbron. A major uplift was identified to have occurred over the middle/late Aalenian and the early Bajocian. It corresponds to the Mid-Cimmerian Unconformity. Throughout the Middle Jurassic and Oxfordian, tectonics controlled sedimentation rate and platform architecture; it also triggered two major phases of carbonate growth and demise. Uplifts favoured low sedimentation rates (i.e. late Aalenian to early Bajocian), the occurrence of exposure surfaces and prograding systems, as observed around Montbron during the early to mid Callovian. Tectonic subsidence promoted high sedimentation rates, for example during the Bathonian over the entire western France platform (decompacted sedimentation rate about 70m/my) or during the mid/late Oxfordian around Montbron (decompacted sedimentation rate about 70m/my). The major carbonate production demise at the Bathonian/Callovian boundary

889 was triggered by sharp tectonic subsidence of about 35 m to 55 m, causing an increase in
890 paleodepths. In contrast, the development of the prograding mid-Oxfordian carbonate
891 platform in north-western France was made possible by the tectonic uplift that generated
892 shallow-water and favourable conditions for carbonate growth. A synthesis of sedimentation
893 on western Tethyan platforms was conducted. Two periods of high carbonate production
894 during the Bajocian/Bathonian and middle/late Oxfordian, with prevailing photozoan
895 producers in shallow-marine environments, are synchronous with high eccentricity intervals
896 marked by low $\delta^{13}C$ values (Martinez and Dera, 2015). Carbonate production was promoted
897 by dry climates disturbed by short episodes of intensive rainfalls and storms leading to (1)
898 high evaporation and carbonate sursaturation and (2) low trophic conditions. Both periods of
899 low carbonate production during the Aalenian and from the middle Callovian to early
900 Oxfordian are synchronous with low eccentricity intervals and high $\delta^{13}C$ values. This was
901 marked by a wet climate and the eutrophication of epicontinental seas that tend to diminish
902 growth potential of western Tethyan carbonate platforms. The uplift of the Aalenian
903 (corresponding to the Mid-Cimmerian unconformity) lead to the formation of sedimentation
904 hiatus and condensed levels, whereas the global eustatic sea-level rise of the Callovian-early
905 Oxfordian generated an important accommodation space and favored high sedimentation
906 rates.
907 The present work shows that the development of carbonate platforms in intracontinental
908 settings was influenced by multiple factors, each one exerting a precise control on
909 sedimentation. In particular, we highlitghted the control of basement topography on lateral
910 depth variations and the influence of local and regional tectonics on carbonate platform
911 architecture, even in intracontinental basins. Finally, climate evolution in western Tethys was
912 controlled by long-term eccentricity variations and can be related to the major stages of

913 carbonate platform growth and demise and largely influenced the producer types (photozoan
914 *versus* heterozoan).

915 **Acknowledgements**

916 This work is the result of collaborative project no PO4990 between Paris-Sud University and
917 the BRGM. This project was funded by the BRGM and by a doctoral PhD from the French
918 Ministry of Research and Higher Education. We are grateful to Philippe Blanc (Lithologie
919 Bourgogne) for the high-quality thin-sections and to Christophe Durlet and Philippe Courville
920 for the stratigraphy of Aalenian deposits of Orne.

921 **Figure captions**

922

923 **Fig. 1.** Location of the study outcrops, boreholes, and faults with presumed Mid to Late
924 Jurassic activity on a simplified geological map of western France.

925

926 **Fig. 2. A.** Global palaeogeographical map of the Callovian simplified from R. Blakey's maps
927 (http://cpgeosystems.com) **B.** Location of the study area on a palaeogeographical map of the
928 Western Tethys during the Callovian. **C.** Location of the study area during the Bathonian in a
929 paleogeographic reconstruction (modified from Brigaud et al., 2009; based on Enay and
930 Mangold, 1980; Ziegler, 1988; Thierry and Barrier, 2000; Hendry, 2002) **D.** Location of the
931 study area during the Oxfordian in a paleogeographic reconstruction (modified from Strasser et
932 al., 2015; based on Enay and Mangold, 1980; Ziegler, 1988; Thierry and Barrier, 2000).

933

934 **Fig. 3.** Schematic lithostratigraphic illustration of the north–south transect of the study area.
935 Biostratigraphic ammonite zonation from Gradstein et al. (2012). Standard European sequences
936 from Hardenbol et al. (1998a).

937

938 **Fig. 4.** Location of the Middle Jurassic to Oxfordian facies with allochem distribution on a
939 downdip profile from the lower offshore to backshore in the western Paris to northern
940 Aquitaine basins. The range of variation of the fair-weather wave base and storm-wave base
941 depths are estimated from Walker and James (1992), Lathuilière et al. (2005), and Sahagian
942 (1996).

943

944 **Fig. 5.** Synthetic sedimentological log with geological stages, ammonite biozones, and
945 biostratigraphic data (ammonites, brachiopods, and foraminifers), lithostratigraphic formations,

carbonate textures, depositional environments, third-order sequence stratigraphy and stratigraphic locations of outcrops and samples. The parts of the logs not observed in the field have been completed using boreholes and descriptions from the literature. **A.** Synthetic sedimentological log of the Caen region, completed from Rioult et al. (1989, 1991) and Maurizot et al., 2000). **B.** Synthetic sedimentological log of the Argentan to Alençon region, completed from Kuntz et al. (1989) and Moguedet et al. (1998). **C.** Synthetic log of the Poitiers region completed from Mourier et al. (1986) and Cariou and Joubert, (1989a). **D.** Synthetic log of the Saint-Maixent-l'École region, completed from Cariou et al. (2006). **E.** Synthetic log of the Montbron region, completed from Le Pochat et al. (1986).

Fig. 6. A. Clay/marl to marl/micritic limestone alternations – F1a-b-c – Port-en-Bessin (6) – *Marnes Port-en-Bessin* Formation, sequence MJVIII. **B.** Mudstone – F1c – Pierre Levée quarry (54) – *Banc de Pierre sublithographique* Formation, sequence LJVI. **C.** Historic Bajocian stratotype with ferruginous oncoids (On.), bivalves (Bi.), belemnites (Be.), stromatolites (Str.) and sponges (Sp.) – Sainte-Honorine-des-Pertes (5) – *Malière* Formation (F1c), *Couche verte* Formation (F1f), *Conglomérat de Bayeux* Formation (F1e), *Oolithe ferrugineuse de Bayeux* Formation (F1d), *Calcaire à spongiaires* Formation (F2d), sequences MJIV to MJVI. **D.** Ferruginous oolite (Oo.) wackestone with bivalves (Bi.) – F1d – Sainte-Honorine-des-Pertes (5) – *Oolithe ferrugineuse de Bayeux* Formation, sequence MJVI. **E.** Microbialites – F1e – Feuguerolles quarry (18) – *Conglomérat de Bayeux* Formation, sequence MJV. **F.** Ferruginous oncoid (On.) floatstone with belemnites (Be.) and bivalves (Bi.) – F1e – Feuguerolles quarry (18) – *Oolithe ferrugineuse aalénienne* Formation, sequence MJI. **G.** Glauconite (Gl.) wackestone with quartz (Qz), ferruginous ooids (Oo.), echinoderms (Ech.) and bivalves (Bi.) – F1f – Sainte-Honorine-des-Pertes (5) – *Couche verte* Formation, sequence MJIV.

971

972 **Fig. 7. A.** Marl/echinoderm limestone alternation with gutter clasts – F2a – Tracy-sur-Mer (7)
973 – *Calcaire de Saint-Pierre-du-Mont* Formation, sequence MJVIII. **B.** Echinoderm (Ech.)
974 packstone with peloids (Pe.) – F2a – Cintheaux quarry (20) – *Calcaire de Caen* Formation,
975 sequence MJVIII. **C.** Bivalve (Bi.) packstone – F2b – Moulin à Vent quarry (65) – *Calcaires*
976 *argileux de Pamproux* Formation, sequence MJXIII. **D.** Wackestone with sponge spicules
977 (Spi.) – F2d – Limalonges quarry (71) – *Calcaires à spongiaires et silex* Formation, sequence
978 MJX. **E.** Sponge (Sp.) limestone – F2d – Sainte-Honorine-des-Pertes (5) – *Calcaire à*
979 *spongiaires* Formation, sequence MJVI. **F.** Coral (boundstone) in marls – F2e – Belle-Eau
980 quarry (32) – *Caillasse de Belle-Eau* Formation, sequence MJXI.

981

982 **Fig. 8. A.** Very fine-grained peloidal (Pe.) grainstone with superficial ooids (Su. oo.),
983 foraminifers (Fo.), echinoderms (Ech.), and bivalves (Bi.) – F3a – Bonnillet quarry (55) –
984 *Pierre des Lourdines* Formation, sequence LJV. **B.** Bivalve (Bi.) and brachiopod (Br.)
985 grainstone – F3c – Villedieu-lès-Bailleul quarry (25) – *Calcaires de Villedieu* Formation,
986 sequence MJIX. **C.** Bioclastic peloidal (Pe.) grainstone with crinoids (Cr.), undifferentiated
987 echinoderms (Ech.), gastropods (Ga.), bivalves (Bi.), serpulites (Se.) and a well-developed
988 isopachous early cement (Iso. Ce.) – F3d – Belle-Eau quarry (32) – *Calcaires de Belle-Eau*
989 Formation, sequence MJX. **D.** Echinoderm (Ech.) grainstone with crinoids (Cr.) and bivalves
990 (Bi.) – F3h – Vierville-sur-Mer (3) – *Calcaires de Saint-Pierre-du-Mont* Formation, sequence
991 MJVIII. **E.** Bryozoan (Br.) rudstone – F3i – Luc-sur-Mer (10) – *Calcaires de Langrune*
992 Formation, sequence MJXI. **F.** Ooid (Oo.) sand with crinoids (Cr.) – F3j – Fay quarry (41) –
993 *Oolithe de Vilaines-la-Carelle* Formation, sequence MJVI. **G.** Lithoclast (Li.) rudstone with
994 bryozoans (Br.), echinoderms (Ech.), ooids (Oo.), peloids (Pe.), and microbial peloids (Mi.
995 Pe.) – F3k – Les Aucrais quarry (21) – *Calcaires de Bon-Mesnil* Formation, sequence MJIX.

H. Detritic conglomerate with quartz (Qz), lithoclasts (Li.), feldspaths (Fe.), and echinoderms (Ech.) – F3l – Fay quarry (41) – *Sables et graviers de Tessé* Formation, sequence MJIII.

Fig. 9. A. Channel and large-scale low-angle clinobeds – F3d – Belle-Eau quarry (32) – *Calcaires de Belle-Eau* Formation, sequences MJIX and MJX. **B.** Cross-bedding stratifications – F3e – Fay quarry (41) – *Sables et graviers de Tessé* Formation, sequence MJIII. **C.** Sponge bioherms on bryozoan rudstones – F3f and F3i – Saint-Aubin-sur-Mer (8) – *Caillasses de Basse-Ecarde* Formation, sequence MJXI. **D.** Trough cross-bedding stratifications with alternating fine and coarse levels in echinoderm grainstone – F3h – Creully quarry (12) – *Calcaires de Creully* Formation, sequence MJVIII. **E-F.** Wedge of clinobedded oolitic grainstone foresets – F3j and F3k – Combe Brune quarry (84) – *Calcaires de Combe Brune* Formation, sequences MJIX to MJXI. **G.** Trough cross-bedded oolitic grainstone – F3j – Cosses Noires quarry (85) – *Calcaires Vilhonneur* Formation, sequence MJX. **H.** Lithoclast-oyster rich conglomerate, probably storm deposit – F3l – Fay quarry (41) – *Sables et graviers de Tessé* Formation, sequence MJIII.

Fig 10. A. Bivalve (Bi.) mudstone – F4b – Garat Quarry (86) – *Calcaires coralliens et oolithiques de Garat* Formation, sequence MJXII. **B.** Peloidal (Pe.) and oolitic (Oo.) packstone to grainstone with quartz (Qz) – F4c – Boitron quarry (39) – *Calcaires de Valframbert* Formation, sequence MJIX. **C.** Lithoclast (Li.) and oncoid (On.) rudstone with miliolids (Mi.), ooids (Oo.), echinoderms (Ech.), and microbial peloids (Pe.) – F4d – Vilhonneur quarry (83) – *Calcaires de Vilhonneur* Formation, sequence MJIX. **D.** Lithoclast (Li.) grainstone with meniscus cements (M. Ce.) – F4d – Combre Brune quarry (84) – *Calcaires de Combe Brune* Formation, sequence MJXI. **E.** Birdseye in a lithoclast (Li.) grainstone with ooids (Oo.), peloids (Pe.), and foraminifers (Fo.) – F4d – Chez Trappe quarry

(87) – *Calcaires de Saint-Martial* Formation, sequence MJIX. **F.** Unconformity of Bathonian limestone on Brioverian flyschs – F4b, F4c and F3j – Boitron quarry (39) – *Calcaires de Valframbert* Formation, sequence MJIX. **G.** Dolomite formed in a presumably supratidal protected environment, as evidenced by the presence of stromatolites (Le Pochat et al., 1986) – F5a – La Rochebertier (82) – *Dolomies de Montbron* Formation, sequence MJV. **H.** Lithoclast (Li)/Ooid (Oo) grainstone with gastropods (Ga) displaying an erosive surface (Er. S.) with microbial encrusting (Mi. En.), fibrous (Fi. Ce.), microstalactitic (Mi. Ce.) and meniscus cements (Me. Ce.) – F3h – Les Aucrais quarry (21) – *Calcaires de Bon-Mesnil* Formation, maximum regressive surface Bt2.

Table 1. Position on the downdip profile, lithofacies, non-bioclastic and bioclastic components, sedimentary and biogenic structures, granulometry, sorting, and paleoenvironmental interpretations of the Middle Jurassic and Oxfordian rocks of western France.

Fig. 11. Correlation diagram of the Middle Jurassic and the Oxfordian in western France on a Deauville–Montbron transect. This illustration is composed of 61 outcrop sections studied in this work completed by previous descriptions of 13 outcrop sections (Foucher, 1986 – outcrops 72, 73, 88, and 90; Dugué, 1989 – outcrops 16, 17, and 40; Louail et al., 1989 – outcrop 47; Rioult et al., 1991 – outcrops 1, 4, 8, 10, 13, and 15) and 37 boreholes (Guyader et al., 1970 – borehole A; Bourgueil et al., 1971 – borehole AB; Roger et al., 1979 – borehole AK; Rioult and Doré, 1989 – borehole B; Ménillet et al., 1999 – boreole C; and http://infoterre.brgm.fr/ – remaining boreholes). Correlations are based on biostratigraphy (ammonite, brachiopod and foraminifer associations) and 22 recognized stratigraphic cycles (MJI to LJVII) delimited by sequence boundaries (Aa1 to Ox7).

Fig. 12. Facies distribution on carbonate architecture morphology of western France in nine successive steps from Aalenian to Oxfordian in a third-order sequence stratigraphy framework. Potentially active faults, Paleozoic basement and Lias deposits are represented to illustrate the multiple influences on carbonate platform/ramp morphology. **A.** Ramp geometry marked by the dominance of silty to sandy facies – sequences MJII and MJIII, Aalenian. **B.** Ramp geometry with condensed ferruginous facies in Caen and bioclastic upper offshore facies from Poitiers to Montbron – sequence MJV, Bajocian. **C.** Predominance of a storm dominated ramp with sponges, although oolitic facies develop in shallow environments (Montbron, Le Mans) – sequence MJVII, Bajocian. **D.** Bioclastic ramp rich in echinoderms – sequence MJVIII, Bathonian. **E.** Shallow ramp with echinoderm facies from Deauville to Le Mans, oolitic platform in Poitiers and Montbron – sequence MJX, Bathonian. **F.** Shallow ramp with bryozoan facies and sponge bioherms from Deauville to Le Mans, upper offshore bioclastic ramp in Poitiers, oolitic shallow platform in Montbron– sequence MJX, Bathonian. **G.** Lower offshore clayey ramp from Deauville to Mirebeau, bioclastic upper offshore in Poiters; lagoon protected by an oolitic shoal in Montbron – sequence MJXIV, Callovian. **H.** Shallow protected platforms in Argentan and Montbron, separated by clayey deposits in lower offshore environments – sequence LJV – Oxfordian. **I.** Emerged platform with soil horizon in Argentan separated from a shallow platform in Montbron by clayey deposits in lower offshore environments – sequence LJVI – Oxfordian.

Fig. 13. Synthetic chronostratigraphic diagram showing western France sequences, eustasism curve (Hardenbol et al., 1998b), bathymetry, decompacted sediment thickness, accommodation, subsidence, and tectonic subsidence curves in Caen/Deauville, Argentan, Poitiers, and Montbron.

Fig. 14. Accommodation rate for each western France sequence in Caen/Deauville, Argentan, Poitiers, and Montbron for the Aalenian to Oxfordian interval.

Fig. 15. Synthetic chronostratigraphic diagram from the Aalenian to Oxfordian showing western France sequences, second- and third-order European cycles/sequences (Hardenbol et al., 1998b), $\delta^{13}C$ isotopic curve (Martinez and Dera, 2015), and semi-quantitative estimation of decompacted carbonate production, carbonate producers, and depositional profile on the western France platform.

Fig. 16. Evolution of sedimentation and dominant carbonate producers during the Middle Jurassic and the Oxfordian in western Tethyan platforms represented in its regional palaeogeographical context. Data are compiled from our results (western France) and literature (France, Germany, Spain, England, Scotland, Poland, Italy, Switzerland, Morocco; see table 2 for references).

Fig. 17. A. Qualitative proportions of allochems in heterozoan and photozoan grain associations (modified from James, 1997), and schematic representation of the distribution of Photozoan– Heterozoan carbonates with respect to common temperature/nutrient gradient (modified from Mutti and Hallock, 2003). The width of the bars indicates estimated abundance of each association from 0–100%. **B.** Scheme of palaeoenvironmental, sedimentation and carbonate production changes linked to $\delta^{13}C$ isotopic signal (maxima and minima of eccentricity), local and global tectonism, and eustasy.

References

Ait Addi, A., Chafiki, D., 2013. Sedimentary evolution and palaeogeography of mid-Jurassic deposits of the Central High Atlas, Morocco. Journal of African Earth Sciences 84, 54-69.

Allen, A., Allen, J.R., 2005. Basin Analysis. Blackwell Science Publications, Oxford.

Allenbach, R. P., 2002. The ups and downs of "Tectonic Quiescence" – recognizing differential subsidence in the epicontinental sea of the Oxfordian in the Swiss Jura Mountains. Sedimentary Geology 150, 323-342.

Aurell, M., Robles, S., Bàdenas, B., Rosales, I., Quesada, S., Meléndez, G., Garcìa-Ramos, J.C., 2003. Transgressive-regressive cycles and Jurassic palaeogeography of northeast Iberia. Sedimentary Geology 162, 239-271.

Barron, A.J.M., Sumbler, M.G., Morigi, A.N., 1997. A revised lithostratigraphy for the Inferior Oolite Group (Middle Jurassic) of the Cotswolds, England. Proceedings of the Geologists' Association 108, 269-285.

Bartolini, A., Cecca, F., 1999. 20 My hiatus in the Jurassic of Umbria–Marche Apennines (Italy): carbonate crisis due to eutrophication. Comptes Rendus de l'Académie des Sciences Serie II Fascicule a–Sciences de la Terre et des Planètes 329, 587-595.

Biteau, J-J., Le Marrec, A., Le Vot, M., Masset, J.-M., 2006. The Aquitaine Basin. Petroleum Geoscience 12, 247-273.

Bosellini, A., Morsilli, M., Neri, C., 1999. Long-term stratigraphy of the Apulia platform margin (Upper Jurassic to Eocene, Gargano, southern Italy).

Bourgueil, B., Gabilly J., Lougnon J., 1971. Carte géologique de Chauvigny (1/50000), sondage n°1-10. Éditions du BRGM.

Branger, P., 1989. La marge nord-aquitaine et le seuil du Poitou au Bajocien : Stratigraphie séquentielle, évolution biosédimentaire et paléogéographie. PhD thesis, Université de Poitiers, 206 pp.

Brigaud, B., Durlet, C., Deconinck, J.-F., Vincent B., Pucéat E., Thierry J., Trouiller A., 2009. Facies and climate/environmental changes recorded on a carbonate ramp: A sedimentological and geochemical approach on Middle Jurassic carbonates. Sedimentary Geology 222, 181-206.

Brigaud, B., Vincent, B., Carpentier, C., Robin, C., Guillocheau, F., Yven, B., Huret, E., 2014. Growth and demise of the Jurassic carbonate platform in the intracratonic Paris Basin (France): Interplay of climate change, eustasy and tectonics. Marine and Petroleum Geology 63, 3-29.

Carcel, D., Colombié, C., Giraud, F., Courtinat, B., 2010. Tectonic and eustatic control on a mixed silicoclastic-carbonate platform during the Late Oxfordian-Kimmeridgian (La Rochelle platform, western France). Sedimentary Geology 223, 334-359.

Carrigan, W. J., Cole, C. A., Colling, E. L., and Jones, P. J., 1995. Geochemistry of the Upper Jurassic Tuwaiq Mountain and Hanifa Formation Petroleum Source Rocks of Eastern Saudi Arabia, in Katz B. J., editor, Petroleum Source Rocks. Springer, Berlin, 67-87.

Cariou, E., Gabilly, J., Coirier, B., 1973. Notice explicative de la carte géologique de Ruffec (1/50000). Éditions du BRGM, 10 pp.

Cariou, E., Joubert, J.-M., 1989a. Notice explicative de la carte géologique de Mirebeau-en-Poitou (1/50000). Éditions du BRGM, 36 pp.

Cariou, E., Joubert, J.-M., 1989b. Notice explicative de la carte géologique de Lusignan (1/50000). Éditions du BRGM, 41 pp.

1134 Cariou, E., Poncet, D., Colchen, M., Karnay, G., Becq-Giraudon, J.-F., Lemordant Y., Charnet F., Soyer, C.,
1135 Bouton, P., Branger, P., 2006. Notice explicative de la carte géologique de Saint-Maixent-l'École
1136 (1/50000). Éditions du BRGM, 132 pp.

1137 Carpentier, C., Lathuilière, B., Ferry, S., 2010. Sequential and climatic framework of the growth and demise of a
1138 carbonate platform: implications for the peritidal cycles (Late Jurassic, North-eastern France).
1139 Sedimentology 57, 985-1020.

1140 Catuneanu, O., Abreu, V., Bhattacharya, J.P., Blum, M.D., Dalrymple, R.W., Eriksson, P.G., Fielding, C.R.,
1141 Fisher, W.L., Galloway, W.E., Gibling, M.R., Giles, K.A., Holbrook, J.M., Jordan, R., Kendall, C.G.S.C.,
1142 Macurda, B., Martinsen, O.J., Miall, A.D., Neal, J.E., Nummedal, D., Pomar, L., Posamentier, H.W.,
1143 Pratt, B.R., Sarg, J.F., Shanley, K.W., Steel, R.J., Strasser, A., Tucker, M.E., Winker, C., 2009. Towards
1144 the standardization of sequence stratigraphy. Earth-science Reviews 92, 1-33.

1145 Chamley, H., 1989. Clay Sedimentology. Springer Verlag. 623 pp.

1146 Christ, N., Immenhauser, A., Amour, F., Mutti, M., Tomàs, S., Agar, S. M., Alway, R., Kabiri, L., 2012.
1147 Characterization and interpretation of discontinuity surfaces in a Jurassic ramp setting (High Atlas,
1148 Morocco). Sedimentology 59, 249-290.

1149 Collin, P.-Y., Courville, P., 2006. Sedimentation and palaeogeography of the eastern part of the Paris Basin
1150 (France) at the Middle-Upper Jurassic boundary. Comptes rendus Geoscience 338, 824-833.

1151 Cubaynes, R., Faure, P., Hantzpergue, P., Pelissie, T., Rey, J., 1989. La Jurassique du Quercy : unités
1152 lithostratigraphiques, stratigraphie et organisation séquentielle, évolution sédimentaire. Géologie de la
1153 France 3, 33-62.

1154 Dassidat, C., Doré, F., Kuntz, G., Le Gall, J., Rioult, M., Verron, G., 1982. Notice explicative de la carte
1155 géologique d'Alençon (1/50000). Éditions du BRGM, 70 pp.

1156 Debrabant, P., Chamley, H., Deconinck, J.-F., Récourt, P., Trouiller, A., 1992. Clay sedimentology, mineralogy
1157 and chemistry of Mesozoic sediments drilled in the Northern Paris Basin. Scientific Drilling 3, 138–152.

1158 de Graciansky, C., Jacquin, T., 2003. Évolution des structures et de la paléogéographie au passage Lias-Dogger
1159 dans le bassin de Paris d'après les données de la subsurface. Bulletin de la Société Géologique de France
1160 174, 3-17.

1161 Delavanna, M.F., Steinberg, M., Trauth, N., Holzapffel, T., 1989. Influence des cycles eustatiques et de la
1162 tectonique synsédimentaire sur la minéralogie du Lias et du Dogger du forage de Sancerre-Couy (Cher).
1163 Programme Géologie Profonde de la France. Comptes rendus de l'Académie des Sciences, Paris, II, 308,
1164 111-116.

1165 Dera, G., Pellenard, P., Neige, P., Deconinck, J.-F., Pucéat, E., Dommergues, J.-L., 2009. Distribution of clay
1166 minerals in Early Jurassic Peritethyan seas: palaeoclimatic significance inferred from multiproxy
1167 comparisons. Palaeogeography, Palaeoclimatology, Palaeoecology 271, 39-51.

1168 Dromart, G., Garcia, J.-P., Gaumet, F., Picard, S., Rousseau, M., Atrops, F., Lecuyer, C., Sheppard, S.M.F.,
1169 2003. Perturbation of the carbon cycle at the Middle/Late Jurassic transition: geological and geochemical
1170 evidence. American Journal of Science 303, 667-707.

1171 Dugué, O., 1989. Géodynamique d'une bordure de massifs anciens. La bordure occidentale du Bassin anglo-
1172 parisien au Callovo-Oxfordien. Pulsations épirogéniques et cycles eustatiques. PhD Thesis, Université de
1173 Caen, 593 pp.

1174 Dugué, O., 2007. Le massif armoricain dans l'évolution mésozoïque et cénozoïque du Nord-Ouest de l'Europe.
1175 Contrôles tectonique, eustatique et climatique d'un bassin intracratonique (Normandie, Mer de la Manche,
1176 France). Mémoire d'Habilitation à Diriger des Recherches. Université de Caen, 335 pp.

1177 Dunham, R.J., 1962. Classification of carbonate rocks according to depositional texture. Memoir of American
1178 Association of Petroleum Geologists 1, 108-121.

1179 Embry, A., 2009. Practical Sequence Stratigraphy. Canadian Society of Petroleum Geologists, 79 pp.

1180 Embry, A., and Klovan, J.E., 1971. A late Devonian reef tract on northeastern Banks Island, Northwest
1181 Territories. Bulletin of Canadian Petroleum Geologists 19, 730-781.

1182 Enay, R., Mangold, C., 1980. Synthèse paléogéographique du Jurassique français. Document du Laboratoire de
1183 Géologie de Lyon, Volume 5. Groupe Français d'Etude du Jurassique, 220 pp.

1184 Faugeras, P., 1988. Evolution de la plate-forme carbonatée est-aquitaine du Jurassique Moyen en Périgord.
1185 Stratigraphie, sédimentologie, paléogéographie. PhD thesis, Université de Poitiers, 200pp.

1186 Foucher, N., 1986. Géodynamique sédimentaire et évolution paléogéographique de la plate-forme nord-est
1187 aquitaine au Jurassique moyen (Charente, Dordogne), tome II : Planches. PhD Thesis, Université de
1188 Poitiers, 81 pp.

1189 Gabilly, J., Brillanceau, A., Cariou, E., Ducloux, J., Dupuis, J., Hantzpergue, P., Moreau, P., Santallier, P., Ters,
1190 M., Bourgueil, B., Brunet, M., Beden, M., Jehenne, Y., Dhoste, M., Viaud, J.M., 1978. Guide géologique
1191 régional, Poitou, Vendée, Charentes, 200 pp.

1192 Gigot, P., Dupret L., Le Gall, J., Coutard, J.P., Ozouf, J.C., Pay, T., Lecointe, A., Desloges, J., Deroin, J.P., 1999.
1193 Notice explicative de la feuille de Falaise (1/50000). Éditions du BRGM, 154 pp.

1194 Goldhammer, R.K., 1997. Compaction and decompaction algorithms for sedimentary carbonates. Journal of
1195 Sedimentary Research 67, 26-35.

1196 Gonnin, C., Cariou, E., Bassoullet, J.-P., Gabilly, J., Mourier, J.-P., 1994. La stratigraphie séquentielle, outil
1197 régional complémentaire de la biostratigraphie : application à la reconstitution de la dynamique
1198 sédimentaire des séries bathoniennes de surface du seuil du Poitou (France). Comptes rendus de
1199 l'Académie des Sciences de Paris 318, 235-241.

1200 Gonnin, C., Cariou, E., Branger, P., 1992. Les facteurs de contrôle de la sédimentation au début du Jurassique
1201 moyen sur le seuil du Poitou et ses abords. Comptes rendus de l'Académie des Sciences de Paris 315, 853-
1202 859.

1203 Gonnin, C., Cariou, E., Branger, P., 1993. Stratigraphie séquentielle des séries du Bajocien inférieur au Bathonien
1204 moyen du seuil du Poitou et de son versant aquitain (France). Comptes rendus de l'Académie des Sciences
1205 de Paris 316, 209-215.

1206 Gonzalez, R., Wetzel, A., 1996. Stratigraphy and paleogeography of the Hauptrogenstein and Klingnau
1207 Formations (middle Bajocian to late Bathonian), northern Switzerland. Eclogae Geologicae Helvetiae 89,
1208 695-720.

1209 Gradstein, F. M., Ogg, J. G., Schmitz, M. D., Ogg, G. M., eds., 2012. The geologic time scale 2012: Elsevier,
1210 1.144 pp.

1211 Guillocheau, F., Robin, C., Allemand, P., Bourquin, S., Brault, N., Dromart, G., Friedenberg, R., Garcia, J.-P.,
1212 Gaulier, J.-M., Gaumet, F., Grosdoy, B., Hanot, F., le Strat, P., Mettraux, M., Nalpas, T., Prija, C.,
1213 Rigollet, C., Serrano, O., Grandjean, G., 2000. Meso-Cenozoic geodynamic evolution of the Paris Basin:
1214 3D stratigraphic constraints. Geodinamica Acta 13, 189-245.

1215 Guyader J., Pareyn, C., Viallefond, L., 1970. Carte géologique du Havre (1/50000), sondage 496. Éditions du
1216 BRGM.

1217 Hamon, Y., Merzeraud, G., 2008. Facies architecture and cyclicity in a mosaic carbonate platform: effects of
1218 fault-block tectonics (Lower Lias, Causses platform, south-east France). Sedimentology 55, 155-178.

1219 Haq, B.U., Hardenbol, J., Vail, P.R., 1987. Chronology of fluctuating sea levels since the Triassic. Science 235,
1220 1156-1167.

1221 Hardenbol, J., Thierry, J., Farley, M. B., Jacquin, T., De Graciansky, P.- C., Vail, P. R., 1998a. Jurassic sequence
1222 chronostratigraphy – chart 6. in De Graciansky P.- C., Hardenbol J., Jacquin T., Vail P. R eds. Mesozoic
1223 and Cenozoic Sequence Stratigraphy of European Basins. SEPM Special Publication 60, 3-15.

1224 Hardenbol, J., Thierry, J., Farley, M. B., Jacquin, T., De Graciansky, P.- C., Vail, P. R., 1998b. Mesozoic and
1225 Cenozoic sequence chronostratigraphy – chart 1. in De Graciansky P.- C., Hardenbol J., Jacquin T., Vail
1226 P. R eds. Mesozoic and Cenozoic Sequence Stratigraphy of European Basins. SEPM Special Publication
1227 60, 3-15.

1228 Hautevelle, Y., Michels, R., Malartre, F., Trouiller, A., 2006. Vascular plant biomarkers as proxies for
1229 palaeoflora and palaeoclimatic changes at the Dogger/Malm transition of the Paris Basin (France).
1230 Organic Geochemistry 37, 610-625

1231 Helm, C., Schülke, I., 1998. A Coral-microbialite Patch Reef from the Late Jurassic (*florigemma*-Banck,
1232 Oxfordian) of NW Germany (Süntel Mountains). Facies 39, 75-104..

1233 Hendry, J.-P., 2002. Geochemical trends and palaeohydrological significance of shallow burial calcite and
1234 ankerite cements in Middle Jurassic strata on the East Midlands Shelf (onshore UK). Sedimentary
1235 Geology 151, 149-176.

1236 Hesselbo, S.P., 2008. Sequence stratigraphy and inferred relative sea-level change from the onshore British
1237 Jurassic. Proceedings of the Geologists' Association 119, 19-34.

1238 Hillgärtner, H., Strasser, A., 2003. Quantification of high-frequency sea-level fluctuations in shallow-water
1239 carbonates: an example from the Berriasian-Valanginian (French Jura). Palaeogeography,
1240 Palaeoclimatology, Palaeoecology 200, 43-63.

1241 Homewood, P., Guillocheau, F., Eschard, R., Cross, T.A., 1992. Corrélations haute résolution et stratigraphie
1242 génétique: une démarche intégrée. Bulletin du Centre de Recherche et d'Exploration Production Elf
1243 Aquitaine 16, 357–381.

1244 Iannace, A., Capuano, M., Galluccio, L., 2011. « Dolomites and dolomites » in Mesozoic platform carbonates of
1245 the Southern Apennines : geometric distribution petrography and geochemistry. Palaeogeography,
1246 Palaeoclimatology, Palaeoecology 310, 324-339.

1247 Insalaco, E., 1998. The descriptive nomenclature and classification of growth fabrics in fossil scleractinian reefs.
1248 Sedimentary Geology 118, 159-186.

1249 Jacquin, T., Dardeau, G., Durlet, C., de Graciansky, C., Hantzpergue, P., 1998. The North Sea cycle: an
1250 overview of 2nd-order transgressive/regressive facies cycles in Western Europe. In: de Graciansky, P.-C.,
1251 Hardenbol, J., Jacquin, T., Vail, P.R. (Eds.), Mesozoic and Cenozoic Sequence Stratigraphy of European
1252 Basins, 445-466.

1253 Jacquin, T., Garcia, J.-P., Ponsot, C., Thierry, J., Vail, P.R., 1992. Séquence de dépôt et cycles
1254 régressif/transgressifs en domaine marin carbonaté: exemple du Dogger du Bassin de Paris. Comptes
1255 Rendus de l'Académie des Sciences, Série II, Fascicule a – Sciences de la Terre et des Planètes 315, 353-
1256 362.

1257 Jacquin, T., de Graciansky, P.-C., 1998. Transgressive/Regressive (Second order) facies cycles: the effects of
1258 tectono-eustasy. In: De Graciansky, P.-C., Hardenbol, J., Jacquin, T., Vail, P.-R. (Eds.), Mesozoic and
1259 Cenozoic Sequence Stratigraphy of European Basins, SEPM Special Publication, 31-42.

1260 James, N.P., 1997. The cool-water carbonate depositional realm. Cool-water Carbonates (Eds N. P. James and
1261 J.A.D. Clarke). SEPM Special Publication 56, 20 pp.

1262 Jervey, M., T., 1988. Quantitative modeling of siliciclastic rock sequences and their seismic expression. SEPM
1263 Special Publication 42, 47-69.

1264 Juignet, P., Lebert, A., Le Gall, J., 1984. Notice de la carte géologique de Fresnay-sur-Sarthe (1/50000). Éditions
1265 du BRGM, 56 pp.

1266 Juignet, P., Lebert, A., Le Gall, J., Mary, G., 1989. Notice de la carte géologique de Beaumont-sur-Sarthe
1267 (1/50000). Éditions du BRGM, 63 pp.

1268 Kenig, F., Hayes, J. M., Popp, B. N., and Summons, R. E., 1994. Isotopic biochemistry of the Oxford Clay
1269 Formation (Jurassic), UK, London. Journal of the Geological Society 151, 139-152.

1270 Kuntz, G., Ménillet, F., Le Gall, J., Rioult, M., 1989. Notice explicative de la carte géologique d'Argentan
1271 (1/50000). Éditions du BRGM, 99 pp.

1272 Lathuilière, B., Gaillard, C., Habrant, N., Bodeur, Y., Boullier, A., Enay, R., Hanzo, M., Marchand, D., Thierry,
1273 J., Werner, W., 2005. Coral zonation of an Oxfordian reef tract in the northern French Jura. Facies 50,
1274 545-559.

1275 Lécuyer, C., Picard, S., Garcia, J.-P., M. F. Sheppard, S., Grandjean, P., Dromart, G., 2003. Thermal evolution of
1276 Tethyan surface waters during the Middle-Late Jurassic: Evidence from $\delta^{18}O$ values of marine fish teeth.
1277 Paleoceanography 18, 1076.

1278 Lenoir, F., 2012. Faciès, géométries et déformations du Sud-Ouest du bassin de Paris : un domaine faiblement
1279 subsident, transition avec le bassin d'Aquitaine. PhD thesis, Université de Rennes, 371 pp.

1280 Le Gall, J., Maurizot, P., Lautridou, J.P., Giordano, R., Gaillard, C., 1998. Notice explicative de la carte
1281 géologique de Sillé-le-Guillaume (1/50000). Éditions du BRGM, 123 pp.

1282 Le Pochat, G., Floc'h, J.-P., Platel, J.-P., Recoing, M., 1986. Notice explicative de la carte géologique de
1283 Montbron (1/50000). Éditions du BRGM, 48 pp.

1284 Léonide, P., Floquet, M., Villier, L., 2007. Interaction of tectonics, eustasy, climate and carbonate production on
1285 the sedimentary evolution of an early/middle Jurassic extensional basin (Southern Provence Sub-basin,
1286 SE France). Basin Research 19, 125-152.

1287 Lorenz, J., 1992. Le Dogger du Berry, contribution à la connaissance des plate-formes carbonatées européennes
1288 du Jurassique. Éditions du BRGM, 397 pp.

1289 Louail, J., Morzadec, P., Le Hérissé A., Brossé R., Moguedet G., Etienne H., 1989. Notice explicative de la carte
1290 géologique de La Flèche (1/50000). Éditions du BRGM, 38 pp.

1291 Luczynski, P., 2002. Depostional evolution of the Middle Jurassic carbonate sediments in the High-Tatric
1292 succession, Tatra Mountains, Western Carpathians, Poland.

1293 Maire, P., 1983. Le Jurassique supérieur charentais : plate-forme carbonatée et faciès de bassin, stratigraphie,
1294 sédimentologie, paléogéographie, tome II – planches. PhD Thesis, Université de Poitiers, 131 pp.

1295 Ma W., Tian J., Li Q., Wang P., 2011. Simulation of long eccentricity (400-kyr) cycle in ocean carbon reservoir
1296 during the Miocene Climate Optimum: Weathering and nutrient response to orbital change. Geophysical
1297 Research Letters 38, L10701.

1298 Martinez, M., Dera, G., 2015. Orbital pacing of carbon fluxes by a ~9-My eccentricity cycle during the
1299 Mesozoic. Proceedings of the National Academy of Sciences 112, 12604-12609.

1300 Matyszkiewicz, J., Felisiak, I., 1992. Microfacies and Diagenesis of an Upper Oxfordian Carbonate Buildup in
1301 Mydlnika (Cracow Area, Southern Poland). Facies 27, 179-190.

1302 Maurizot, P., Auffret, J.-P., Baize S., Deroin, J.-P., Dugué, O., Fily, G., Le Gall, J., Leliepault, F., Mazenc, B.,
1303 Pellerin, J., 2000. Notice explicative de la carte géologique de Bayeux-Courseulles-sur-Mer (1/50000).
1304 Editions du BRGM, 151 pp.

1305 Maxwell, E.E., Fernandez, M.S., Schoch, R.R., 2012. First Diagnostic Reptile Remains from the Aalenian
1306 (Middle Jurassic): A new Ichthyosaur from Southwestern Germany. Plos one 7, 1-13.

1307 Mégnien, C., Mégnien, F., 1980. Synthèse géologique du Bassin de Paris. BRGM.

1308 Ménillet, F., Bourdillon, C., Fauconnier, D., Houari, A., Langevin, C., Hérard, B., Béguin, P., 1999. Notice
1309 explicative de la carte géologique de Livarot (1/50000). Éditions du BRGM, 98 pp.

1310 Ménillet, F., Gérard, J., Hérard, B., Langevin, C., Lemoine, B., Leturcq, T., Pellerin, J., Quesnel, F., 1997.
1311 Notice explicative de la carte géologique de Sées (1/50000). Éditions du BRGM, 103 pp.

1312 Ménillet, F., Lebret, P., Béguin, P., Charnet, F., Hérard, B., Lemoine, B., Perron, C., 1998. Notice explicative de
1313 la carte géologique de l'Aigle (1/50000). Éditions du BRGM, 114 pp.

1314 Ménillet, F., Rioult, M., Havlicek, P., Lecointe, A., Monciardini, C., Pascaud, P., 1994. Notice explicative de la
1315 carte géologique de Vimoutiers (1/50000). Editions du BRGM, 91 pp.

1316 Merino-Tomé, Ó., Porta, G.D., Kenter, J.A.M., Verwer, K., Harris, P., Adams, E.W., Playton, T.E.D.,
1317 Corrochano, D., 2012. Sequence development in an isolated carbonate platform (Lower Jurassic, Djebel
1318 Bou Dahar, high Atlas, Morocco): influence of tectonics, eustacy and carbonate production.
1319 Sedimentology 59, 118-155.

1320 Miller, K. G., Kominz, M. A., Browning, J., V., Wright, J., D., Mountain, G., S., Katz, M., E., Sugarman, P., J.,
1321 Cramer, B., S., Christie-Blick, N., Pekar, S., F., 2005. The Phanerozoic Record of Global Sea-Level
1322 Change, Science 310, 1293-1298.

1323 Moguedet, G., Charnet, F., Gresselin, F., Lemoine, B., 1998. Notice explicative de la carte géologique de
1324 Mortagne-au -Perche (1/50000). Éditions du BRGM, 87 pp.Morettini, E., Santantonio, M., Bartolini, A.,
1325 Cecca, F., Baumgartner, P.O., Hunziker, J.C., 2002. Carbon isotope stratigraphy and carbonate
1326 production during the Early-Middle Jurassic : examples from the Umbria-Marche-Sabina Apennines
1327 (central Italy). Palaeogeography, Palaeoclimatology, Palaeoecology 184, 251-273.

1328 Mourier, J.-P., 1983. Le versant parisien du Seuil du Poitou de l'Hettangien au Bathonien. Stratigraphie,
1329 Sédimentologie, Caractères paléontologiques, Paléogéographie. Université de Poitiers, 191 pp.

1330 Mourier, J.-P., Gabilly, J., Platel, J.-P., 1986. Notice explicative de la carte géologique de Poitiers (1/50000).
1331 Éditions du BRGM, 47 pp.

1332 Mutti, M., Hallock, P., 2003. Carbonate systems along nutrient and temperature gradients: some
1333 sedimentological and geochemical constraints. International Journal of Earth Sciences 92, 465-475.

1334 Ohmert, W., 1994. The *frechi* horizon (Humphriesianum Zone, Lower Bajocian) from the Oberrhein (South
1335 West Germany). Geobios 17, 359-367.

1336 Pareyn, C., 1970. Notice explicative de la carte géologique de Lisieux (1/50000). Éditions du BRGM, 14 pp.

1337 Pellenard, P., Deconinck, J.-F., 2006. Mineralogical variability of Callovo-Oxfordian clays from the Paris Basin
1338 and the Subalpine Basin. Geomaterials (Mineralogy) 338, 854-966.

1339 Pierre, A., Durlet, C., Razin, P., Chellai, E.H., 2010. Spatial and temporal distribution of ooids along a Jurassic
1340 carbonate ramp: Amellago outcrop transect, High-Atlas, Morocco. Geological Society, Special
1341 publication 326, 65-88.

1342 Pittet, B., Strasser, A., 1997. Long-distance correlations by sequence stratigraphy and cyclostratigraphy:
1343 examples and implications (Oxfordian from Swiss jura, Spain, and Normandy). Geol Rundsch 86, 852-
1344 874.

1345 Pittet, B., Strasser, A., Mattioli, E., 2000. Depositional sequences in deep-shelf environements: a response to sea-
1346 level changes and shallow-platform carbonate productivity (Oxfordian, Germany and Spain). Journal of
1347 Sedimentary Geology 70, 392-407.

1348 Pomar, L., 2001. Types of carbonate platforms: a genetic approach. Basin Research 13, 313-334.

1349 Préat, A., Mamet, B., De Ridder, C., Boulvain, F., Gillan, D., 2000. Iron bacterial and fungal mats, Bajocian
1350 stratotype (Mid-Jurassic, northern Normandy, France). Sedimentary Geology 137, 107-126.

1351 Préat, A., Morano, S., Loreau, J.-P., Durlet, C., Mamet, B., 2006. Petrography and biosedimentology of the
1352 Rosse Ammonitico Veronese (middle-upper Jurassic, north-eastern Italy). Facies 52, 265-278.

1353 Price, 2010. Carbon-isotope stratigraphy and temperature change during the Early-Middle Jurassic (Toarcian-
1354 Aalenian), Raasay, Scotland, UK. Palaeogeography, Palaeoclimatology, Palaeoecology 285, 255-263.

1355 Pucéat, E., Joachimski, M.M., Bouilloux, A., Monna, F., Bonin, A., Motreuil, S., Morinière, P., Hénard, S.,
1356 Mourin, J., Dera, G., Quesne, D., 2010. Revised phosphate-water fractionation equation reassessing
1357 paleotemperatures derived from biogenic apatite. Earth and Planetary Science Letters 298, 135-142.

1358 Reolid, M., M., J.M., Löser, H., Navarro, V., Ruiz-Ortiz, P.A., 2009. Coral biostromes of the Middle Jurassic
1359 from the Subbetic (Betic Cordillera, southern Spain): facies, coral taxonomy, taphonomy, and
1360 palaeoecology. Facies 55, 575-593.

1361 Rioult, M., Coutard, J.-P., Helluin, M., Larsonneur, C., Pellerin, J., 1989. Notice explicative de la carte
1362 géologique de Caen (1/50000). Éditions du BRGM, 104 pp.

1363 Rioult, M., Doré, F., 1989. Carte géologique de Caen (1/50000), sondage Touffreville n°1 (6-6). Éditions du
1364 BRGM.

1365 Rioult, M., Dugué, O., Fily, G., Juignet, P., 1992. Regards nouveaux sur le Jurassique normand. Bulletin
1366 d'information géologique du bassin de Paris 29, 7-44.

1367 Rioult, M., Dugué, O., Jan du Chêne, R., Ponsot, C., Fily, G., Moron, J. M., Vai,l P. R., 1991. Outcrop sequence
1368 stratigraphy of the Anglo-Paris Basin Middle to Upper Jurassic (Normandy, Maine, Dorset). Bulletin
1369 Centres Recherche Exploration-Production Elf Aquitaine 15, 1-194.

1370 Rioult, M., Fily, G., 1975. Discontinuités de sédimentation et unités lithostratigraphiques dans le Jurassique de
1371 Normandie. 9ème Congrès international de sédimentologie, 353-360.

1372 Robin, C., Guillocheau, F., Allemand, P., Bourquin, S., Dromart, G., Gaulier, J.M., Prijac, C., 2000. Time and
1373 space-scales of the tectonic control on a flexural intracratonic basin: the Paris Basin. Bulletin de la
1374 Société géologique de France 171, 181-196.

1375 Roger, P., Platel, J.-P., Barde, J-P., Doche, J.-L., Geffrault, E., Gouin, M., Jansana, P., Lombard, C., Poitevin, E.,
1376 Rambaud, D., Gottis, M., Humbert, L., Lenguin, M., Sellier, E., Floc'h, J.-P., Laville, H., Texier, J.-P.,
1377 Raynal, J.-P., 1979. Carte géologique de Nontron (1/50000), forage de la Tour-Blanche. Éditions du
1378 BRGM.

1379 Rousselle, B., Dromart, G., 1996. Partition stratigraphique des environnements et produits carbonatés dans
1380 l'Aalénien du sud-est de la France. Bulletin de la Société géologique de France 167, 399-408.

1381 Rowley, D., B., 2013. Sea Level: Earth's Dominant Elevation—Implications for Duration and Magnitudes of
1382 Sea Level Variations. The Journal of Geology 121, 445-454.

1383 Sahagian, D., Pinous, O., Olferiev, A., Zakharov, V., 1996. Eustatic curve for the Middle Jurassic–Cretaceous
1384 based on Russian platform and Siberian stratigraphy: zonal resolution. AAPG Bulletin 80, 1433– 58.

1385 Sandoval, J., O'Dogherty, L., Aguado, R., Bartolini, A., Bruchez, S., Bill, M., 2008. Aalenian carbon-isotope
1386 stratigraphy: Calibration with ammonite, radiolarian and nannofossil events in Western Tethys.
1387 Palaeogeography, Palaeoclimatology, Palaeoecology 267, 115-137.

1388 Schlager, W., 1993. Accommodation and supply – a dual control on stratigraphic sequences. Sedimentary
1389 Geology 86, 111-136.

1390 Schlager, W., 2004. Fractal nature of stratigraphic sequences. Geology 32, 185-188.

1391 Schlager, W., 2005. Carbonate Sedimentology and Sequence Stratigraphy. In: SEPM Concepts in Sedimentology
1392 and Paleontology.

1393 Sellwood, B.W., Scott, J., Mikkelsen, P., Akroyd, P., 1985. Stratigraphy and sedimentology of the Great Oolite
1394 Group in the Humbly Grove Oilfield, Hampshire. Marine and Petroleum Geology 2, 44-55.

1395 Sellwood, B.W., Sladen, C.P., 1981. Mesozoic and Tertiary argillaceous units: distribution and composition.
1396 Quarterly Journal of Engineering Geology and Hydrogeology 14, 263-275.

1397 Strasser, A., Hillgärtner, H., Hug, A., W., Pittet, B., 2000. Third-order depositional sequences reflecting
1398 Milankovitch cyclicity. Terra Nova 12, 303-311.

1399 Strasser, A., Pittet, B., Wolfgang, H., 2015. Palaeogeography of a shallow carbonate platform: The case of the
1400 Middle to Late Oxfordian in the Swiss Jura Mountains. Journal of Palaeogeography 4, 251-268.

1401 Steckler, M.S., Watts, A.B, 1978. Subsidence of the Atlantic–type continental margin off New-York. Earth and
1402 Planetary Science Letters 41, 1-13.

1403 Thierry, J., Barrier, E., 2000. Late Sinemurian, Middle Toarcian, Middle Callovian, Early Kimmeridgian, Early
1404 Tithonian. In: Crasquin, S. (Ed.), Atlas Peri-Tethys, Palaeogeographical maps–Explanatory notes.
1405 CCGM/CGMW Edit. Paris, 49-110.

1406 Tomas, A., Homann, M., Mutti, M., Amour, F., Christ, N., Immenhauser, A., Agar, S.M., Kabiri, L., 2013.
1407 Alternation of microbial mounds and ooid shoals (Middle Jurassic, Morocco): Response to
1408 palaeoenvironmental changes. Sedimentary Geology 294, 68-82.

1409 Tyszka, J., Kaminski, M.A. 1995. Factors controlling distribution of agglutinated foraminifera in Aalenian—
1410 Bajocian dysoxic facies (Pieniny Klippen Belt, Poland). In: M.A. Kaminski, S. Geroch, and M.A. Gasinski
1411 (eds.), Proceedings of the Fourth International Workshop on Agglutinated Foraminifera. Grzybowski
1412 Foundation Special Publication 3, 271–291.

1413 Tyszka, J., 1994. Response of Middle Jurassic benthic foraminiferal morphogroups to dysoxic/anoxic conditions
1414 in the Pieniny Klippen Basin, Polish Carpathians. Palaeogeography, Palaeoclimatology, Palaeoecology
1415 110, 55-81.

1416 Underhill, J.R., Partington, M.A., 1993. Jurassic thermal doming and deflation in the North Sea: implications of
1417 the sequence stratigraphic evidence. In: Parker, R.J. (Ed.), Petroleum Geology of Northwest Europe:
1418 Proceedings of the 4th Conference, Geological Society of London. Petroleum Geology 86 Ltd, London,
1419 337-345.

1420 Van Wagoner, J.C., Posamentier, H.W., Mitchum, R.M., Vail, P.R., Sarg, J.F., Loutit, T.S., Hardenbol, J., 1988.
1421 An overview of the fundamentals of sequence stratigraphy and key definitions, In: Wilgus, C., Hastings,
1422 B.S., Kendall, C.G., Posamentier, H.W., Ross, C.A. and Van Wagoner, J.C., (eds.). Sea level changes: an
1423 integrated approach. SEPM Special Publication 42, 39-46.

1424 Walker, R. G. and James, N. P., 1992. Facies Models, response to sea level change. Geological Association of
1425 Canada, 454 pp.

1426 Weissert H., Mohr H., 1996. Late Jurassic climate and its impact on carbon cycling. Palaeogeography,
1427 Palaeoclimatology, Palaeoecology 122, 27-43.

1428 Wetzel, A., Weissert, H., Schaub, M., Voegelin, A.R., 2013. Sea-water circulation on an oolite-dominated
1429 carbonate system in an epeiric sea (Middle Jurassic, Switzerland). Sedimentology 60, 19-35.

1430 Wiezrbowski, H., 2015. Seawater temperatures and carbon isotope variations in central European at the Middle-
1431 Late Jurassic transition (Late Callovian-Early Kimmeridgian). Palaeogeography, Palaeoclimatology,
1432 Palaeoecology 440, 506-523.

1433 Wright, J.K., 2014. A new section through the Corallian Group (Oxfordian, Upper Jurassic) rocks of Calne,
1434 Wiltshire, southern England. Proceedings of the Geologists' Association 125, 83-95.

1435 Zaton, M., Marynowski, L., Szczepanik, P., Bond, D.P.G., Wignall, P.B., 2009. Redox conditions during
1436 sedimentation of the Middle (Upper Bajocian-Bathonian) clays of the Polish Jura (south-central Poland).
1437 Facies 55, 103-114.

1438 Ziegler, P-A., 1988. Evolution of the Arctic - North Atlantic and the Western Tethys. AAPG Memoir 43 (charts).

1439 Zimmermann, J., Franz, M., Heunisch, C., Wilhelm Luppold, F., Mönnig, E., Wolfgramm, M., 2015. Sequence
1440 stratigraphic framework of the Lower and Middle Jurassic in the North German Basin: Epicontinental
1441 sequences controlled by Boreal cycles. Palaeogeography, Palaeoclimatology, Palaeoecology 440, 395-
1442 416.

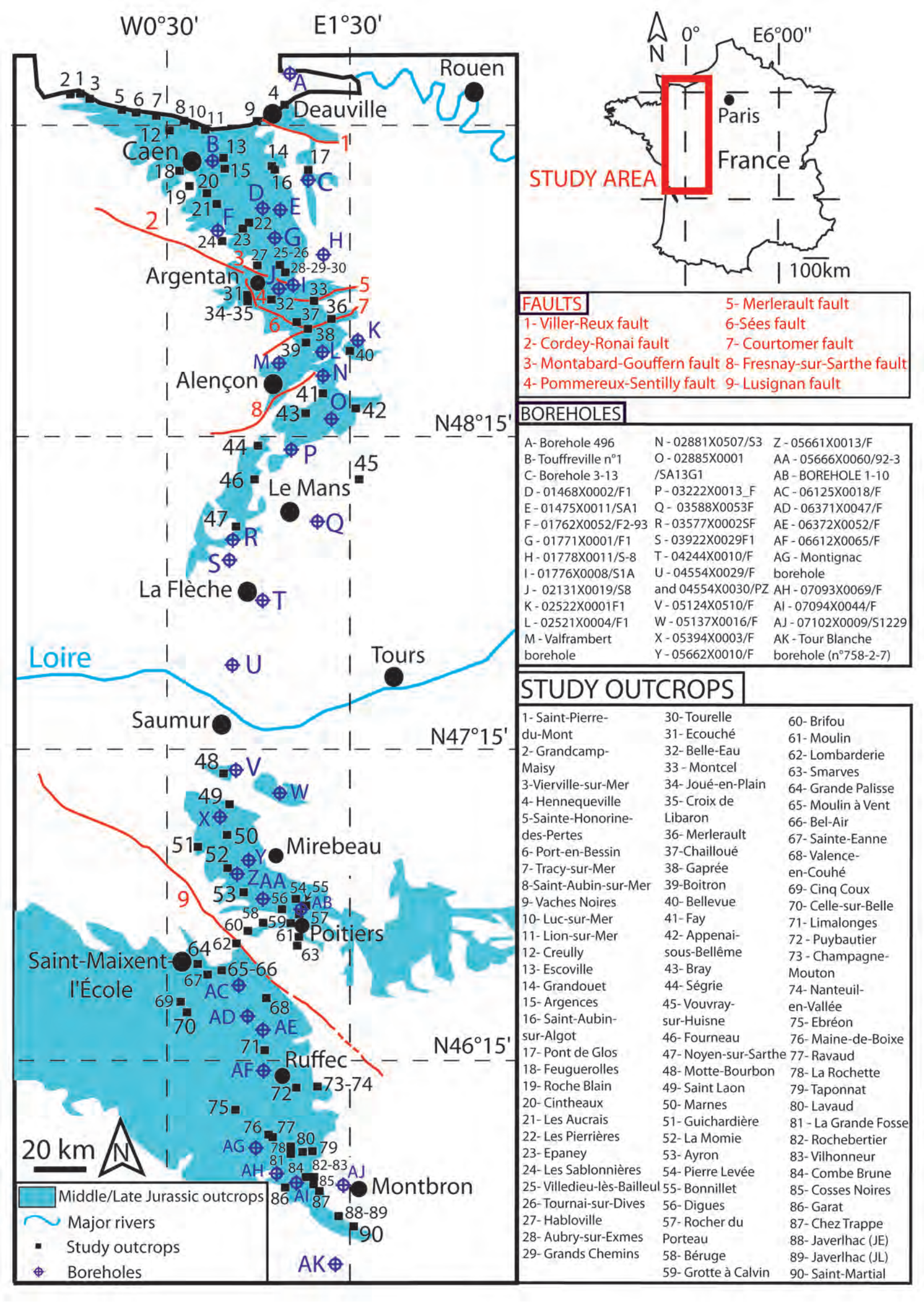

FAULTS

1- Viller-Reux fault
2- Cordey-Ronai fault
3- Montabard-Gouffern fault
4- Pommereux-Sentilly fault
5- Merlerault fault
6-Sées fault
7- Courtomer fault
8- Fresnay-sur-Sarthe fault
9- Lusignan fault

BOREHOLES

A- Borehole 496
B- Touffreville n°1
C- Borehole 3-13
D - 01468X0002/F1
E - 01475X0011/SA1
F - 01762X0052/F2-93
G - 01771X0001/F1
H - 01778X0011/S-8
I - 01776X0008/S1A
J - 02131X0019/S8
K - 02522X0001F1
L - 02521X0004/F1
M - Valframbert borehole
N - 02881X0507/S3
O - 02885X0001 /SA13G1
P - 03222X0013_F
Q - 03588X0053F
R - 03577X0002SF
S - 03922X0029F1
T - 04244X0010/F
U - 04554X0029/F and 04554X0030/PZ
V - 05124X0510/F
W - 05137X0016/F
X - 05394X0003/F
Y - 05662X0010/F
Z - 05661X0013/F
AA - 05666X0060/92-3
AB - BOREHOLE 1-10
AC - 06125X0018/F
AD - 06371X0047/F
AE - 06372X0052/F
AF - 06612X0065/F
AG - Montignac borehole
AH - 07093X0069/F
AI - 07094X0044/F
AJ - 07102X0009/S1229
AK - Tour Blanche borehole (n°758-2-7)

STUDY OUTCROPS

1- Saint-Pierre-du-Mont
2- Grandcamp-Maisy
3-Vierville-sur-Mer
4- Hennequeville
5-Sainte-Honorine-des-Pertes
6- Port-en-Bessin
7- Tracy-sur-Mer
8-Saint-Aubin-sur-Mer
9- Vaches Noires
10- Luc-sur-Mer
11- Lion-sur-Mer
12- Creully
13- Escoville
14- Grandouet
15- Argences
16- Saint-Aubin-sur-Algot
17- Pont de Glos
18- Feuguerolles
19- Roche Blain
20- Cintheaux
21- Les Aucrais
22- Les Pierrières
23- Epaney
24- Les Sablonnières
25- Villedieu-lès-Bailleul
26- Tournai-sur-Dives
27- Habloville
28- Aubry-sur-Exmes
29- Grands Chemins
30- Tourelle
31- Ecouché
32- Belle-Eau
33 - Montcel
34- Joué-en-Plain
35- Croix de Libaron
36- Merlerault
37-Chailloué
38- Gaprée
39-Boitron
40- Bellevue
41- Fay
42- Appenai-sous-Bellême
43- Bray
44- Ségrie
45- Vouvray-sur-Huisne
46- Fourneau
47- Noyen-sur-Sarthe
48- Motte-Bourbon
49- Saint Laon
50- Marnes
51- Guichardière
52- La Momie
53- Ayron
54- Pierre Levée
55- Bonnillet
56- Digues
57- Rocher du Porteau
58- Béruge
59- Grotte à Calvin
60- Brifou
61- Moulin
62- Lombarderie
63- Smarves
64- Grande Palisse
65- Moulin à Vent
66- Bel-Air
67- Sainte-Eanne
68- Valence-en-Couhé
69- Cinq Coux
70- Celle-sur-Belle
71- Limalonges
72 - Puybautier
73 - Champagne-Mouton
74- Nanteuil-en-Vallée
75- Ebréon
76- Maine-de-Boixe
77- Ravaud
78- La Rochette
79- Taponnat
80- Lavaud
81 - La Grande Fosse
82- Rochebertier
83- Vilhonneur
84- Combe Brune
85- Cosses Noires
86- Garat
87- Chez Trappe
88- Javerlhac (JE)
89- Javerlhac (JL)
90- Saint-Martial

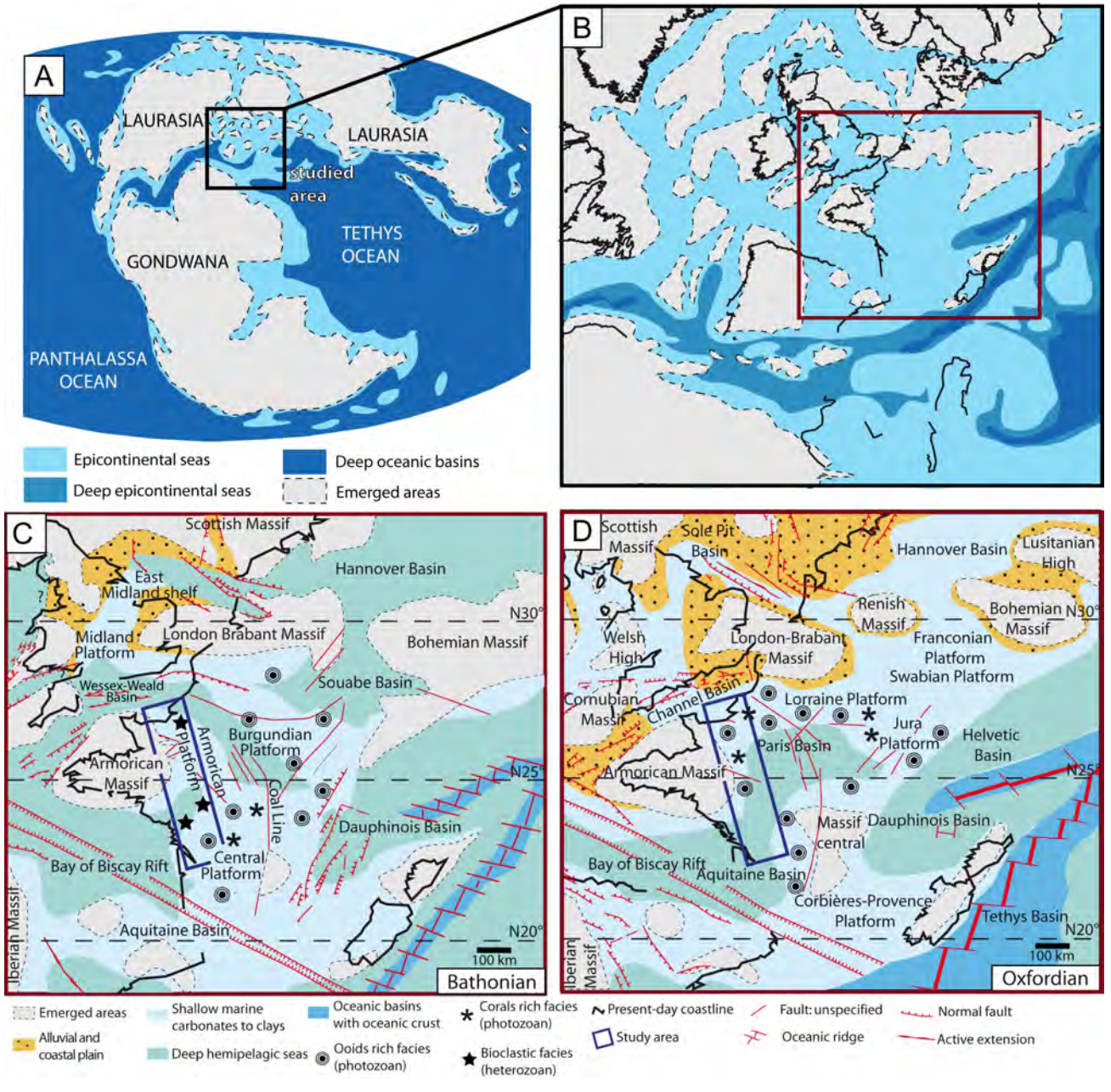
A
LAURASIA
LAURASIA
studied area
TETHYS OCEAN
GONDWANA
PANTHALASSA OCEAN
Epicontinental seas
Deep epicontinental seas
Deep oceanic basins
Emerged areas
B
C
Scottish Massif
East Midland shelf
Hannover Basin
N30°
Midland Platform
London Brabant Massif
Bohemian Massif
Wessex-Weald Basin
Souabe Basin
Armorican Massif
Armorican Platform
Burgundian Platform
Coal Line
N25°
Dauphinois Basin
Bay of Biscay Rift
Central Platform
Aquitaine Basin
N20°
Iberian Massif
100 km
Bathonian
D
Scottish Massif
Sole Pit Basin
Hannover Basin
Lusitanian High
Renish Massif
Bohemian Massif
N30°
Welsh High
London-Brabant Massif
Franconian Platform
Swabian Platform
Cornubian Massif
Channel Basin
Lorraine Platform
Jura Platform
Helvetic Basin
Paris Basin
Armorican Massif
N25°
Massif central
Dauphinois Basin
Bay of Biscay Rift
Aquitaine Basin
Corbières-Provence Platform
Tethys Basin
N20°
Iberian Massif
100 km
Oxfordian
Emerged areas
Alluvial and coastal plain
Shallow marine carbonates to clays
Deep hemipelagic seas
Oceanic basins with oceanic crust
Ooids rich facies (photozoan)
Corals rich facies (photozoan)
Bioclastic facies (heterozoan)
Present-day coastline
Study area
Fault: unspecified
Oceanic ridge
Normal fault
Active extension

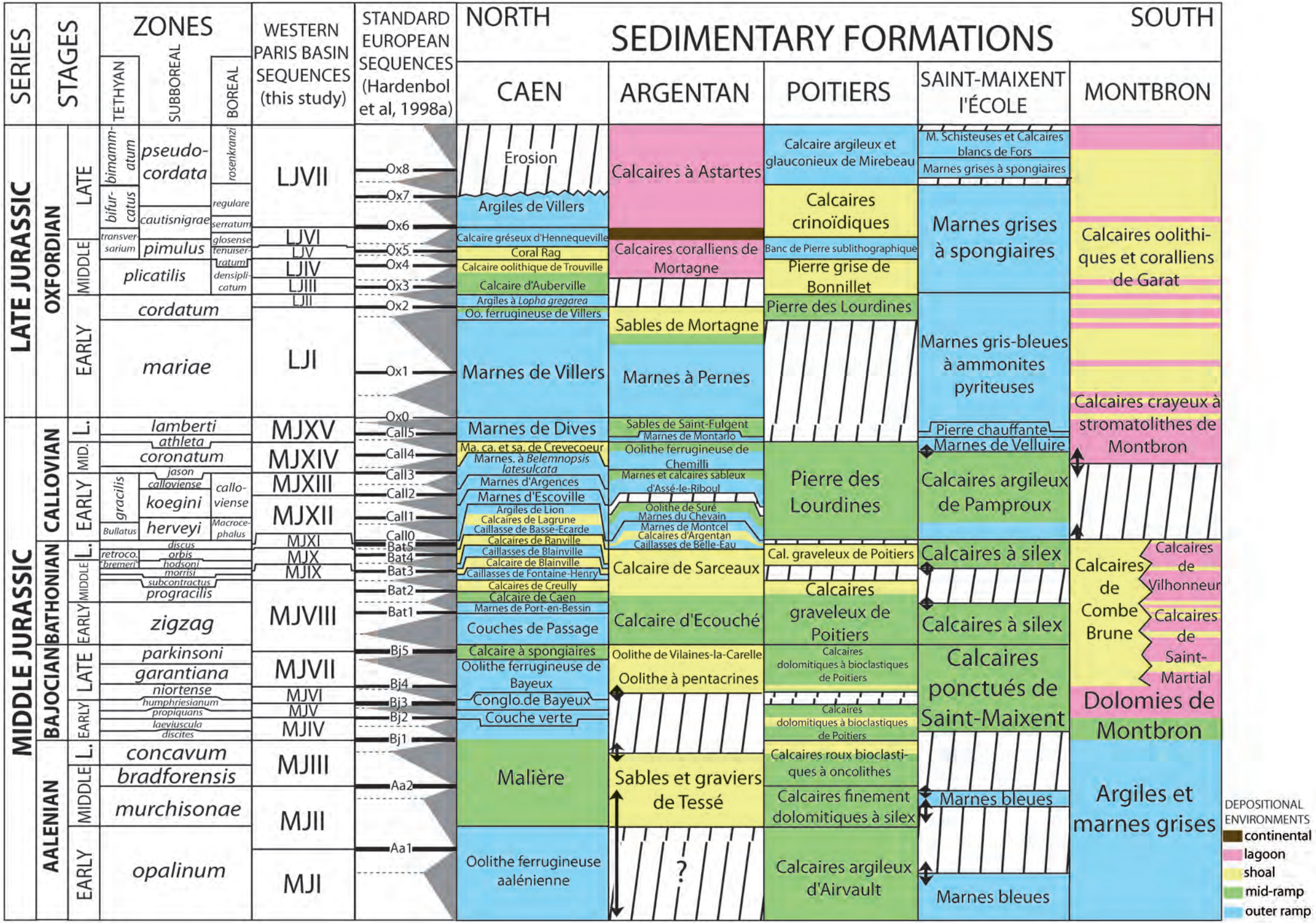
SERIES
STAGES
ZONES
TETHYAN
SUBBOREAL
BOREAL
WESTERN PARIS BASIN SEQUENCES (this study)
STANDARD EUROPEAN SEQUENCES (Hardenbol et al, 1998a)
NORTH
SOUTH
SEDIMENTARY FORMATIONS
CAEN
ARGENTAN
POITIERS
SAINT-MAIXENT l'ÉCOLE
MONTBRON
LATE JURASSIC
MIDDLE JURASSIC
OXFORDIAN
CALLOVIAN
BATHONIAN
BAJOCIAN
AALENIAN
LATE
MIDDLE
EARLY
L.
MID.
MIDDLE
EARLY
L.
MIDDLE
EARLY
bimammatum
bifurcatus
transversarium
plicatilis
cordatum
mariae
lamberti
athleta
coronatum
jason
gracilis
calloviense
koegini
herveyi
Bullatus
Macrocephalus
discus
retroco. bremeri
orbis
hodsoni
morrisi
subcontractus
progracilis
zigzag
parkinsoni
garantiana
niortense
humphriesianum
propiquans
laeviuscula
discites
concavum
bradforensis
murchisonae
opalinum
pseudocordata
cautisnigrae
pimulus
rosenkranzi
regulare
serratum
glosense
tenuiserratum
densiplicatum
callo-viense
LJVII
LJVI
LJV
LJIV
LJIII
LJII
LJI
MJXV
MJXIV
MJXIII
MJXII
MJXI
MJX
MJIX
MJVIII
MJVII
MJVI
MJV
MJIV
MJIII
MJII
MJI
Ox8
Ox7
Ox6
Ox5
Ox4
Ox3
Ox2
Ox1
Ox0
Call5
Call4
Call3
Call2
Call1
Call0
Bat5
Bat4
Bat3
Bat2
Bat1
Bj5
Bj4
Bj3
Bj2
Bj1
Aa2
Aa1
Erosion
Argiles de Villers
Calcaire gréseux d'Hennequeville
Coral Rag
Calcaire oolithique de Trouville
Calcaire d'Auberville
Argiles à Lopha gregarea
Oo. ferrugineuse de Villers
Marnes de Villers
Marnes de Dives
Ma. ca. et sa. de Crevecoeur
Marnes. à Belemnopsis latesulcata
Marnes d'Argences
Marnes d'Escoville
Argiles de Lion
Calcaires de Lagrune
Caillasse de Basse-Ecarde
Calcaires de Ranville
Caillasses de Blainville
Calcaire de Blainville
Caillasses de Fontaine-Henry
Calcaires de Creully
Calcaire de Caen
Marnes de Port-en-Bessin
Couches de Passage
Calcaire à spongiaires
Oolithe ferrugineuse de Bayeux
Conglo.de Bayeux
Couche verte
Malière
Oolithe ferrugineuse aalénienne
Calcaires à Astartes
Calcaires coralliens de Mortagne
Sables de Mortagne
Marnes à Pernes
Sables de Saint-Fulgent
Marnes de Montarlo
Oolithe ferrugineuse de Chemilli
Marnes et calcaires sableux d'Assé-le-Riboul
Oolithe de Suré
Marnes du Chevain
Marnes de Montcel
Calcaires d'Argentan
Caillasses de Belle-Eau
Calcaire de Sarceaux
Calcaire d'Ecouché
Oolithe de Vilaines-la-Carelle
Oolithe à pentacrines
Sables et graviers de Tessé
?
Calcaire argileux et glauconieux de Mirebeau
Calcaires crinoïdiques
Banc de Pierre sublithographique
Pierre grise de Bonnillet
Pierre des Lourdines
Cal. graveleux de Poitiers
Calcaires graveleux de Poitiers
Calcaires dolomitiques à bioclastiques de Poitiers
Calcaires dolomitiques à bioclastiques de Poitiers
Calcaires roux bioclastiques à oncolithes
Calcaires finement dolomitiques à silex
Calcaires argileux d'Airvault
M. Schisteuses et Calcaires blancs de Fors
Marnes grises à spongiaires
Marnes grises à spongiaires
Marnes gris-bleues à ammonites pyriteuses
Pierre chauffante
Marnes de Velluire
Calcaires argileux de Pamproux
Calcaires à silex
Calcaires à silex
Calcaires ponctués de Saint-Maixent
Marnes bleues
Marnes bleues
Calcaires oolithiques et coralliens de Garat
Calcaires crayeux à stromatolithes de Montbron
Calcaires de Combe Brune
Calcaires de Vilhonneur
Calcaires de Saint-Martial
Dolomies de Montbron
Argiles et marnes grises
DEPOSITIONAL ENVIRONMENTS
continental
lagoon
shoal
mid-ramp
outer ramp

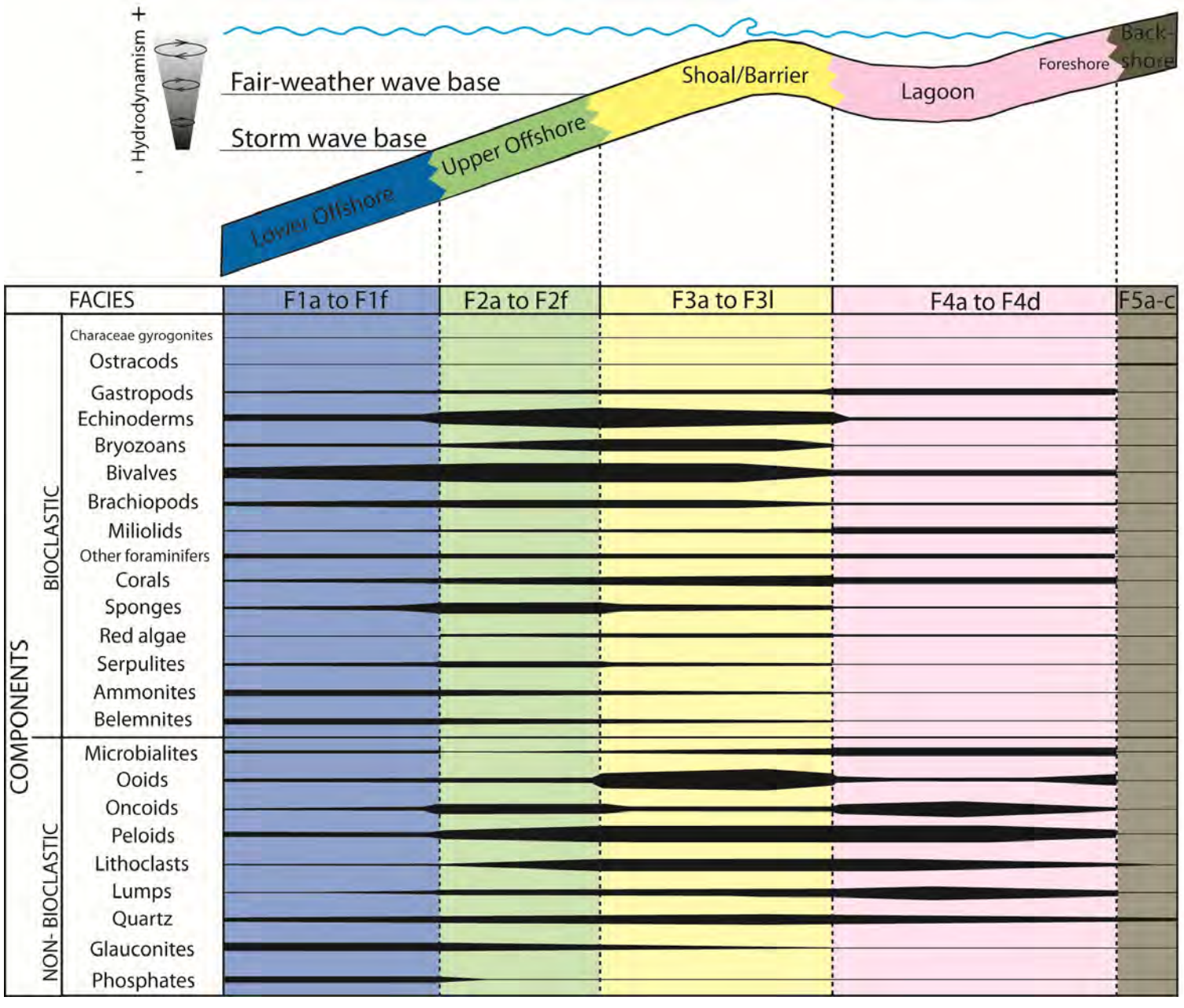
Hydrodynamism +
-
Fair-weather wave base
Storm wave base
Lower Offshore
Upper Offshore
Shoal/Barrier
Lagoon
Foreshore
Back-shore
FACIES
F1a to F1f
F2a to F2f
F3a to F3l
F4a to F4d
F5a-c
COMPONENTS
BIOCLASTIC
NON- BIOCLASTIC
Characeae gyrogonites
Ostracods
Gastropods
Echinoderms
Bryozoans
Bivalves
Brachiopods
Miliolids
Other foraminifers
Corals
Sponges
Red algae
Serpulites
Ammonites
Belemnites
Microbialites
Ooids
Oncoids
Peloids
Lithoclasts
Lumps
Quartz
Glauconites
Phosphates

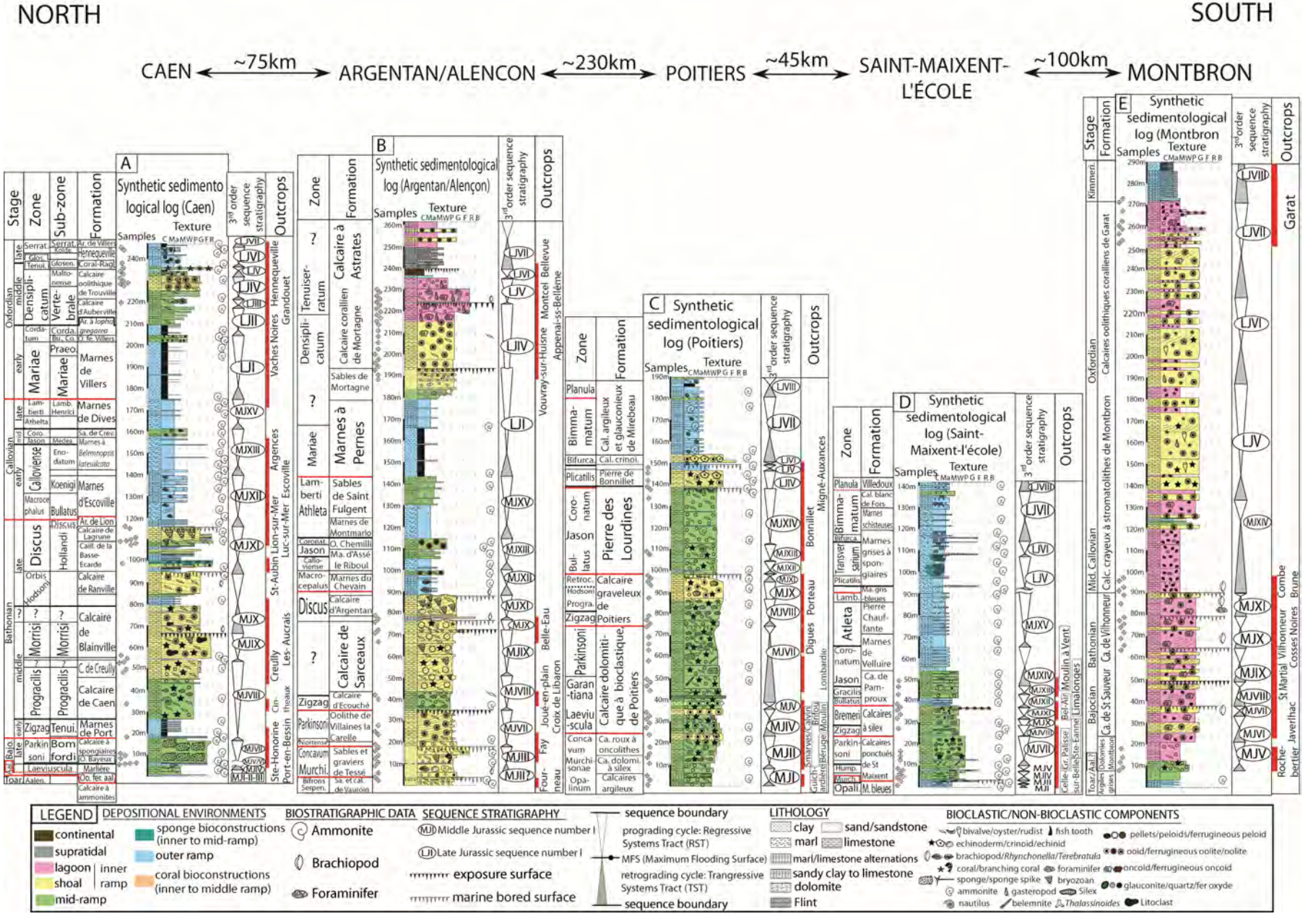
NORTH
SOUTH
CAEN
~75km
ARGENTAN/ALENCON
~230km
POITIERS
~45km
SAINT-MAIXENT-L'ÉCOLE
~100km
MONTBRON
A
Synthetic sedimento logical log (Caen)
B
Synthetic sedimentological log (Argentan/Alençon)
C
Synthetic sedimentological log (Poitiers)
D
Synthetic sedimentological log (Saint-Maixent-l'école)
E
Synthetic sedimentological log (Montbron
Stage
Zone
Sub-zone
Formation
Samples
Texture
3rd order sequence stratigraphy
Outcrops
LEGEND
DEPOSITIONAL ENVIRONMENTS
continental
supratidal
lagoon
shoal
inner ramp
mid-ramp
sponge bioconstructions (inner to mid-ramp)
outer ramp
coral bioconstructions (inner to middle ramp)
BIOSTRATIGRAPHIC DATA
Ammonite
Brachiopod
Foraminifer
SEQUENCE STRATIGRAPHY
MJI Middle Jurassic sequence number I
LJI Late Jurassic sequence number I
exposure surface
marine bored surface
sequence boundary
prograding cycle: Regressive Systems Tract (RST)
MFS (Maximum Flooding Surface)
retrograding cycle: Trangressive Systems Tract (TST)
sequence boundary
LITHOLOGY
clay
sand/sandstone
marl
limestone
marl/limestone alternations
sandy clay to limestone
dolomite
Flint
BIOCLASTIC/NON-BIOCLASTIC COMPONENTS
bivalve/oyster/rudist
fish tooth
echinoderm/crinoid/echinid
brachiopod/Rhynchonella/Terebratula
coral/branching coral
foraminifer
sponge/sponge spike
bryozoan
ammonite
gasteropod
Silex
nautilus
belemnite
Thalassinoides
Litoclast
pellets/peloids/ferruginous peloid
ooid/ferruginous oolite/oolite
oncoid/ferruginous oncoid
glauconite/quartz/fer oxyde

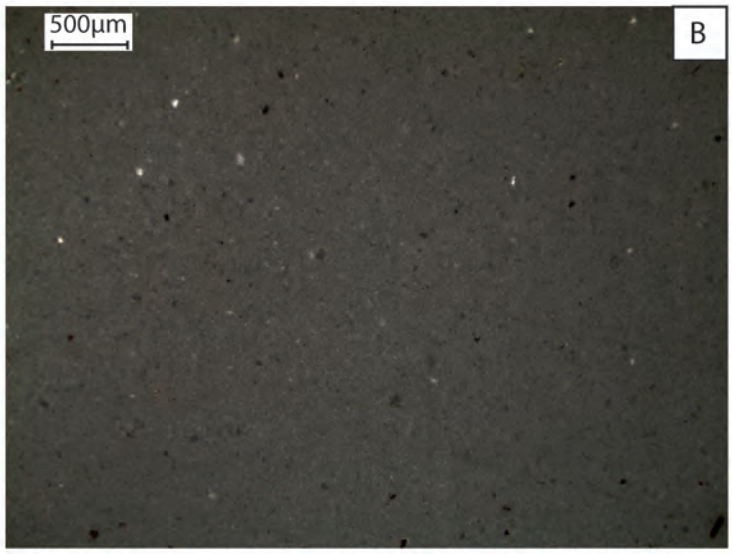

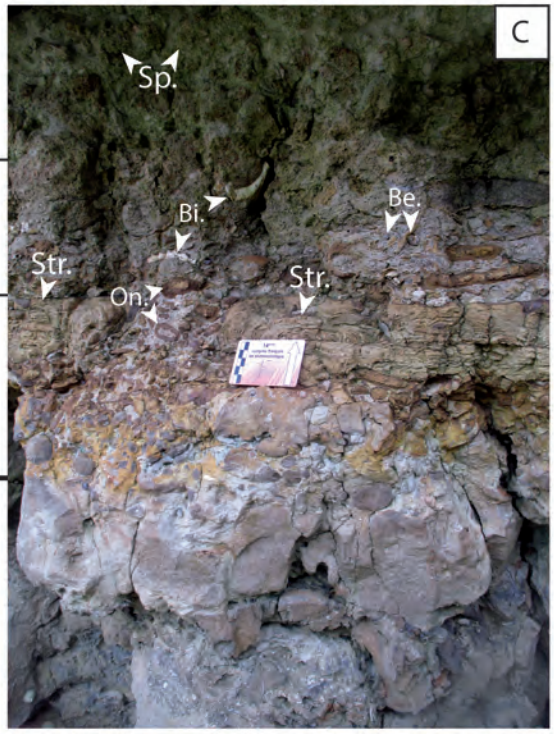

Calcaire à spongaires

Oolithe ferrugineuse de Bayeux

Conglomérat de Bayeux

Couche verte

Malière

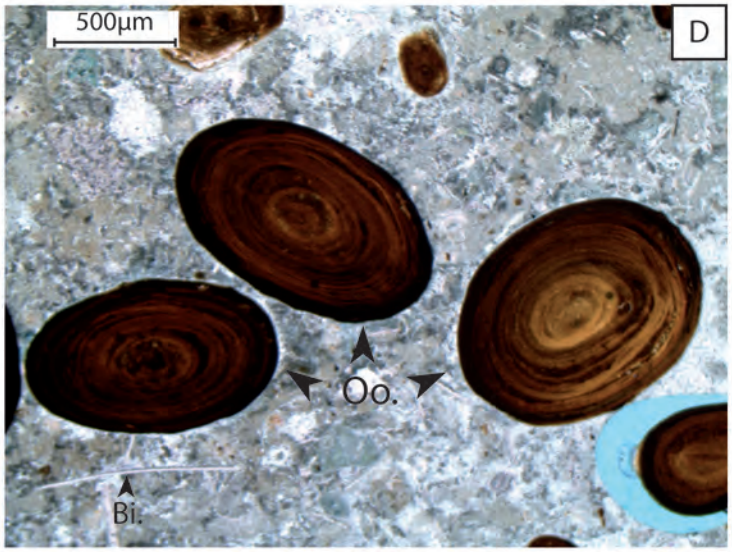

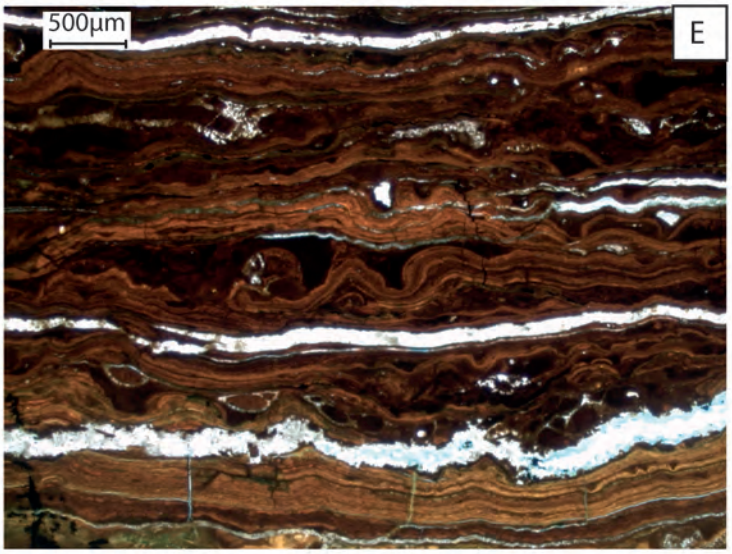

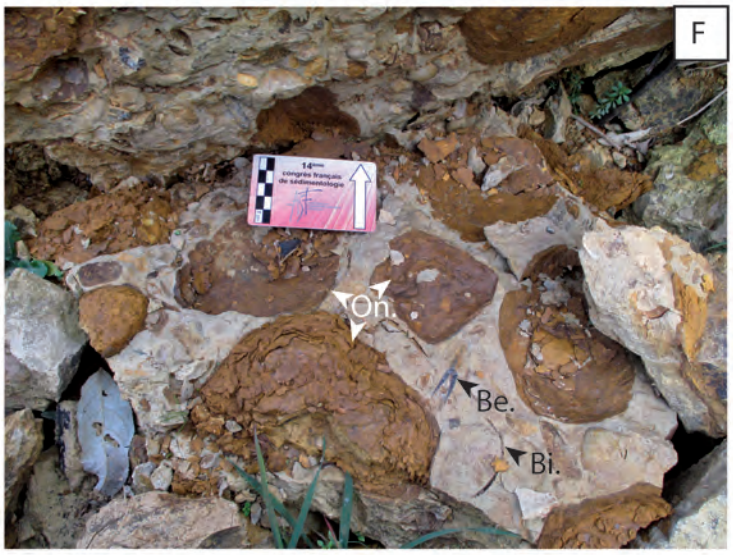

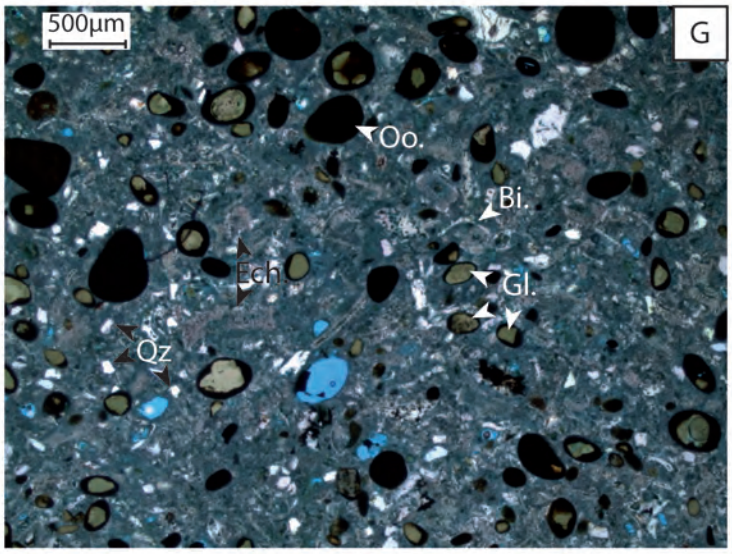


A

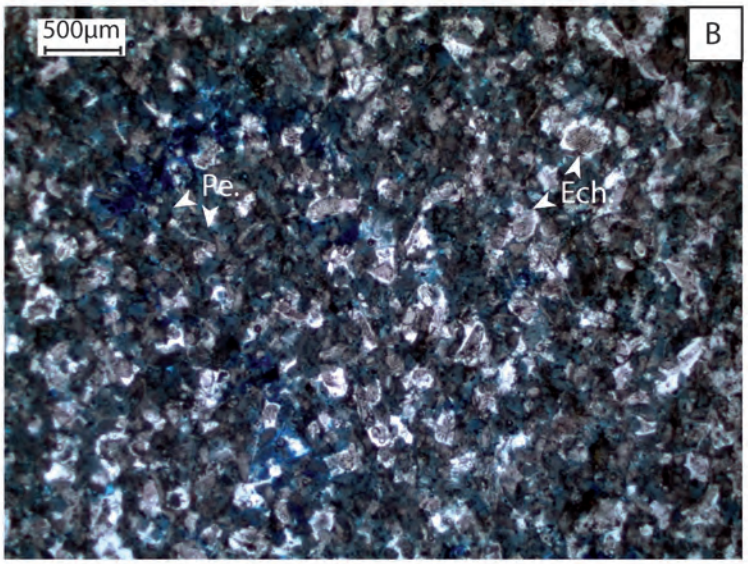
500µm
B
Pe.
Ech.

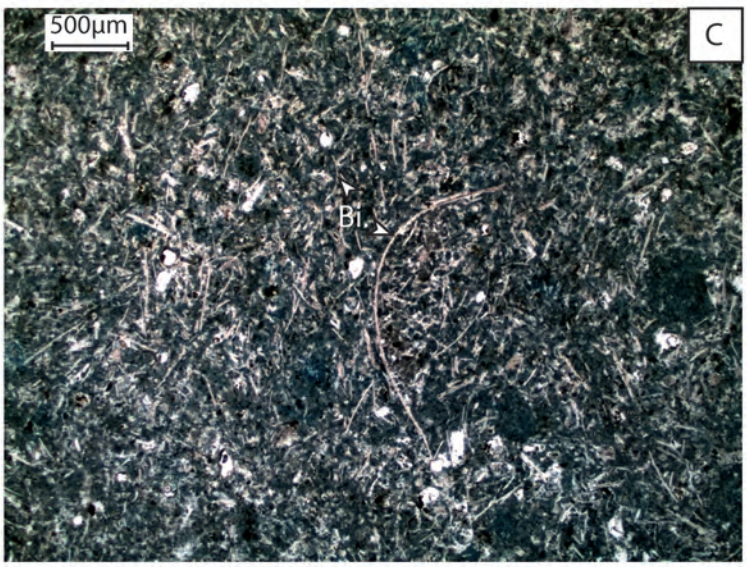
500µm
C
Bi.

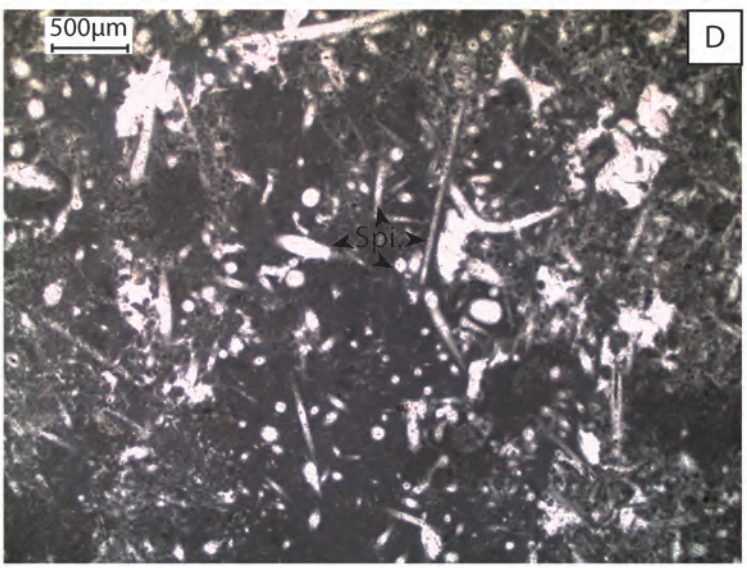
500µm
D
Spi.


E
Sp.
Sp.

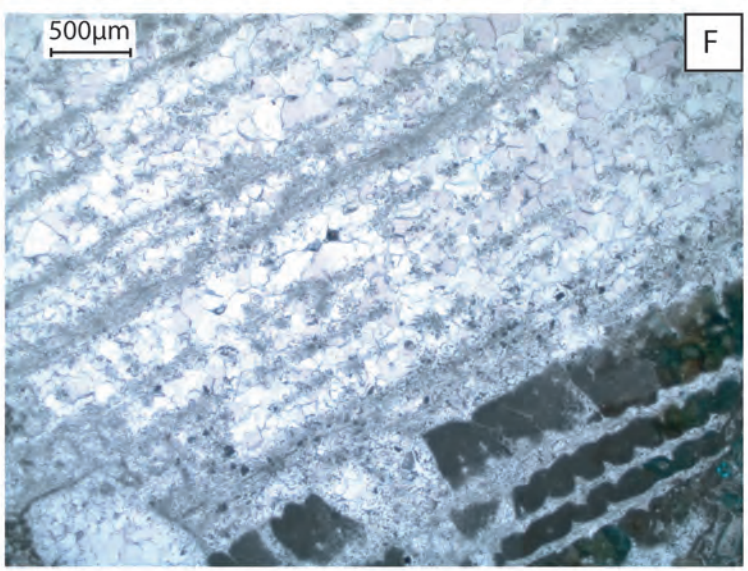
500µm
F

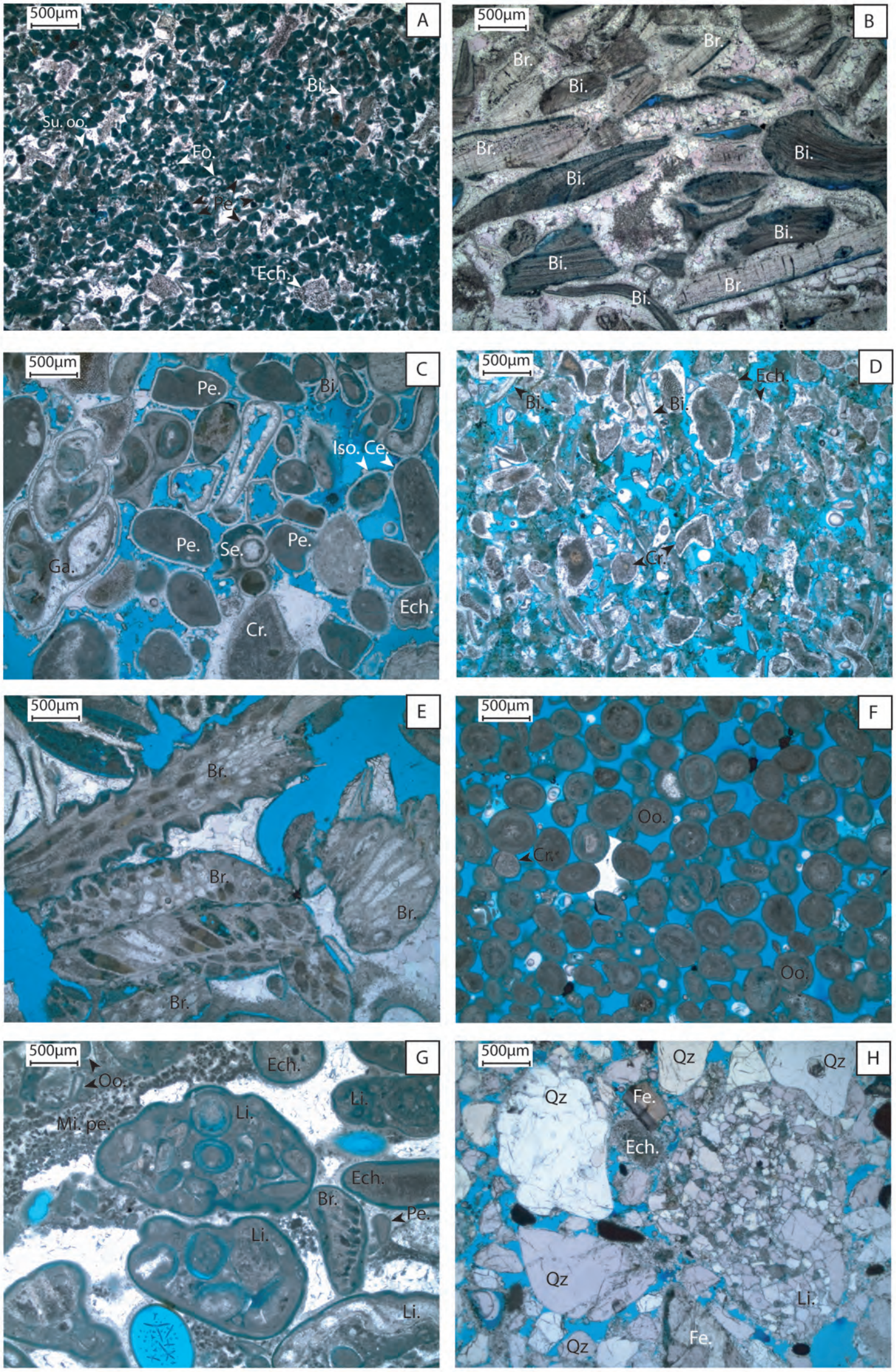
500µm
A
Bi.
Su. oo.
Fo.
Pe.
Ech.
500µm
B
Br.
Br.
Bi.
Br.
Bi.
Bi.
Bi.
Bi.
Br.
Bi.
500µm
C
Pe.
Bi.
Iso. Ce.
Pe.
Se.
Pe.
Ga.
Ech.
Cr.
500µm
D
Ech.
Bi.
Bi.
Cr.
500µm
E
Br.
Br.
Br.
Br.
500µm
F
Oo.
Cr.
Oo.
500µm
G
Ech.
Oo.
Li.
Li.
Mi. pe.
Ech.
Br.
Pe.
Li.
Li.
500µm
H
Qz
Qz
Qz
Fe.
Ech.
Qz
Li.
Qz
Fe.

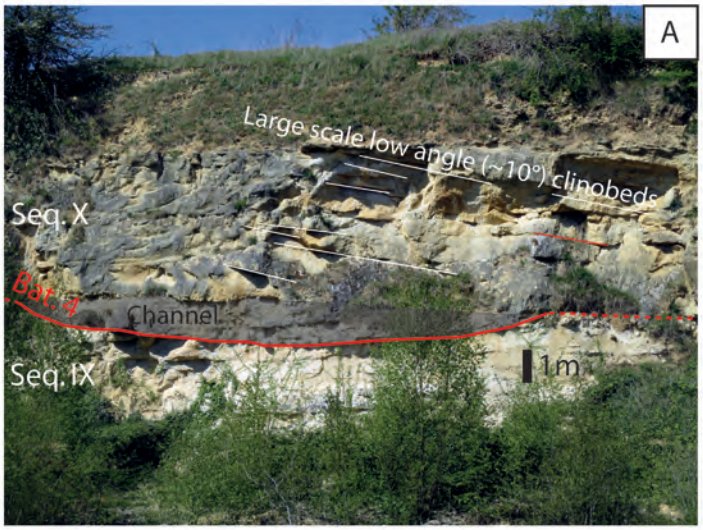
A
Large scale low angle (~10°) clinobeds
Seq. X
Bar 4
Channel
Seq. IX
1m


B

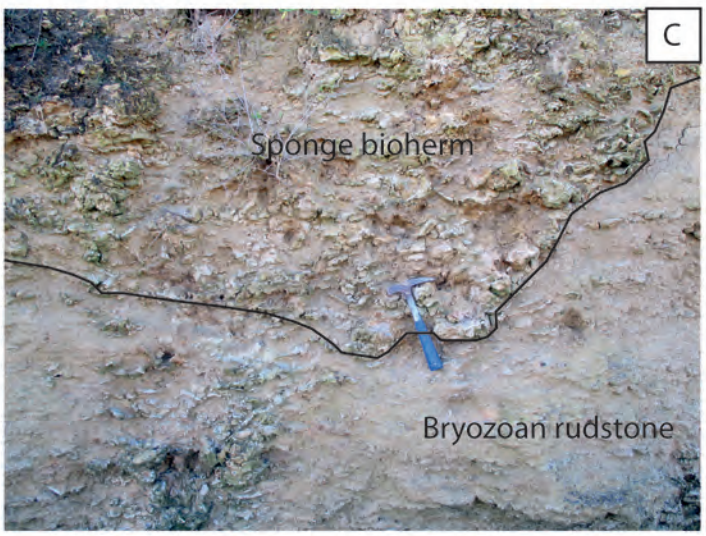
C
Sponge bioherm
Bryozoan rudstone


D
Hammer


E


F


G

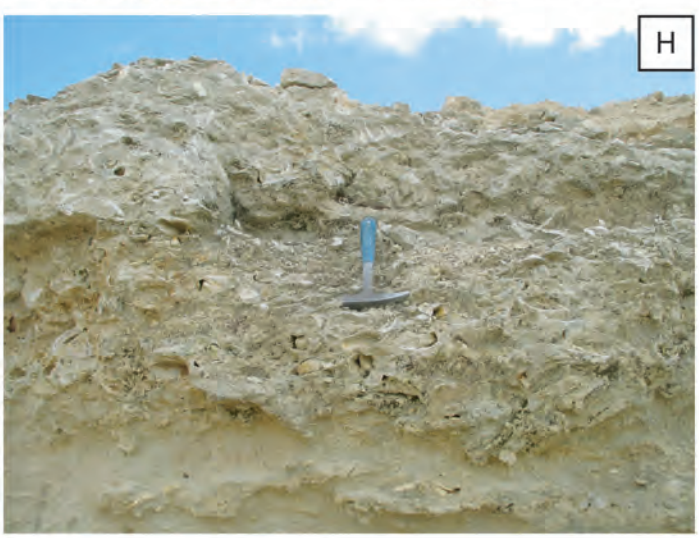
H

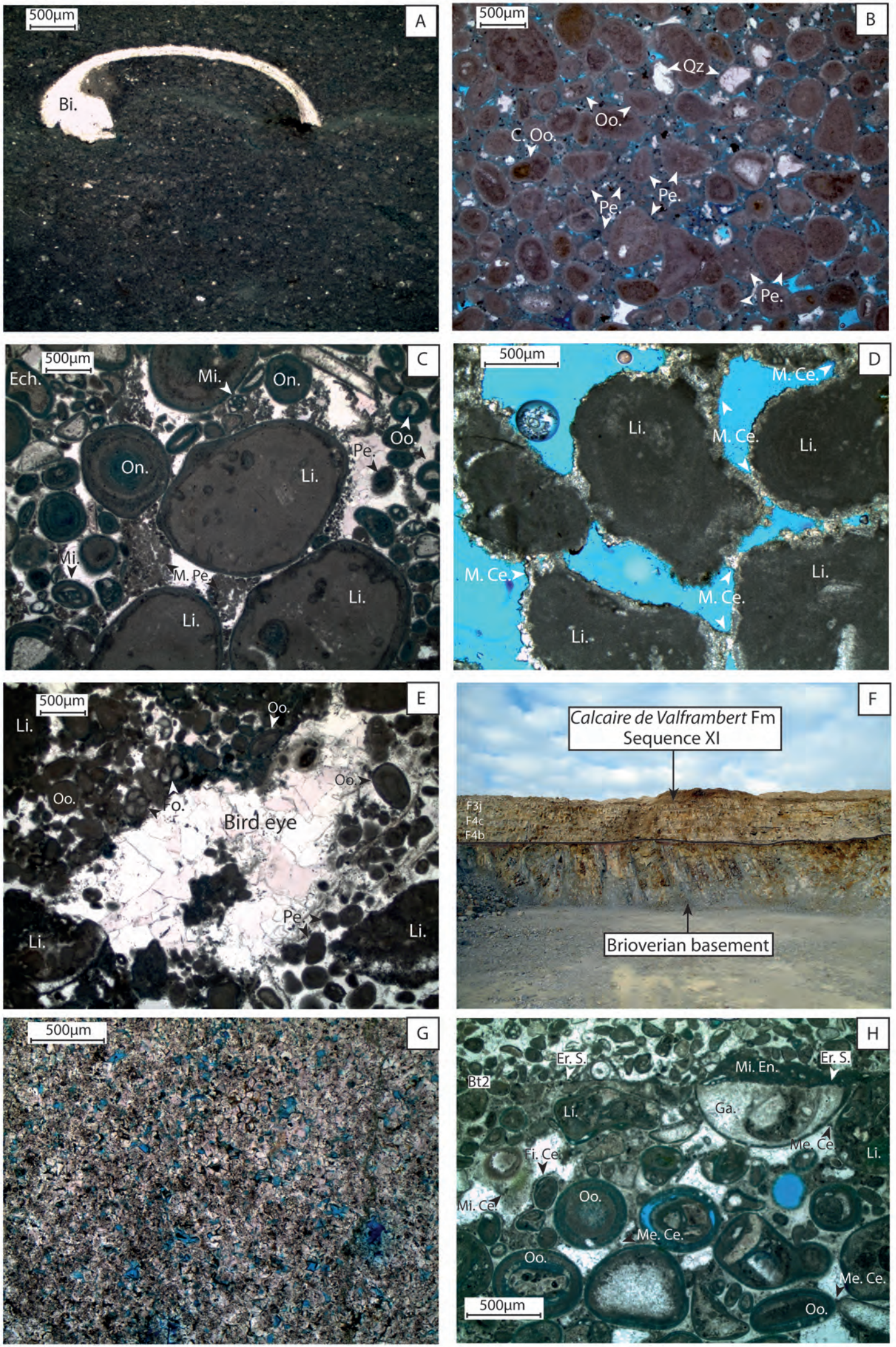
500µm
A
Bi.
500µm
B
Qz
Oo.
C. Oo.
Pe.
Pe.
Pe.
Pe.
500µm
C
Ech.
Mi.
On.
Oo.
Pe.
On.
Li.
Mi.
M. Pe.
Li.
Li.
500µm
D
M. Ce.
Li.
M. Ce.
Li.
M. Ce.
Li.
M. Ce.
Li.
500µm
E
Li.
Oo.
Oo.
Oo.
Bird eye
Pe.
Li.
Li.
F
Calcaire de Valframbert Fm
Sequence XI
F3j
F4c
F4b
Brioverian basement
500µm
G
500µm
H
Er. S.
Mi. En.
Er. S.
Bt2
Li.
Ga.
Me. Ce.
Fi. Ce.
Li.
Mi. Ce.
Oo.
Me. Ce.
Oo.
Me. Ce.
500µm
Oo.

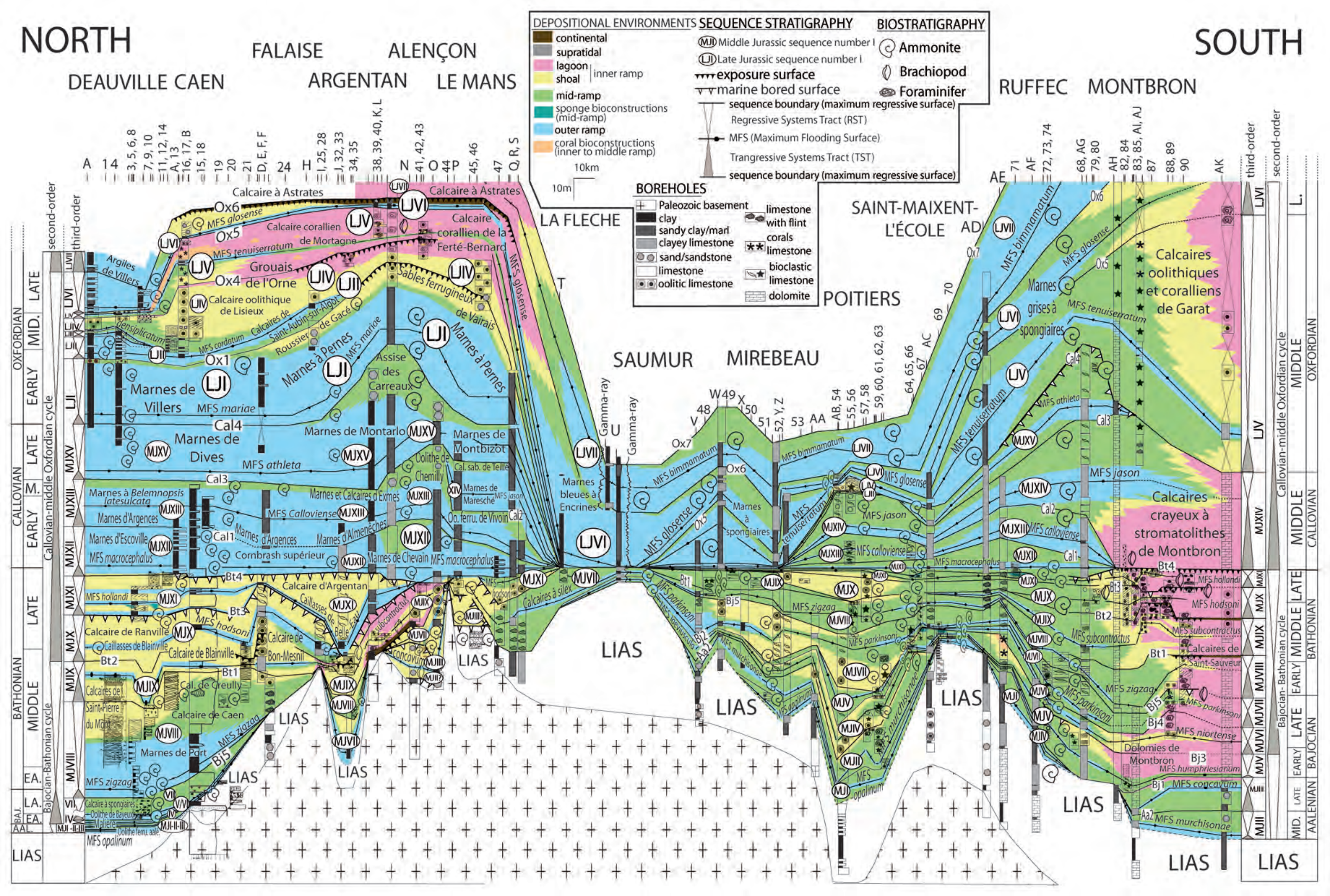

NORTH
SOUTH
DEAUVILLE CAEN
FALAISE
ARGENTAN
ALENÇON
LE MANS
LA FLECHE
SAUMUR
MIREBEAU
POITIERS
SAINT-MAIXENT-L'ÉCOLE
RUFFEC
MONTBRON
DEPOSITIONAL ENVIRONMENTS
continental
supratidal
lagoon
shoal
inner ramp
mid-ramp
sponge bioconstructions (mid-ramp)
outer ramp
coral bioconstructions (inner to middle ramp)
10km
10m
SEQUENCE STRATIGRAPHY
Middle Jurassic sequence number I
Late Jurassic sequence number I
exposure surface
marine bored surface
sequence boundary (maximum regressive surface)
Regressive Systems Tract (RST)
MFS (Maximum Flooding Surface)
Trangressive Systems Tract (TST)
sequence boundary (maximum regressive surface)
BIOSTRATIGRAPHY
Ammonite
Brachiopod
Foraminifer
BOREHOLES
Paleozoic basement
clay
sandy clay/marl
clayey limestone
sand/sandstone
limestone
oolitic limestone
limestone with flint
corals limestone
bioclastic limestone
dolomite
second-order
third-order
LIAS
Calcaire à Astrates
Calcaire corallien de Mortagne
Calcaire corallien de la Ferté-Bernard
Argiles de Villers
Grouais de l'Orne
Calcaire oolithique de Lisieux
Sables ferrugineux de Vairais
Marnes de Villers
Marnes à Pernes
Assise des Carreaux
Marnes de Dives
Marnes de Montarlo
Marnes de Montbizot
Marnes bleues à Encrines
Marnes à spongiaires
Marnes grises à spongiaires
Calcaires oolithiques et coralliens de Garat
Calcaires crayeux à stromatolithes de Montbron
Calcaire d'Argentan
Calcaire de Ranville
Calcaire de Blainville
Calcaire de Bon-Mesnil
Calcaire de Caen
Marnes de Port
Calcaires à silex
Dolomies de Montbron
Calcaires de Saint-Sauveur
Gamma-ray
CALLOVIAN
OXFORDIAN
BATHONIAN
BAJOCIAN
AALENIAN
EARLY
MIDDLE
LATE
Callovian-middle Oxfordian cycle
Bajocian-Bathonian cycle

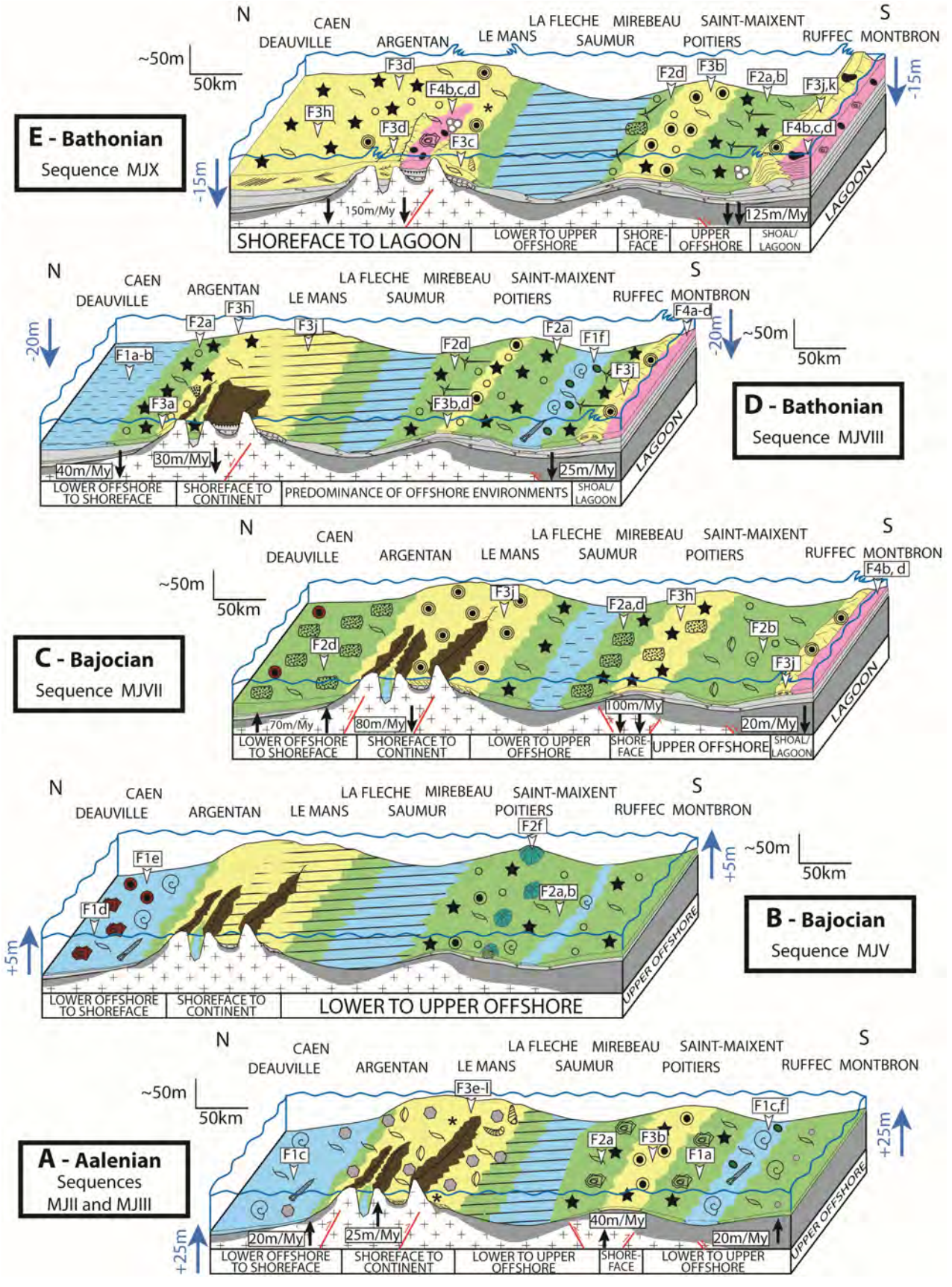
N
CAEN
DEAUVILLE
ARGENTAN
LE MANS
LA FLECHE
MIREBEAU
SAUMUR
SAINT-MAIXENT
POITIERS
RUFFEC
MONTBRON
S
~50m
50km
-15m
E - Bathonian
Sequence MJX
F3d
F4b,c,d
F3h
F3d
F3c
F2d
F3b
F2a,b
F3j,k
F4b,c,d
150m/My
125m/My
SHOREFACE TO LAGOON
LOWER TO UPPER OFFSHORE
SHORE-FACE
UPPER OFFSHORE
SHOAL/ LAGOON
LAGOON
-20m
F2a
F3h
F3j
F1a-b
F3a
F2d
F2a
F1f
F3j
F3b,d
F4a-d
40m/My
30m/My
25m/My
LOWER OFFSHORE TO SHOREFACE
SHOREFACE TO CONTINENT
PREDOMINANCE OF OFFSHORE ENVIRONMENTS
D - Bathonian
Sequence MJVIII
F4b, d
F3j
F2a,d
F3h
F2b
F3j
F2d
70m/My
80m/My
100m/My
20m/My
C - Bajocian
Sequence MJVII
+5m
F2f
F1e
F1d
F2a,b
B - Bajocian
Sequence MJV
F3e-l
F1c,f
F1c
F2a
F3b
F1a
+25m
20m/My
25m/My
40m/My
20m/My
A - Aalenian
Sequences
MJII and MJIII

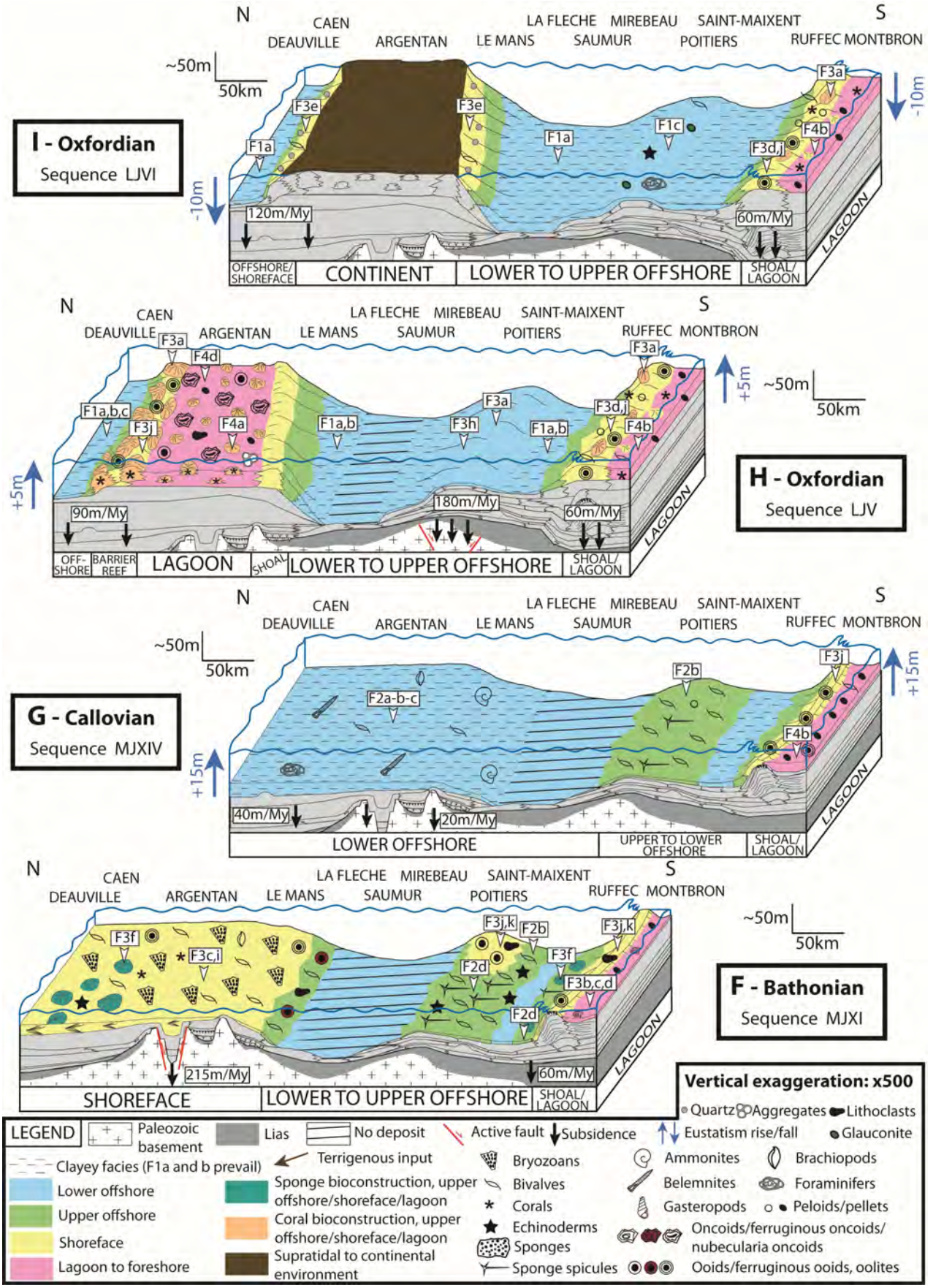
N
S
CAEN
DEAUVILLE
ARGENTAN
LE MANS
LA FLECHE
SAUMUR
MIREBEAU
POITIERS
SAINT-MAIXENT
RUFFEC
MONTBRON
~50m
50km
I - Oxfordian
Sequence LJVI
-10m
F1a
F3e
F1c
F3a
F4b
F3d,j
120m/My
60m/My
OFFSHORE/ SHOREFACE
CONTINENT
LOWER TO UPPER OFFSHORE
SHOAL/ LAGOON
LAGOON
H - Oxfordian
Sequence LJV
+5m
F1a,b,c
F3j
F4a
F4d
F1a,b
F3h
90m/My
180m/My
OFF-SHORE
BARRIER REEF
LAGOON
SHOAL
G - Callovian
Sequence MJXIV
+15m
F2a-b-c
F2b
F3j
40m/My
20m/My
LOWER OFFSHORE
UPPER TO LOWER OFFSHORE
F - Bathonian
Sequence MJXI
F3f
F3c,i
F3j,k
F2d
F3b,c,d
215m/My
SHOREFACE
Vertical exaggeration: x500
Quartz
Aggregates
Lithoclasts
Glauconite
LEGEND
Paleozoic basement
Lias
No deposit
Active fault
Subsidence
Eustatism rise/fall
Clayey facies (F1a and b prevail)
Terrigenous input
Lower offshore
Upper offshore
Shoreface
Lagoon to foreshore
Sponge bioconstruction, upper offshore/shoreface/lagoon
Coral bioconstruction, upper offshore/shoreface/lagoon
Supratidal to continental environment
Bryozoans
Bivalves
Corals
Echinoderms
Sponges
Sponge spicules
Ammonites
Belemnites
Gasteropods
Brachiopods
Foraminifers
Peloids/pellets
Oncoids/ferruginous oncoids/ nubecularia oncoids
Ooids/ferruginous ooids, oolites

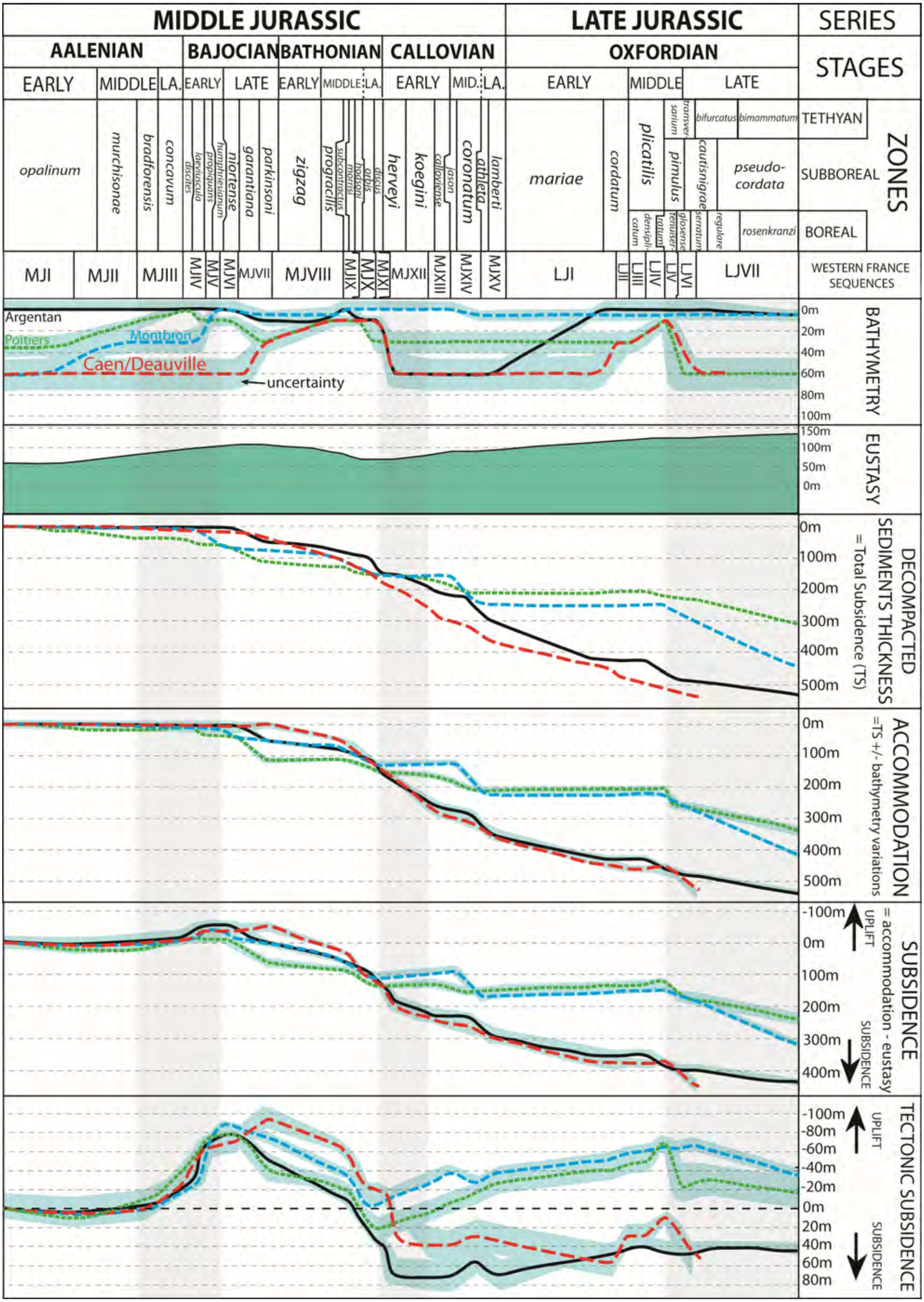

MIDDLE JURASSIC
LATE JURASSIC
SERIES
AALENIAN
BAJOCIAN
BATHONIAN
CALLOVIAN
OXFORDIAN
STAGES
EARLY
MIDDLE
LA.
LATE
MID.
TETHYAN
SUBBOREAL
BOREAL
ZONES
opalinum
murchisonae
bradforensis
concavum
zigzag
herveyi
koegini
coronatum
athleta
lamberti
mariae
cordatum
plicatilis
pimulus
pseudo-cordata
bifurcatus
bimammatum
rosenkranzi
MJI
MJII
MJIII
MJIV
MJV
MJVI
MJVII
MJVIII
MJIX
MJX
MJXI
MJXII
MJXIII
MJXIV
MJXV
LJI
LJII
LJIII
LJIV
LJV
LJVI
LJVII
WESTERN FRANCE SEQUENCES
Argentan
Poitiers
Montbron
Caen/Deauville
uncertainty
BATHYMETRY
EUSTASY
DECOMPACTED SEDIMENTS THICKNESS
= Total Subsidence (TS)
ACCOMMODATION
=TS +/- bathymetry variations
SUBSIDENCE
= accommodation - eustasy
UPLIFT
TECTONIC SUBSIDENCE

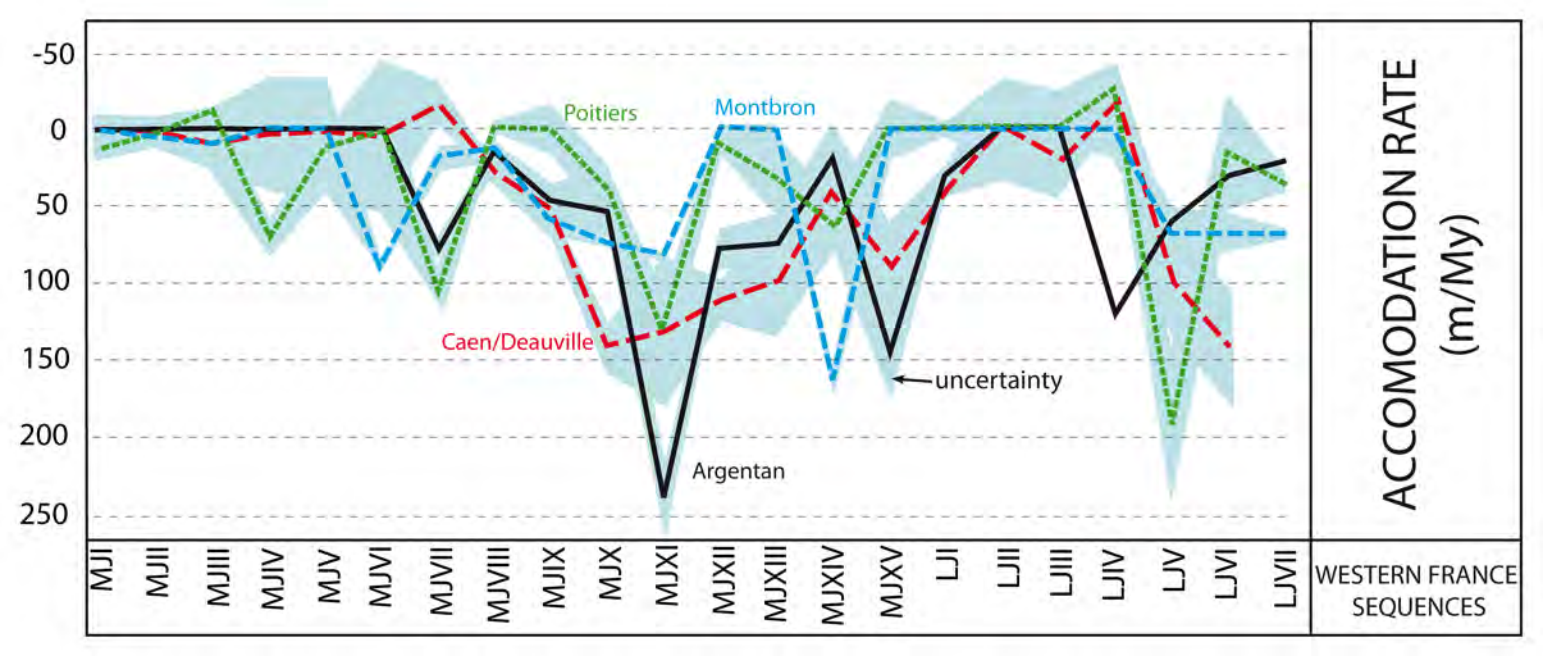
-50
0
50
100
150
200
250
Poitiers
Montbron
Caen/Deauville
uncertainty
Argentan
ACCOMODATION RATE
(m/My)
MJI
MJII
MJIII
MJIV
MJV
MJVI
MJVII
MJVIII
MJIX
MJX
MJXI
MJXII
MJXIII
MJXIV
MJXV
LJI
LJII
LJIII
LJIV
LJV
LJVI
LJVII
WESTERN FRANCE
SEQUENCES

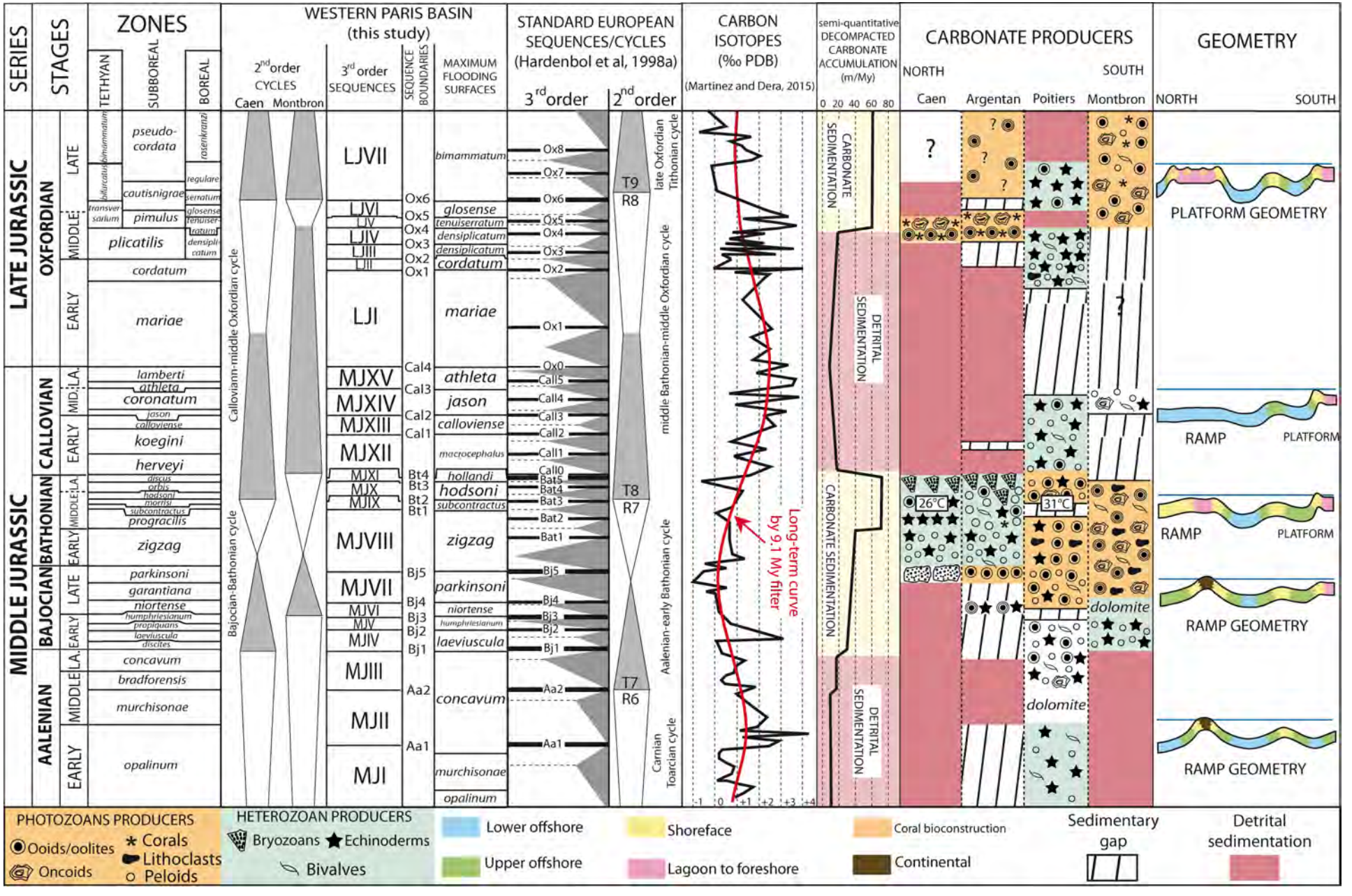
SERIES
STAGES
ZONES
TETHYAN
SUBBOREAL
BOREAL
WESTERN PARIS BASIN
(this study)
2nd order CYCLES
Caen
Montbron
3rd order SEQUENCES
SEQUENCE BOUNDARIES
MAXIMUM FLOODING SURFACES
STANDARD EUROPEAN SEQUENCES/CYCLES
(Hardenbol et al, 1998a)
3rd order
2nd order
CARBON ISOTOPES (‰ PDB)
(Martinez and Dera, 2015)
semi-quantitative DECOMPACTED CARBONATE ACCUMULATION (m/My)
0 20 40 60 80
CARBONATE PRODUCERS
NORTH
SOUTH
Caen
Argentan
Poitiers
Montbron
GEOMETRY
NORTH
SOUTH
LATE JURASSIC
MIDDLE JURASSIC
OXFORDIAN
CALLOVIAN
BATHONIAN
BAJOCIAN
AALENIAN
LATE
MIDDLE
EARLY
pseudo-cordata
cautisnigrae
pimulus
plicatilis
cordatum
mariae
lamberti
athleta
coronatum
jason
calloviense
koegini
herveyi
discus
orbis
hodsoni
morrisi
subcontractus
progracilis
zigzag
parkinsoni
garantiana
niortense
humphriesianum
propinquans
laeviuscula
discites
concavum
bradforensis
murchisonae
opalinum
LJVII
LJVI
LJV
LJIV
LJIII
LJII
LJI
MJXV
MJXIV
MJXIII
MJXII
MJXI
MJX
MJIX
MJVIII
MJVII
MJVI
MJV
MJIV
MJIII
MJII
MJI
Ox8
Ox7
Ox6
Ox5
Ox4
Ox3
Ox2
Ox1
Ox0
Cal5
Cal4
Cal3
Cal2
Cal1
Cal0
Bat5
Bat4
Bat3
Bat2
Bat1
Bj5
Bj4
Bj3
Bj2
Bj1
Aa2
Aa1
Cal4
Cal3
Cal2
Cal1
Bt4
Bt3
Bt2
Bt1
Bj5
Bj4
Bj3
Bj2
Bj1
Aa2
Aa1
T9
R8
T8
R7
T7
R6
Calloviann-middle Oxfordian cycle
Bajocian-Bathonian cycle
late Oxfordian Tithonian cycle
middle Bathonian-middle Oxfordian cycle
Aalenian-early Bathonian cycle
Carnian Toarcian cycle
Long-term curve by 9.1 My filter
-1 0 +1 +2 +3 +4
CARBONATE SEDIMENTATION
DETRITAL SEDIMENTATION
CARBONATE SEDIMENTATION
DETRITAL SEDIMENTATION
26°C
31°C
dolomite
dolomite
PLATFORM GEOMETRY
RAMP
PLATFORM
RAMP
PLATFORM
RAMP GEOMETRY
RAMP GEOMETRY
PHOTOZOANS PRODUCERS
Ooids/oolites
Oncoids
Corals
Lithoclasts
Peloids
HETEROZOAN PRODUCERS
Bryozoans
Echinoderms
Bivalves
Lower offshore
Upper offshore
Shoreface
Lagoon to foreshore
Coral bioconstruction
Continental
Sedimentary gap
Detrital sedimentation

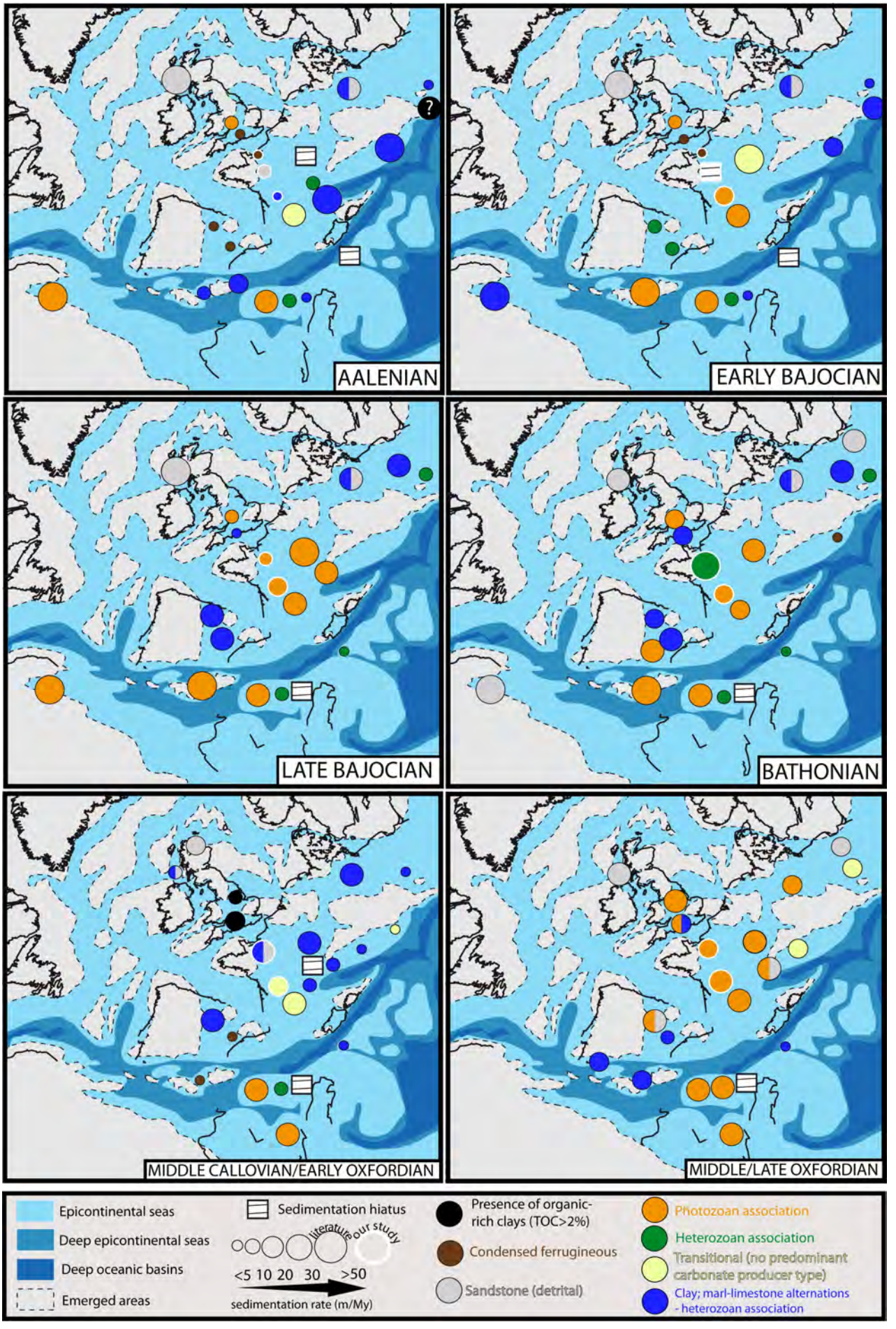
AALENIAN
EARLY BAJOCIAN
LATE BAJOCIAN
BATHONIAN
MIDDLE CALLOVIAN/EARLY OXFORDIAN
MIDDLE/LATE OXFORDIAN
?
Epicontinental seas
Deep epicontinental seas
Deep oceanic basins
Emerged areas
Sedimentation hiatus
literature
our study
<5 10 20 30 >50
sedimentation rate (m/My)
Presence of organic-rich clays (TOC>2%)
Condensed ferrugineous
Sandstone (detrital)
Photozoan association
Heterozoan association
Transitional (no predominant carbonate producer type)
Clay; marl-limestone alternations - heterozoan association

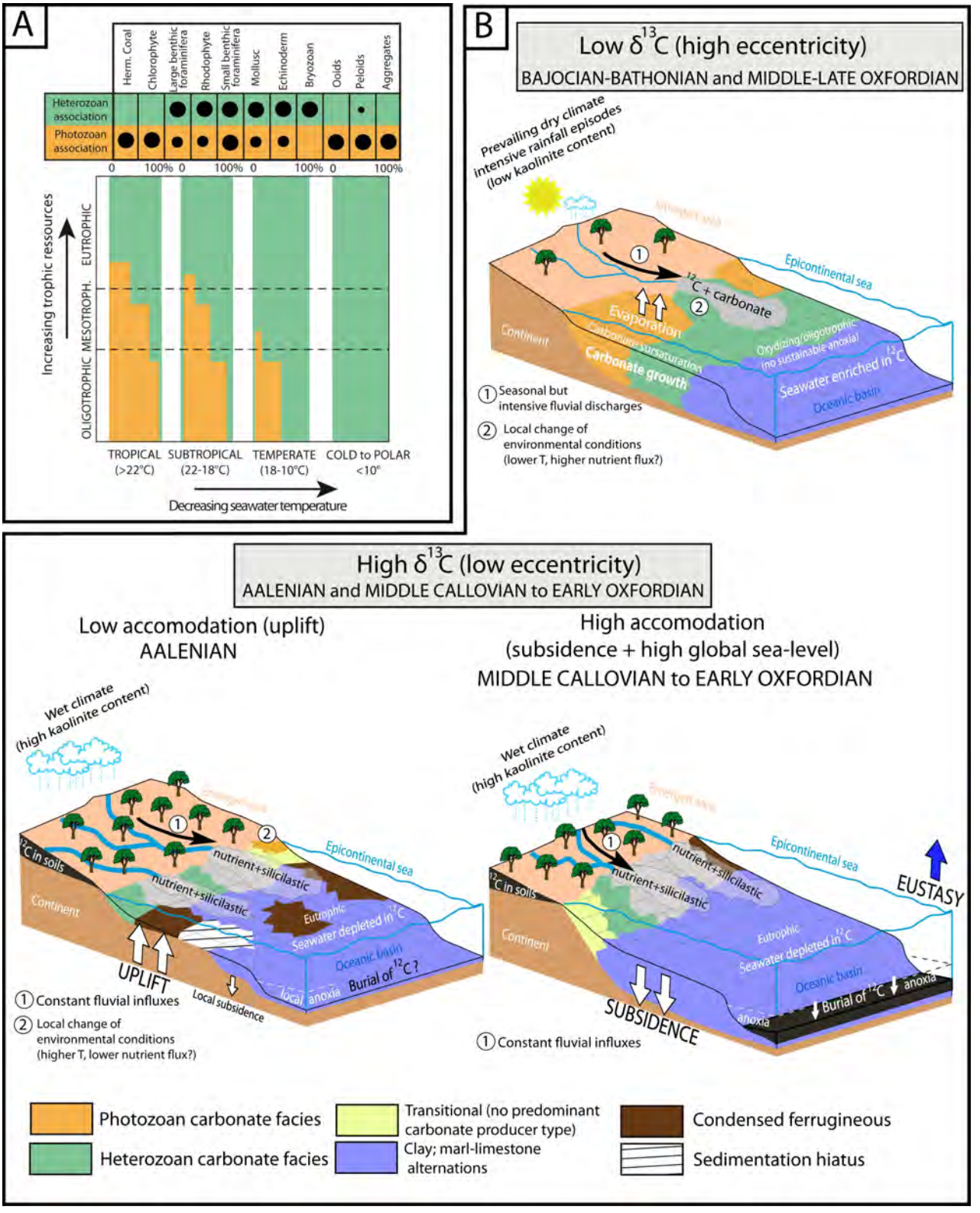
A
Herm. Coral
Chlorophyte
Large benthic foraminifera
Rhodophyte
Small benthic foraminifera
Mollusc
Echinoderm
Bryozoan
Ooids
Peloids
Aggregates
Heterozoan association
Photozoan association
0 100% 0 100% 0 100% 0 100%
Increasing trophic ressources
EUTROPHIC
MESOTROPH.
OLIGOTROPHIC
TROPICAL (>22°C)
SUBTROPICAL (22-18°C)
TEMPERATE (18-10°C)
COLD to POLAR <10°
Decreasing seawater temperature
B
Low δ13C (high eccentricity)
BAJOCIAN-BATHONIAN and MIDDLE-LATE OXFORDIAN
Prevailing dry climate
intensive rainfall episodes
(low kaolinite content)
Epicontinental sea
12C + carbonate
Evaporation
Carbonate supersaturation
Carbonate growth
Oxydizing/oligotrophic (no sustainable anoxia)
Continent
Seawater enriched in 12C
Oceanic basin
1 Seasonal but intensive fluvial discharges
2 Local change of environmental conditions (lower T, higher nutrient flux?)
High δ13C (low eccentricity)
AALENIAN and MIDDLE CALLOVIAN to EARLY OXFORDIAN
Low accomodation (uplift)
AALENIAN
Wet climate
(high kaolinite content)
12C in soils
nutrient+silicilastic
Epicontinental sea
Continent
Eutrophic
Seawater depleted in 12C
Oceanic basin
UPLIFT
Burial of 12C ?
local anoxia
Local subsidence
1 Constant fluvial influxes
2 Local change of environmental conditions (higher T, lower nutrient flux?)
High accomodation
(subsidence + high global sea-level)
MIDDLE CALLOVIAN to EARLY OXFORDIAN
Wet climate
(high kaolinite content)
12C in soils
nutrient+silicilastic
Epicontinental sea
EUSTASY
Continent
Eutrophic
Seawater depleted in 12C
Oceanic basin
Burial of 12C
anoxia
SUBSIDENCE
1 Constant fluvial influxes
Photozoan carbonate facies
Heterozoan carbonate facies
Transitional (no predominant carbonate producer type)
Clay; marl-limestone alternations
Condensed ferrugineous
Sedimentation hiatus

Position within the downdip profile (hydrodynamism)	Lithofacies	Non-bioclastic components	Bioclastic components	Predominant grain association	Sedimentary and biogenic structures	Sorting and grain size	Energy and depositional environment
Lower offshore	F1a: claystone	Silts (R), wood fragments (R)	Ammonites (R), belemnites (R), bivalves (R), sponge spicules (R), foraminifers (R), ostracods (R)		Abundant bioturbation: *Chondrites, Thalassinoïdes, Walthonensis*	Very well sorted; < 4 µm	Very low energy, lower offshore
	F1b: marls	Silts (C), wood fragments (R)	Ammonites (R), belemnites (R), bivalves (R), brachiopods (R), sponge spicules (R), foraminifers (R), ostracods (R), echinoderms (R), dinoflagellates (R)	Heterozoan	Abundant bioturbation: *Chondrites, Thalassinoïdes, Walthonensis*	Very well sorted	Very low energy, lower offshore
	F1c: marl/micritic limestone alternations	Peloids (A), quartz (C), glauconite (C), intraclasts (R)	Echinoderms (F), bivalves (F), foraminifers (R), serpulites (R)	Heterozoan	Abundant bioturbation	Very well sorted	Very low energy, lower offshore
	F1d: ferrugineous ooids packstone to wackestone	Ferruginous ooids (A), intraclasts (R), quartz (R), glauconite (R)	Bivalves (F), echinoderms (C), sponges (R), foraminifers (R), brachiopods (R), gastropods (R), bryozoans (R)	Heterozoan	Bioturbation	Poorly sorted, 100 µm – 5 cm	Very low energy, lower offshore
	F1e: ferruginous oncoid-ooid floatstone	Ferruginous oncoids (A), ferruginous ooids (F), peloids (R), quartz (R), glauconite (R)	Bivalves (C), echinoderms (C), foraminifers (R), brachiopods (R)	Heterozoan	Ferruginous stromatolites, bioturbation	Very poorly sorted, 100 µm – 10 cm	Very low energy, lower offshore
	F1f: Glauconitic to phosphate bioclastic wackestone to floatstone	Glauconite (F), phosphate (C), quartz (C)	Echinoderms (F), bivalves (F), belemnites (C), ammonites (C), brachiopods (R), foraminifers (R)	Heterozoan	Abundant bioturbation	Poorly sorted, 100 µm – 5 cm	Very low energy, lower offshore
Upper offshore	F2a:marl/echinoderm-peloid packstone to grainstone alternations	Peloids (F), quartz (R), oncoids (R), superficial ooids (R), lithoclasts (R)	Echinoderms (A), bivalves (C), brachiopods (R), bryozoans (R), miliolids (R), corals (R), serpulites (R)	Heterozoan	Gutter casts, shell graded layers, bioturbation	Well sorted, 200 µm – 500 µm	Low to moderate energy, upper offshore

	F2b: marl/bivalve-brachiopod wackestone to packstone alternations	Peloids (C), lumps (C), oncoids (C), glauconite (R)	Bivalves (A), brachiopods (C), crinoids (C), sponges spicules (C), foraminifers (R), serpulites (R)	Heterozoan	Gutter casts, hummocky cross-stratification (HCS), shell graded layers	Well sorted, 100 µm – 1cm	Low to moderate energy, upper offshore
	F2c: marl/ooid grainstone alternations	Oolites (F), radial ooids (C), superficial ooids (R), micritic ooids (R), quartz (R), peloids (R), intraclasts (R), grapstones (R)	Crinoids (C), echinoids (R), bivalves (R), foraminifers (R), brachiopods (R), bryozoans (R)	Transitional	Gutter casts	Moderately sorted, 200 µm – 3 cm	Low to moderate energy, upper offshore
	F2d: sponge wackestone to floatstone	Peloids (C), oncoids (C), superficial ooids (R), intraclasts (R)	Sponges (A), sponge spicules (F), echinoderms (F), bivalves (C), bryozoans (R), brachiopods (R), miliolids (R), corals (R), gastropods (R), serpulites (R)	Transitional	Bioturbation, reversed sponges	Very poorly sorted, 100 µm – 10 cm	Low to moderate energy, upper offshore
	F2e: coral bioconstructions (sheetstone to platestone) in marls	Peloids (R)	Lamellar corals (A), bivalves (R), echinoderms (R), sponge spicules (R)	Photozoan	Biostroms (50 cm to 1 m thick and 2-15 m wide)		Upper offshore
	F2f: sponge bioconstruction (boundstone) in marls		Sponges (A), bivalves (C)	Heterozoan	Biostroms (50 cm thick and 2-5 m wide)		Upper offshore
Shoreface	F3a: very fine peloidal grainstone	Peloids (A), superficial ooids (R), intraclasts (R), quartz (R), intraclasts (R)	Echinoderms (C), bivalves (C), miliolids (R), foraminifers (R), brachiopods (R), gastropods (R)	Transitional	Cross stratification in megaripples, bioturbations	Well sorted, 100 µm	Moderate energy, wave dominated shoreface
	F3b: superficial ooid grainstone	Superficial ooids (A), radial ooids (C), micritic ooids (C), oolites (C), peloids (C), grapstones (R), quartz (R), oncoids (R), intraclasts (R)	Bivalves (R), echinoderms (R), miliolids (R), bryozoans (R)	Photozoan	SCS (swaley cross stratification), cross stratification, bioturbations	Well sorted, 50 µm – 1 cm	Moderate energy, wave dominated shoreface
	F3c: bivalve grainstone to rudstone	Quartz (R), peloids (R), ooids (R), oncoids (R), intraclasts (R)	Bivalves (A), echinoderms (C), brachiopods (C), corals (C), bryozoans (R), gastropods (R), red	Heterozoan	Cross stratification in megaripples	Very poorly sorted, 300 µm – 10 cm	Moderate to high energy, wave dominated shoreface

			algae (R), foraminifers (R)				
	F3d: bioclastic peloidal grainstone	Peloids (F), intraclasts (C), micritic ooids, superficial ooids, radial ooids, oolites (C), oncoids (R)	Bivalves (C), echinoderms (C), bryozoans (C), miliolids (R), foraminifers (R), gastropods (R), brachiopods (R), corals (R)	Transitional	Tangential cross-bedding in megaripples, erosive channels (1-2 m thick and 2-5 m wide)	Moderately sorted, 300 µm – 5 cm	High energy, wave dominated shoreface
	F3e: quartz/bioclastic sand to sandstone	Quartz (A), peloids (R), feldspar (R), glauconite (R), iron oxides, intraclasts (R), ferruginous ooids (R)	Echinoderms (R), bivalves (R), gastropods (R), brachiopods (R), foraminifers (R)		Tangential cross-bedding in megaripples, herring bone stratification	Well sorted, 200 µm – 500 µm	High energy, wave to tidally dominated shoreface
	F3f: sponge bioconstruction (boundstone) in bioclastic grainstones		Sponges (*Platychonia magna*) (A), bivalves (C), bryozoans (C), serpulites (R), brachiopods (R), echinoids (R)	Heterozoan	Bioherms (2-3 m thick and 2-5 m wide)		High energy wave dominated shoreface
	F3g: coral bioconstructions (mixstone) in oolitic grainstones		Branching corals (*Thecosmilia*), lamellar corals, massive corals (*Isastrea*) (A), bivalves (F), gastropods (R), bryozoans (R), crinoids (R), echinoids	Photozoan	Bioherms and biostroms		High energy wave dominated shoreface
	F3h: echinoderm grainstone	Peloids (C), oncoids (R), ooids (R), quartz (R)	Echinoderms (A), bivalves (F), brachiopods (R), bryozoans (R), corals (R), green algae (R), miliolids (R)	Heterozoan	Tangential cross bedding in megaripples, herring bone stratification, hydraulic dunes	Well sorted, 100 µm – 2 cm	High energy, wave to tidally dominated shoreface, hydraulic dunes
	F3i: bryozoan grainstone to rudstone	Peloids (R), ooids (R), oncoids (R), intraclasts (R)	Bryozoans (A), bivalves (C), echinoderms (C), sponges (R), corals (R), serpulites (R), red algae (R), brachiopods (R), gastropods (R)	Heterozoan	Cross bedding in megaripples	Poorly sorted, 500 µm – 5 cm	High energy, wave dominated shoreface
	F3j: ooid grainstone to sand	Oolites, micritic ooids, radial ooids, superficial	Echinoderms (C), bivalves (C), foraminifers (R), bryozoans (R),	Photozoan	Tangential cross bedding in	Moderately sorted, 200 µm	High energy, wave to tidally dominated

		ooids (A), peloids (C), nubecularia oncoids (R), intraclasts (R), grapstones (R), quartz (R)	brachiopods (R), gastropods (R), corals (R)		megaripples, large scale cross stratification (foresets of about 20°), herring bone stratification, decimetric channels	– 1 cm	shoreface, dunes near sea surface or carbonate platform margin
	F3k: lithoclast-ooid grainstone to rudstone	Lithoclasts (F), oolites, micritic ooids, superficial ooids, radial ooids (F), peloids (C), grapstones (R)	Echinoderms (C) bryozoans (R), gastropods (R), brachiopods (R), bivalves (R), red algae (R),	Photozoan	Tangential cross-bedding in megaripples, large scale cross stratification (foresets of about 20°), microbial peloids	Poorly sorted, 200 µm – 5 cm	High energy, wave dominated shoreface, carbonate platform margin
	F3l: lithoclast-oyster calcareous conglomerate	Quartz (A), intraclasts (C), peloids (R), ferruginous ooids (R), glauconite (R), iron oxide (R), feldspar (R)	Bivalves (F), echinoderms (R)		Erosive basal surface	Very poorly sorted, 200 µm – 5 cm	High energy, probably storm deposits
Lagoon and intertidal environments	F4a : coral bioconstructions (mixstone) in micritic limestones		Branching corals (*Thomanesteria dendroidea*) massive corals (A), bivalves (C), gastropods (R), brachiopods (R)	Photozoan	Bioherms and biostroms		Low to moderate energy, protected environment
	F4b: bioclastic/ peloid/quartz mudstone	Peloids (F), quartz (F), lithoclasts (C), micritic ooids, oolites (C), oncoids (R)	Bivalves (F), corals (C), gastropods (C), miliolids (R)	Transitional	Washover deposit	Well sorted, 500 µm – 2 cm	Low energy, protected environment
	F4c: pellet/peloid grainstone/packstone	Pellets (A), peloids (F), lithoclasts (F) superficial ooids (C), oncoids (R), aggregates (R), micritic ooids, radial ooids (R), quartz (R)	Miliolids (R), bryozoans (R), bivalves (R), echinoderms (R), gastropods (R)	Photozoan	Planar-bedding, Meniscus and microstalactitic cements, birdseyes, stromatolites	Moderately sorted, 50 µm – 500 µm	Moderate to high energy, lagoon to foreshore (beach)
	F4d: oncoid-ooid	Oolites, micritic ooids,	Miliolids (R), corals (R), bivalves	Photozoan	Planar-bedding,	Very poorly	Moderate to high

	rudstone to packstone with aggregates and lithoclasts	superficial ooids (F), nubecularia oncoids (F), aggregates (F), lithoclasts (F), peloids (R)	(R), gastropods (R), echinoderms (R)		sigmoid cross-bedding in megaripples, meniscus and microstalactitic cements, birdseyes, microbialites, microbial peloids	sorted, 100 µm – 3 cm	energy, lagoon to foreshore (beach)
Supratidal to continental environments	F5a: dolomite	Quartz (R)			Stromatolites		Sabkha: very low energy, backshore
	F5b: lignite	Silts (F)	Characeae gyrogonites (R), ostracods (R)			Very well sorted; < 4 µm	Brackish environment: very low energy, backshore
	F5c: paleosoil	Clays (F), silts (F), quartz (F), iron hydroxides (C)	Characeae gyrogonites (R), oysters (R)		Roots	Very well sorted; < 4 µm	Continental environment

R = rare: <10%; C = common: 10–20%; F = frequent: 20–40%; A = abundant: >40%

Country	Location	Age	Depositional environment	Lithology/carbonate producers	Reference
England	Wessex and Worcester basins, London platform	Aalenian to Oxfordian	Offshore to shallow marine	Marl-limestone alternations, condensed ferruginous, oolitic limestones (photozoan), sandstones	Hesselbo, 2008
England	Worcester Basin, London platform	Aalenian to Bajocian	Shallow marine	Oolitic limestone (photozoan)	Barron et al., 1997
England	Worcester Basin, London platform	Bathonian	Shallow marine	Oolitic limestone (photozoan)	Sellwood et al., 1985
France	Eastern Paris Basin	Aalenian to Oxfordian	Lower offshore to shoreface	Ooid/coral limestones (photozoan), crinoid/coral limestones (transitional) and marls	Brigaud et al., 2014
France	Eastern Paris Basin	Callovian		Hiatus	Collin and Courville, 2006
France	Southeastern France	Aalenian to early Bajocian	Mainly wave to tidal-dominated shoreface	Crinoid limestones (heterozoan)	Rouselle and Dromart, 1996
France	Quercy (southwestern France)	Aalenian to Oxfordian	Shallow platform	Bioclastic (mixed grain association, Aalenian and Callovian) to ooid (photozoan, Bajocian, Bathonian, Oxfordian) limestones	Cubaynes et al., 1989
Germany	Oberrhein (southwestern Germany)	Early Bajocian	Offshore	Marl-limestone alternations	Ohmert, 1994
Germany	Southwestern Germany	Aalenian	Offshore	Marl-limestone alternations	Maxwell et al., 2012
Germany	Southwestern Germany	Late Oxfordian	Upper offshore	Sponge wackestone to packstone with marl interbeds (transitional)	Pittet et al., 2000

Germany	Süntel Mountains (northwestern Germany)	Callovian-Oxfordian	Lower offshore (Callovian and early Oxfordian) to shallow marine (middle-late Oxfordian)	Marl to sandstone (Callovian and early Oxfordian) and oolitic limestone (photozoan, middle-late Oxfordian)	Helm and Schülke, 1998
Germany	North German Basin	Middle Jurassic (Aalenian-Callovian)	Offshore to shallow-marine (Wave dominated)	Claystone to sandstone	Zimmermann et al., 2015
Italy	Umbria-Marche Basin, Central Italy	Aalenian to Oxfordian	Offshore/shallow marine	Marl-limestone alternations	Bartolini et al., 1996
Italy	Umbria-Marche Basin, Central Italy	Aalenian to Oxfordian	Offshore	Marl-limestone alternations/ Heterozoan limestones	Morettini et al., 2002
Italy	Lazio-Abruzzi Platform, Central Italy	Aalenian to Oxfordian	Shallow marine	Heterozoan (Aalenian-early Oxfordian) to photozoan (middle-late Oxfordian) limestones	Bartolini et al., 1996
Italy	Apulia platform, southern Italy	Callovian to Oxfordian	Oolitic shoals and lagoon	Peloidal mudstones to packstones/oolitic grainstones (photozoan)	Bosellini et al., 1999
Italy	Apennines platform, southern Italy, Sorrento Peninsula	Aalenian to Oxfordian	Very shallow	Ooid limestone with Chlorophyte	Iannace et al., 2011
Italy	Trento Plateau, north-eastern Italy	Aalenian to Oxfordian	Offshore	Marl-limestone alternations/ Heterozoan limestones	Préat et al., 2006
Morocco	High Atlas	Aalenian	Inner to mid-ramp	Oolitic limestones (photozoan)	Pierre et al., 2010
Morocco	High Atlas	Aalenian to Bathonian	Inner ramp (Aalenian, late Bajocian, Bathonian) to lower offshore (early Bajocian)	Oolitic/bioclastic limestones (photozoan, Aalenian, late Bajocian), marls (early Bajocian) and sandstones (Bathonian)	Tomas et al., 2013; Ait Addi and Chafiki, 2013
Morocco	High Atlas	Late Bajocian	Inner ramp	Oolitic to bioclastic ramp with corals patch reef (photozoan)	Christ et al., 2012

Poland	Pieniny Kippen Basin, Carpathians (southern Poland)	Aalenian to early Bajocian	Lower offshore	Organic-rich claystones	Tyska, 1994; Tyszka and Kaminski, 1995
Poland	Polish Jura (south-central Poland)	Late Bajocian-Bathonian	Lower offshore	Clays	Zaton et al., 2009
Poland	Cracow Area, southern Poland	Callovian-Oxfordian	Lower offshore (Callovian and early Oxfordian) to shallow marine (middle-late Oxfordian)	Marl to sandstone (Callovian and early Oxfordian) and sponge-rich limestone (transitional, middle-late Oxfordian)	Matyszkiewicz and Felisiak, 1992
Poland	Tatra Mountains, southern Poland	Aalenian to Callovian	Offshore to shallow-marine	Crinoidal limestones (heterozoan), ferruginous condensed,	Luczynski, 2002
Poland	Polish Jura chain (southwestern Poland)	Late Oxfordian	Shallow marine	Sponge limestone (transitional)	Wierzbowski, 2015
Scotland	Cleveland Basin	Aalenian-Oxfordian	Shallow marine	Siliciclastic sandstone	Hesselbo, 2008
Spain	Asturias, Basque-Cantabrian, Pyrenean and Iberian basins; northern Spain	Aalenian-Oxfordian	Offshore to shallow marine	Marl-limestone alternations, condensed ferruginous, heterozoan/photozoan limestones , sandstones	Aurell et al., 2003
Spain	Betic Cordillera, southern Spain	Middle to late Oxfordian	Lower offshore	Marl-limestone alternations	Pittet et al., 200
Spain	Betic Cordillera, southern Spain	Aalenian	Lower offshore	Marl-limestone alternations	Sandoval et al., 2008
Spain	Betic Cordillera, southern Spain	Bajocian and Bathonian	Shoreface	Oolitic limestone (photozoan)	Reolid et al., 2009
Switzerland	Swiss Jura	Middle/late Oxfordian	Shoal/tidal flat/lagoon	Ooid/coral grainstoens to boundstones (photozoan)	Pittet and Strasser, 1997

Switzerland	Swiss Jura	Late Bajocian	Shallow water ramp (shoreface)	Oolitic limestone (photozoan)	Gonzalez and Wetzel, 1996
Switzerland	Swiss Jura	Late Bajocian	Shallow water ramp (shoreface)	Oolitic limestone (photozoan)	Wetzel et al., 2013

- Carbonate platform evolution was reconstructed along a 500 km cross-section
- Tectonism triggered two major phases of rise and fall in carbonate production
- Basement topography acted as a major control over lateral variations of paleodepth
- Photozoan carbonate production was promoted by dry climate and low nutrient input
- Wet climate and the eutrophication of epireic seas lead to low carbonate production